ATTENTION: The Singapore Copyright Act applies to the use of this document. Nanyang Technological University Library

Electrical Reliability of Ultra-low k Dielectric of an IC Device and Its Optical Spectroscopic Characterization

Jeffrey Lam Chor Keung
Supervisor: Associate Prof. Sun Handong

A report submitted to Nanyang Technological University
In partial fulfillment of the requirements
for the Degree of Doctor of Philosophy

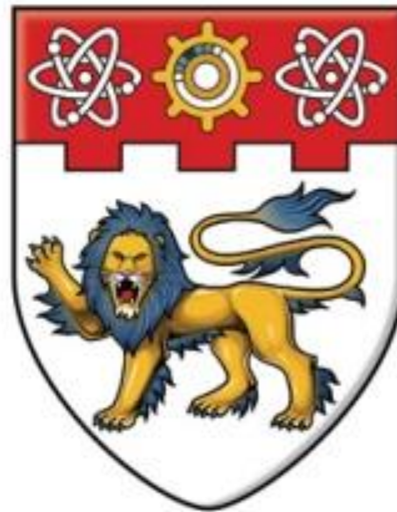

Division of Physics and Applied physics
School of Physical and Mathematical Science
Nanyang Technological University

November, 2013

ATTENTION: The Singapore Copyright Act applies to the use of this document. Nanyang Technological University Library

ACKNOWLEDGEMENT

I wish to express my deepest gratitude to my supervisor Dr. Handong Sun for his continuing support to me in this project, to which I have devoted my past three years. His broad knowledge and strong research capability enable him to provide an in-depth guidance and clear direction in the project.

Special thanks to Prof. Sheng Zexiang for his invaluable technical advices during my PhD degree study in NTU.

Almost as important to a graduate student is moral support, which keeps life tolerable if not downright fun. For this I give my thanks to all of my classmates in the Division of Physics and Applied Physics in NTU.

I would like to thank Dr. Maggie Huang for her help in the installation of the Raman and FTIR spectroscopy systems and other facilities required in the experiments. I also thank Dr. Zhang Fan for providing appropriate silicon wafers for TDDB analysis and Dr. Du Anyan's for performing TEM analysis to allow me to study the root cause of TDDB failure mechanisms.

ATTENTION: The Singapore Copyright Act applies to the use of this document. Nanyang Technological University Library

Summary

In summary, electrical reliability of ultra-low k dielectrics of leading edge semiconductor Integrated circuits (IC) was investigated using complimentary vibrational spectroscopy of Raman and Fourier Transform Infra-Red (FTIR).

In order to reduce the resistance and capacitance (RC) delay in advanced semiconductor IC process, Cu and ultra-low k dielectric was introduced to replace aluminum (Al) and silicon dioxide (SiO_2) as metal interconnects and inter-metal dielectrics, respectively. However, low k and ultra-low k dielectric reliabilities become a concern due to their weak mechanical strength and chemical bonding.

In this project, time dependent dielectric breakdown (TDDB) failure of ultra low-k dielectrics is investigated. TDDB is the standard for low k dielectric reliability stress test. There are several TDDB studies carried out to investigate the mechanism of TDDB failure of low k dielectrics.

The complementary vibrational spectroscopy techniques, Raman and FTIR spectroscopy, were used to investigate the failure mechanism of the TDDB failure. These techniques can obtain the information of the molecular bonding and structure in low k dielectrics. Many researchers have investigated characteristics of low k or ultra-low k dielectrics on blank wafers. However, little research involves Raman and FTIR analysis on low k and ultra-low k dielectric in realistic IC devices. Hence, in TDDB analysis, the mechanism is still arguable and damage of the low k dielectric in TDDB test is uncertain. Raman and FTIR spectroscopy could be one of the most promising techniques to identify the chemical bonding change during TDDB stress test.

ATTENTION: The Singapore Copyright Act applies to the use of this document. Nanyang Technological University Library

In this work, a methodology to study SiCOH low k/ultra-low k dielectric thin films on patterned wafers by overcoming technique limitation of Raman and FTIR spectroscopy due to the fluorescence in Raman spectroscopy and weak signal from patterned Cu/ultra-low k structures, has been developed.

Ultra-low k dielectric TDDB process is characterized using complementary Raman and FTIR vibrational spectroscopy. Under the applied electrical field, the ultra-low k dielectric would first degrade. Ta ions would then migrate into ultra-low k along interfacial weakness of Cu/Ta/TaN/SiCOH, resulting in a more severe damage to the ultra-low k dielectric. The Ta ions inside the ultra-low k induced an increased local electrical field between Cu electrodes and thus accelerated the ultra-low k degradation to final breakdown. No out-diffusion of Cu ions is observed.

For the first time, a new TDDB failure mechanism based on Ta/TaN barrier metal migration which occurred some distance away from capping layers is proposed. The pores in ultra-low k materials were degraded under high electrical field, resulting in the Ta ionic migration into the degraded inter-metal dielectric (IMD). This failure mechanism fits well to the "square root of E" $\sqrt{E}$ model. Additionally, wafers with Reactive ion etching (RIE) etch experiments are devised to explore the line edge roughness (LER) effect on TDDB. A unified model and understanding for the spacing variations is established. In summary, we can see that more dense Ultralow k dielectric material, a better slopped trench/via profile and more tightened control on metal roughness are needed for a robust ultra-low k TDDB performance.

ATTENTION: The Singapore Copyright Act applies to the use of this document. Nanyang Technological University Library

Contents

Table List

Figure Captions

List of Abbreviation

Chapter 1: Introduction..19

1.1 General introduction 19

1.1.1 Semiconductor Technology Roadmap.. 19

1.1.2 Interconnects 20

1.1.3 Low k and ultra-low k dielectrics in IC technology 21

1.1.4 Low k and ultra-low k dielectric classification and preparation method............. 22

1.1.5 Material Characterization.. 25

1.1.6 Difficulties and challenges for low k/ultra-low k with Cu interconnects 26

1.2 Low k dielectric mateterial reliability 27

1.2.1 Low k dielectric reliability 27

1.2.2 Low k dielectric reliability anslysis method 30

1.3 Vibraional spectroscopy of low k and ultra-low k dielectrics 34

1.3.1 Raman spectroscopy 35

ATTENTION: The Singapore Copyright Act applies to the use of this document. Nanyang Technological University Library

1.3.2 Fourier Transform Infrared Spectrometry (FTIR)... 36

1.3.3 Vibrational spectroscopy on low k dielectrics 37

1.4 Summary and conclusions... 43

Chapter 2 Experimental setup 46

2.1 Introduction 46

2.2 The Process of Cu/Ultra low k dielectrics.. 49

2.3 Process integration of low k/Cu interconnects 51

2.4 Process tools and their configurations 52

2.5 Setup for TDDB test 54

2.6 Raman spectroscopy system.. 55

2.7 Fourier Transform Infrared (FTIR) spectrometry.. 67

Chapter 3 Vibrational spectroscopy of low k/ultra-low k dielectrics on patterned wafers...70

3.1 Introduction 70

3.2 Experiments.. 73

3.3 Results and discussions 85

3.3.1 Vibrational spectroscopy on SiCOH low k dielectric on patterned wafers 75

3.3.2 Vibrational spectroscopy on SiCOH ultra-low k dielectric on patterned wafer 80

ATTENTION: The Singapore Copyright Act applies to the use of this document. Nanyang Technological University Library

3.3.3 Vibrational spectroscopy on SiCOH/Cu mixed 82

3.4 Summary and conclusions 85

Chapter 4 FTIR spectroscopy of ultra-low k dielectric on patterned wafers............ 86

4.1 Introduction 86

4.2 Experiments 88

4.3 Results and discussions 89

4.3.1 FTIR Spectroscopy on low k dielectric on patterned wafe rs: reflection mode 89

4.3.2 FTIR Spectroscopy on low k dielectric on patterned wafers: ATR mode 91

4.3.3 FTIR Signal Analysis on Mixed FTIR Spectroscopy: mapping mode 94

4.4 Summary and conclusions 95

Chapter 5 Ultra-Low k Dielectric TDDB Failure 96

5.1 Introduction 96

5.2 Experiments 98

5.3 Results and discussion 99

5.4 Summary and conclusions 105

ATTENTION: The Singapore Copyright Act applies to the use of this document. Nanyang Technological University Library

Chapter 6 A Model Analysis and the Process Improvement on the Cu/Ultra-Low k Dielectric TDDB Failure Caused by Dielectric Degradation and Barrier Metal Migration Into the Degraded Dielectrics 106

6.1 Introduction 106

6.2 Experimental details 108

6.3 Summary and conclusions 116

Chapter 7 Conclusions and Future Work 118

References 123

Publications 139

ATTENTION: The Singapore Copyright Act applies to the use of this document. Nanyang Technological University Library

Table List

Table 1.1 Improvement trends for feature scaling of IC devices.

Table 1.2 Summary of low k dielectrics.

Table 3.1 k value and optical properties of low k and ultra-low k SiCOH.

ATTENTION: The Singapore Copyright Act applies to the use of this document. Nanyang Technological University Library

Figure Captions

Figure 1.1 2009 ITRS technology trends.

Figure 1.2 The relation of leakage current density versus electric field for different low k dielectrics.

Figure 1.3 The TDDB test of an E-test structure with 50nm ½ pitch low k interconnects after with a testing time of almost one year.

Figure 2.1. A cross section view of a device fabricated with a standard Cu/low k process.

Figure 2.2 Schematic diagram of a Cu/low k dual damascence process.

Figure 2.3 XTEM image on a 20 nm IC device.

Figure 2.5 Keithly 4200-SCS semiconductor parameter analyzer.

Figure 2.6 A Raman mapped image of a stressed Silicon interface by T64000.

Figure 2.7 The T64000 Raman spectroscopy system.

ATTENTION: The Singapore Copyright Act applies to the use of this document. Nanyang Technological University Library

Figure 2.8 The overall of the precision tilt platform.

Figure 2.9 The schematic of the tilt platform.

Figure 2.10 Raman spectra captured for the SRAM sample with tilt 0° (no-tilt) and tilt 15°, respectively.

Figure 2.11. The schematic for enhanced Raman scattering on nanometer scaled Cu/low k interconnect.

Figure 2.12 FITR principle.

Figure 2.13 the Nicolet 6700 FTIR system.

Figure 3.1 Low k dielectric breakdown (indicated by the arrow) during the reliability test, IM.

Figure 3.2 A typical cross-section TEM of an IC device with low k/Cu CMOS process.

Figure 3.3 Raman spectrum excited by 532 nm laser of the dense SiCOH low k dielectric deposited on the second via in the first IC device.

ATTENTION: The Singapore Copyright Act applies to the use of this document. Nanyang Technological University Library

Figure 3.4 Raman spectrum excited by 325 nm laser of the porous SiCOH ultra-low k dielectric deposited on the second via in the second IC device.

Figure 3.5 FTIR spectrum of the dense SiCOH low k dielectric at the same location corresponding to the Fig. 3.3.

Figure 3.6 Raman spectrum excited by 325 nm laser of the porous SiCOH ultra-low k dielectric deposited on the second via in the second IC device.

Figure 3.7 Comparison of FTIR spectra, in a range of 2700–3200 cm^{-1}, between the dense (bottom curve) and porous SiCOH (top curve) dielectrics in the two IC devices, respectively.

Figure 3.8 Raman spectra excited by 532 nm laser of the individual SiCOH ultra-low k dielectric and the ultra-low k/Cu mixed structure in the second IC device.

Figure 3.9 Raman spectrum excited by 532 nm laser of the ultra-low k/TaN/Cu mixed structure in the second IC device.

Figure 4.1. Optical micrograph of a pattern wafer with low k dielectric. Areas of interest are indicated on the graph.

ATTENTION: The Singapore Copyright Act applies to the use of this document. Nanyang Technological University Library

Figure 4.2. FTIR spectra of SiCOH layer structure from the patterned wafer recorded under reflection mode.

Figure 4.3. Comparison of FTIR spectra recorded by reflection and ATR mode from the same area of interest on the patterned wafer.

Figure 4.4. Comparison of FTIR spectra recorded by reflection and ATR mode over CH_x band.

Figure 4.5. FTIR mapping over a rectangular area on a patterned wafer.

Figure 5.1 A plot showing the leakage current as a function of time in Cu/ultra-low k comb structure. The insert shows the top-down schematics of the comb structure used in the study.

Figure 5.2 In-situ FTIR spectroscopy on the Cu/ultra-low k comb structure at different stress status.

Figure 5.3 Raman spectroscopy on the Cu/ultra-low k comb structure at different stress status.

ATTENTION: The Singapore Copyright Act applies to the use of this document. Nanyang Technological University Library

Figure 5.4 TEM cross-section images of the Cu/ultra-low k comb structure for the original sample before stress (a) and the sample with a certain time of stress with leakage current (b). EDX line profile of the Ta migration along the interface of Cu/Ta/TaN/SiCOH before stress (c) and after stress (d), respectively.

Figure 6.1 Cu/Ta/TaN/Low k SiCOH Damascene structure

Figure 6.2 TDDB Test Structure

Figure 6.3 Measured TDDB on POR wafers under different stress Fields

Figure 6.4 Measured TDDB @ T63.2(s) shows consistent with Square Root E Model for Ta Migration wafer

Figure 6.5 TEM cross-section images of the Cu/ultra-low k comb structure for the original sample before stress (a) and the sample with a certain time of stress with leakage current (b). EDX line profile of the Ta migration along the interface of Cu/Ta/TaN/SiCOH before stress (c) and after stress (d), respectively [3].

Figure 6.6 Simulation of the electric field distributionrepartition during CVS test on Interdigited-on a E-test comb structure

ATTENTION: The Singapore Copyright Act applies to the use of this document. Nanyang Technological University Library

Figure 6.7 bond diagram for Ta Migration

Figure 6.8 Metal Profile after Metal RIE & CMP for split wafers

Figure 6.9 Tbd of bad LER Wafer(138) & Good LER Wafer(1400)

Figure 6.10 Measured TDDB @ T63.2(s) shows consistent with Square Root E Model, the bad LER wafer shows degradation on the TDDB.

ATTENTION: The Singapore Copyright Act applies to the use of this document. Nanyang Technological University Library

List of Abbreviation

ATR – Attenuated Total Reflectance

BLS – Brillion Elastic Modulus

CA – Contact

CVD – Chemical Vapor Deposition

CLC – Charge Limited Current

CMP – Chemical-Mechanical Planarization (or Polishing)

CW laser – Continuous Wave Laser

DOE – Design of Experiments

DUT – Device Under Test

DRAM – Dynamic Random Access Memory

BEOL – Backend of Line

EDX – Energy Dispersive X-ray

EFTEM –Energy Filtered TEM

EP – Ellipsometric Porosity

ESR – Electron Spin Resonance

ET – Electrical Test

FEOL – Frontend of Line

FIB – Focused Ion Beam

FTIR – Fourier Transform Infrared

ATTENTION: The Singapore Copyright Act applies to the use of this document. Nanyang Technological University Library

IC – Integrated Circuit

ILD – Inter-Layer Dielectrics

IMD – Inter-Metal Dielectrics

ITRS – International Technology Roadmap for Semiconductors

HFS – Hydrogen Forward Scattering

HRTEM – High Resolution TEM

IR – Infrared

LER –Line Edge Roughness

MCT –Mercury Cadmium Telluride, HgCdTe

NMR – Nuclear Magnetic Resonance

ORTC – Overall Roadmap Technology Characteristics

PAS – Positron Annihilation Spectroscopy

PECVD – Plasma Enhance CVD

PF cuurent – Poole-Frenkel Current

PIDS – Process Integration, Device and Structure

RC – Resistance and Capacitance

RBS – Rutherford Backscattering

SAWS – Surface Acoustic Spectroscopy

SEM – Scanning Electron Microscope

SRAM – Static Random Access Memory

ATTENTION: The Singapore Copyright Act applies to the use of this document. Nanyang Technological University Library

TEM – Transmission Electron Microscope

TBD – Time of Breakdown

TDDB – Time Dependent Dielectric Breakdown

ToFSMIS – Time of Flight Secondary Ion Mass Spectrometry

TVS – Triangular Voltage Sweep

TTF – Time to Failure

RIE – Reactive Ion Etch

RF – Radio Frequency

SiCO – Carbon Doped Silicon Dioxide

ULK – Ultra-Low k

UV – Ultra Violet

XPS – X-ray Photoelectron Spectroscopy (XPS)

ATTENTION: The Singapore Copyright Act applies to the use of this document. Nanyang Technological University Library

Chapter 1 Introduction and Motivation

1.1 General Introduction

1.1.1 Semiconductor Technology Roadmap [1].

In the past decades, the semiconductor industry advanced with rapid pace in its product improvements. The major categories of improvement are shown in Table 1.1 [1]. Most of advancements benefits from the exponential decreased minimum feature sizes, which was used to fabricate an IC device. Moore's Law shows that the number of electrical components per chip doubles in every 2 years. The manufacturing cost will be greatly decreased.

Table 1.1 Improvement trends for feature scaling of IC device [1].

TREND	*EXAMPLE*
Integration Level	**Components/chip, Moore's Law**
Cost	**Cost per function**
Speed	**Microprocessor throughput**
Power	**Laptop or cell phone battery life**
Compactness	**Small and light-weight products**
Functionality	**Nonvolatile memory, imager**

ATTENTION: The Singapore Copyright Act applies to the use of this document. Nanyang Technological University Library

The Overall Roadmap Technology Characteristics (ORTC) Technology Pacing Trends drivers for the International Technology Roadmap for Semiconductors (ITRS) Roadmap Update provides the introduction of "equivalent scaling" technologies. An example of "equivalent scaling" technology was shown in Figure 1.1.

Different company has different technology implementation. The time to market for differing reasons was based on the market needs, competition, resulting difference in their individual technology roadmap.

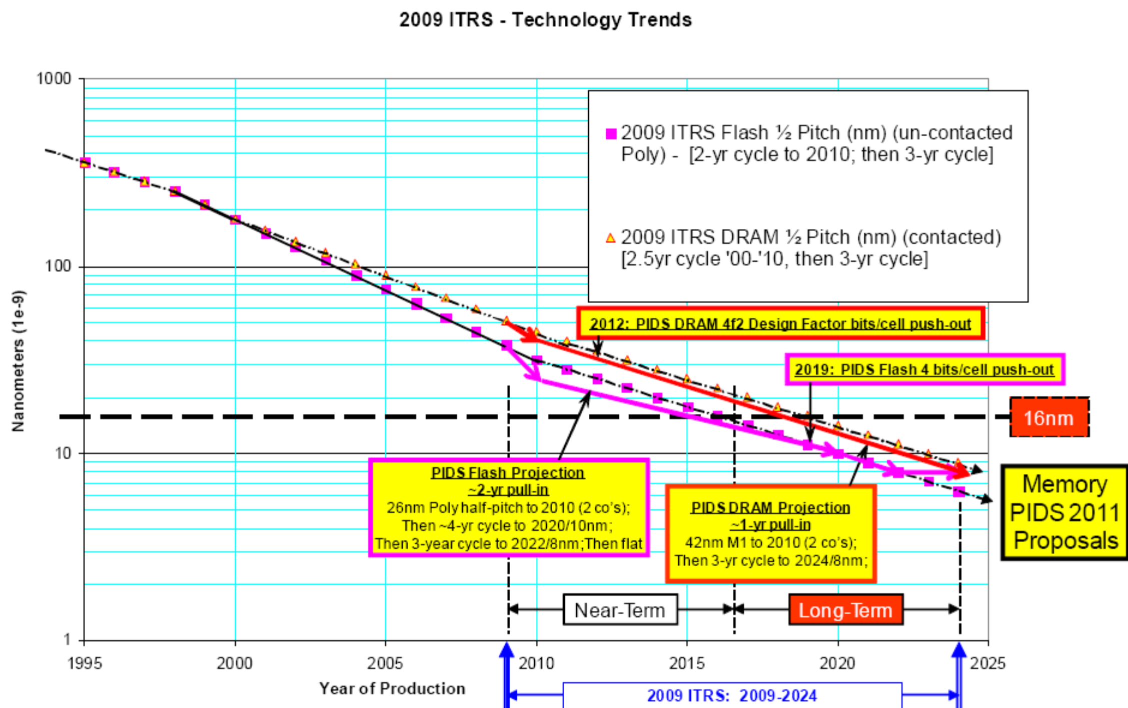

Figure 1.1 2009 ITRS technology trends [1].

1.1.2 Interconnects [1, 3].

Due to the continuous scaling in device feature size, IC devices increased their storage capacity and overall function with faster transistors. In the past twenty years, device feature size was scaled down from 1 μm to 20 nm and 10 nm process technology started. However, with the decrease of the device feature size, the interconnection RC

ATTENTION: The Singapore Copyright Act applies to the use of this document. Nanyang Technological University Library

delay decreases. Smaller cross-section of a wire and the smaller spacing between interconnects lead to higher resistance and larger parasitic capacitance. Therefore, RC delay is becoming a serious limitation to performance improvement. It has negative impact to further scaling down transistor dimensions. In order to reduce resistance and capacitance, conventional Al and SiO_2 need to be replaced with lower resistive metal and lower k dielectric materials, respectively.

Copper (Cu) has a resistivity 36% lower than Aluminum. The replacement of Al with Cu as the new interconnect metal will effectively reduce the RC delay. In the past decade Cu has been successfully integrated into IC manufacturing and the damascene processing was developed.

The wiring system in an IC device includes the clock and other signals to functional blocks, and different power supply distributions and ground connections. Since 2008, the contact level was included to the local wiring. The biggest challenge is the global wiring delay which is still a primary focus for RC delay reduction.

1.1.3 Low k and ultra-low k dielectric in IC technology

The dielectric constant of a low k dielectric is smaller than that of silicon dioxide. Low k dielectric material implementation allows us continuously scale down microelectronic devices. With the device feature size decreased, transistors are closer to each other, resulting in the reduction of the insulating dielectrics thickness. The charge building up at the thinner dielectrics and crosstalk becoming more severe due to the increase of the parasitic capacitance affect the general device performance. Using a low k dielectric to replace the SiO_2 will reduce the parasitic capacitance and, hence, the IC device can switch at faster speeds with lower heat dissipation.

ATTENTION: The Singapore Copyright Act applies to the use of this document. Nanyang Technological University Library

SiO_2, which was used as IMD in IC devices, has dielectric constant of 3.9. Many dielectric materials have lower dielectric constants. However, not all of them can be integrated into current semiconductor manufacturing process.

Low dielectric material can not only reduce RC delay but also suppress the cross talk between interconnect wires. The dielectric constant can be reduced with smaller dipole strength or less number of dipoles. The dielectric materials with chemical bond of lower polarizability (Si-F, Si-C) than Si-O has smaller dipole strength and the lower density materials have less number of dipoles. Many researches have been done to develop the low k dielectric materials and to integrate them, such as Black Diamond, CORAL, SiLK, into IC manufacturing process.

To further reduce the dielectric constant, subtractive pores can be introduced into low k dielectric materials. This may be achieved by adding thermally degradable material, porogen, into the precursor. Later on, the porogen can be removed by a post thermal treatment or some other process. In general however, simply reducing the dielectric constant decreases the film strength and thermal stability. Although porous low k dielectric materials have ultra low dielectric constant, they have lower thermal and mechanical stability compared to SiO_2. Therefore, it is challenging to integrate low k dielectric materials into Cu damascene and dual damascene process.

1.1.4 Low k and ultra-low k dielectric classification and preparation method

Dependent on their elementary composition and spatial structure, low k or ultra-low k dielectrics have two groups of Si based and non-Si based. In Si-based materials, it can be divided into the Silica based materials and the Silsesquioxane (SSQ) based materials. Because SiO_2 has traditionally been well understood as ILD materials and

ATTENTION: The Singapore Copyright Act applies to the use of this document. Nanyang Technological University Library

seamless integrated into ULSI fabrication technology, the first low k dielectrics are Silica-based with k value of 3.9 - 4.1. In silica, oxygen atoms in the Si-O bond are replaced with F, C, or CH_3 atom. Compared to Si-O bond, Si-H, Si-F and Si-CH_3 bonds have lower polarizability. At the same time, H, F and CH_3 atoms can create additional volume and steric hindrance, both of which are critical to get lower K value. SSQ-based materials have lower material's density with cubic structure different from tetrahedral structure of Silica-based materials. Thus, lower density or k value of 2.5 to 3.5 can be achieved by replacing oxygen atom with H (HSQ) or CH_3 (MSQ).

Non-Si based materials are mainly organic polymers consisting of nonpolar C-C bonds. Dielectric constant as low as two has been obtained in some research labs. But their application was limited by the poor thermal stability, mechanical properties, and incompatibility with traditional SiO_2 based process.

The low k dielectrics are also obtained with decreased material density or increased free volume by introducing porosity into the materials. There are two ways to create porosity: constitutive and subtractive. In constitutive materials, a material can be porous without any additional treatment. The part of the materials has to be removed in subtractive materials. Well dispersed spherical pores with a diameter of 2 nm without severe aggregation have been achieved by Byeongdu *etc.* using polymethylsilsesquioxance (PMSSQ) as precursor [2]. An overall materials summary is listed in table 1.2 below.

There are two main deposition methods for low k dielectrics: chemical vapor deposition (CVD) and Spun-on coating. Spun-on coating can be applied to both inorganic and organic films deposition. In some of the study, spin-on method was employed

ATTENTION: The Singapore Copyright Act applies to the use of this document. Nanyang Technological University Library

because it can be performed under room temperature; while CVD thin film deposition usually requires high temperature (~300C) and is often enhanced by plasma. Hitachi Ltd. and Hitachi Chemical Co. had already announced that they had developed pin-on type ultra low dielectric constant materials with a dielectric constant of k=2.4.

Table 1.2 Summary of low k dielectrics [3].

Materials Class	Feature	Examples	Dielectric constant
Silica (SiO_2)	Silicon dioxide glass	Thermal TEOS	3.9-4.1
Modified Silica	Fluorinated Silica Carbon doped Silica	SiCOH	<3.0
Porous Silica	Nanoporous Silica	Aerogel , Zerogel	1.0-3.0
Inorganic Polymer	Organic modified SIlica	Polysilesquioxane (SSQ)	2.5-3.5
Porous Hybrids	Phase separated organic and inorganic	PSL/SSQ hybrids	2.3-3.0
Organic polymers	Fluorinated and non Fluorinated polymers	Polymide, parylene, and polynaphthalene families benzocyclobutene (BCB) Aromatic Hydrocarbon (SILK) amorphous carbon films	1.8-3.5

Porosity can be obtained by constitutive and subtractive methods. High temperature annealing is not only necessary to remove porogen to leave behind the pores; it also forms chemical cross-link to achieve a stable film structure for desirable

ATTENTION: The Singapore Copyright Act applies to the use of this document. Nanyang Technological University Library

mechanical and thermal requirement. Currently, samples are annealed at temperature range of 300 to 700 ^{o}C to produce cross link structure or remove the precursor at a vacuum or N_2 ambient [4-7].

1.1.5 Material Characterization

To determinate the thin film composition, a complementary analytical approach is usually used. Those approaches include hydrogen forward scattering (HFS) and Rutherford backscattering (RBS), time of flight secondary ion mass spectrometry (ToFSIMS) or Auger, and Raman spectroscopy and Fourier Transform Infra-red (FTIR). Raman and FTIR spectroscopy are complementary vibrational spectroscopy techniques, which obtain the information of the molecular bonding and structure of a material.

Nuclear magnetic resonance (NMR) can also be used for the analysis of the molecular bonding and structure of a material. It gives information both on the elemental composition and the bonding polarity.

High resolution Transmission Electron Microscope (HRTEM) with atomic resolution is the most excellent technique to study the low k dielectrics in very thin dimensions. Cross section profiles of ultra-low k dielectric can be observed to provide quantitative information of pore structure and distribution [3]. Combined with energy filtered TEM (EFTEM), element sensitive analysis can be applied to materials in small features. X-ray reflectivity (SXR) and Ellipsometric porosimetry (EP) can measure the density and the porosity of the materials.

The noncontact optical techniques of Brillouin light scattering (BLS) and Surface acoustical wave spectroscopy (SAWS) can measure the elastic modulus [8]. BLS and

ATTENTION: The Singapore Copyright Act applies to the use of this document. Nanyang Technological University Library

SAWS are able to measure the correlations between the OSG films thickness and the porosity if the film density and thickness of low k dielectric was carefully calibrated.

1.1.6 Difficulties and Challenges for low k and ultra-low k with Cu interconnects [1-8].

For low k and ultra-low k with interconnects, we are facing the following challenges.

1. **Materials:** When a new material was introduced into the process, it was always challenging for process integration and material characterization. For low and ultra-low k process with Cu as the interconnects, the size effects impact the interconnect structures. The common issues for the new materials include defective metal line and roughness of the line edge and surface, resulting in high resistivity of the Cu lines.
2. **Manufacturing Integration**: In the manufacturing integration, the Chemical-mechanical polishing (CMP) damage during processing, dielectric constant degradation, resist poisoning, optical proximity correction (OPC), and interconnect/packaging architecture design optimization tool performance is the key concerns for a successful process development. Patterning techniques of lithography and etching, cleaning process, and material filling at nano dimensions will be challenging too. With the reduction of the features size, the process of lithography, etch, clean, film deposition for gap fill, etc, will be the key focus. The increased complexity to processes integration, manufacturing and device structures will impact the time to the market of a newly developed process. The

ATTENTION: The Singapore Copyright Act applies to the use of this document. Nanyang Technological University Library

thermo-mechanical effects due to the increased number of levels and transistors need to be carefully considered also.

3. **Reliability:** All the new materials, structures, and processes, which are to ensure chip reliability (electrical, thermal, and mechanical), need to be assessed for every new process development. The key concerns are test, failure location detection, modeling, and understanding of failure mechanisms.
4. **Metrology:** To achieve desirable circuit performance and reliability, precise control of interconnect critical dimensions, layer thickness and structures is required by applying associated metrology. Trench depth and profile, line edge roughness (LER), via shape, and the new materials and its multiplicity of levels, feature size reduction, and pattern optimization is challenging for metrology techniques.
5. **Cost & Yield for Manufacturability:** To meet the cost and performance requirements, Manufacturability and defect management is critical to the process development too. Plasma damage, defect tolerant processes, contamination, cleaning of high aspect ratio features, thermal budgets, and cost control have to be concerned.

1.2 Low k dielectric reliability

1.2.1 Low k dielectric reliability [1, 4, 5].

Low k dielectric reliability has been the subject of back-end-of-line (BEOL) reliability research for about a decade. It has gradually gained industrial acceptance and

ATTENTION: The Singapore Copyright Act applies to the use of this document. Nanyang Technological University Library

currently, BEOL time-dependent dielectric breakdown (TDDB) is part of technology qualifications. Although numerous aspects have been investigated, not all details are fully understood. The reduction of dielectric spacing, the introduction of more and more porosity into low k dielectrics and ultimately adopting air gaps in BEOL architectures fuels the need for concentrated efforts in characterizing and understanding low k dielectric reliability aspects of scaled interconnects. Typical characterization methods include wafer and package level TDDB tests, leakage and conduction studies using voltage ramp measurements, finite element modeling for electric field simulation, triangular voltage sweep (TVS) method for detection of ionic species, electron spin resonance (ESR) for defect characterization as well as various failure analysis methods. For understanding some of the active mechanisms simple planar structures are well suited. At the same time, the study of single- and dual-damascene vertical capacitors is important, because the fabricated IMD structures form the same effective vertical parasitic capacitors. However, the damascene process introduces several undesirable effects, such as LER, dielectric thickness variation, dielectric modification, metallic contamination, etc. TDDB performance is typically impacted by the integration methods and all fabrication steps.

Leakage and breakdown properties become important selection criteria for low k dielectrics. Typical industrial low k dielectrics are silica based. The silica based low k dielectrics have the Si-O bonds of their silica matrix replaced by the Si-CH_3 (or Si-H) bonds, which have less polar. To achieve lower k values, higher porosity and carbon doping are necessary. However, with the increased porosity the leakage current density will increase and the breakdown electrical field strength will decrease. It was shown that

ATTENTION: The Singapore Copyright Act applies to the use of this document. Nanyang Technological University Library

besides the intentional carbon doping of the skeleton itself, sp^2 residual carbon is also present in virtually all CVD porogen based low k dielectrics, resulting in the leakage current density increasing by several orders of magnitude while lowering the k value. This leakage current increase will cause early failures. Figure 1.2 showed the relation of the leakage current density versus the electric field for different low k dielectrics. In this experiment, TVS measurement was used on a micro-probing probe station with a hot chuck. A pico-Ampere semiconductor parameter analyzer, HP4140, was used for measurement and voltage sweeping. A constant sweeping rate of 1V/s was applied at a temperature of 100°C. Low k dielectrics with different k values were tested to validate the physical origin of TDDB thermal acceleration results and to characterize the experimental samples qualitatively. The TVS technique is based on the measurement of the displacement current response to a slow linear ramp voltage at elevated temperatures and can be used on either metal-insulator-semiconductor (MIS) or metal-insulator-metal (MIM) capacitor structures, making it suitable for inter-metal dielectric testing. The ramp yields an ionic displacement current peak whose area is proportional to the total mobile ionic space charge. Additionally, the TVS technique may be used for distinguishing between mobile ionic species such as sodium and potassium. Recently, TVS was successfully applied in damascene structures and can distinguish copper ions from moisture content.

ATTENTION: The Singapore Copyright Act applies to the use of this document. Nanyang Technological University Library

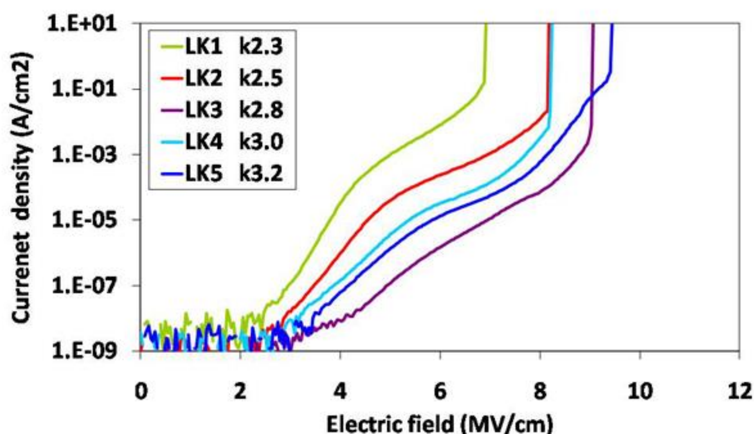

Figure 1.2 The relation of leakage current density versus electric field for different low k dielectrics [5].

1.2.2 Low k reliability analysis method

In the past several years, many studies have been carried out on the electrical field dependence of the TDDB time to failure (TTF). McPerson, etc., [9]. used a three-year TDDB study at low electrical field to get better understanding on TDDB model, E or 1/E. His results strongly suggested that the E-model described much better the failure physics. The proposed E and root-E models are currently being used by most researchers to fit TDDB plots. Theoretical support is mainly the assumed weak bonds broken in the dielectric can be broken, or copper ion drift either into the dielectric or at interfaces. Another possible model is the impact damage model which suggests that at low field, the dependence is dominated by 1/E model. Other than the above models, which work well for BEOL TDDB, pure 1/E-model and power law are widely considered to study the gate oxide TDDB. However, there is no direct measurement at normal operating temperatures reported. Package level TDDB experiments have been conducted on damascene structures. The purpose was to validate existing models and to determine low electrical

ATTENTION: The Singapore Copyright Act applies to the use of this document. Nanyang Technological University Library

field TDDB behavior. High electrical field data was used for the prediction of the median TTF at low electrical fields. Study showed that even the most optimistic E and Square root-E model were unable to fully describe the low field data. Further investigation showed that lifetime models can be used to predict longer lifetimes better than the E and the square root-E models. The experimental data obtained at 100°C are in excellent agreement with earlier proposed theoretical models that describe the dynamics of trap creation physics.

Jingyong [10]. investigated, over a wide range of areas and electric fields test, the TDDB characteristics of low k dielectric carbon doped silicon oxide (SiOC). Figure 1.3 is the TDDB test of an E-test structure with 50nm ½ pitch low k interconnects with a testing time of almost one year.

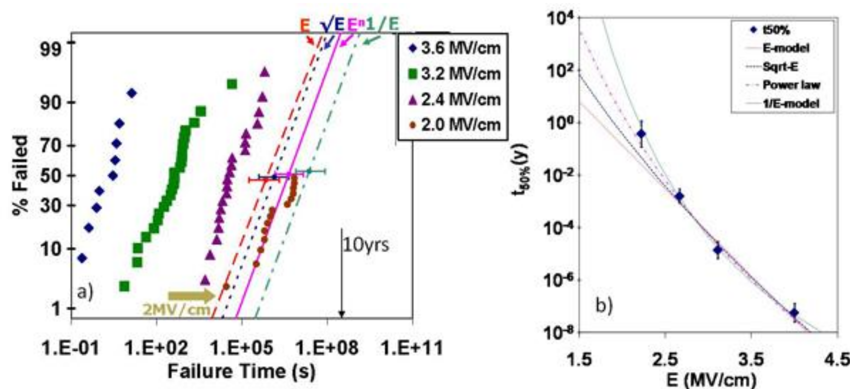

Figure 1.3 The TDDB test of an E-test structure with 50nm ½ pitch low k interconnects after with a testing time of almost one year: (a) breakdown distributions and the fit; (b) acceleration models.

TDDB of low k dielectric was investigated for different materials, failure mechanism and process effects. Stucchi's TDDB lifetime model can be used to predict the impact of LER on Cu interconnect reliability [11]. The accuracy of the model together with the E test structure and validity were studied in details. A interconnect

ATTENTION: The Singapore Copyright Act applies to the use of this document. Nanyang Technological University Library

scaling scenario was fitted with this model by including spacer-defined patterning and other conventional patterning of Cu wires in nanometer scale.

J. Noguchi's publication reported dominant factors causing TDDB failure of low k dielectrics [12]. He studied the electrical field acceleration factor, γ, for the TDDB E model in different E-test structures with low k dielectrics. For p-type SiCN E-test structures is larger than that of p-type SiN E-test structures. The γ is independent of the low k dielectrics and the processes. The relationship of the breakdown electric field strength (EBD) versus the TDDB lifetime demonstrated that experimentally measured EBD and γ can predict the TDDB lifetime. Under 0.2 MV/cm operations, an EBD larger than 4.2 MV/cm is required to assure ten-year reliability. And, the Cu CMP, the post-CMP annealing, the LER, and the fine line effect will influence the TDDB lifetime of low k dielectrics.

Yohei Yamada, etc., studied the factors in TDDB degradation of Cu CMP related Cu/low k integration [13]. In their study, the TDDB reliability was tested on the Cu interconnects with Cu/low k integration. The TDDB lifetime dependence on SiOC damage was caused by CMP processes and sputtering. Without a cap-SiO layer, the TDDB lifetime of the structure was three orders of magnitude shorter than that of the structure with a cap layer. However, when the cap-SiO thin film thickness is thinner than 30 nm, a leakage path was formed in the film which to cause TDDB degradation. The study also confirmed that, when the metal-to-metal spacing approaching 100 nm , TDDB performance degrades. Moreover, it is possible that mechanical destruction and chemical attack during the CMP process could result in TDDB degradation. The line-to-line insulating reliability, such as TDDB and leakage current, can be improved by eliminating

ATTENTION: The Singapore Copyright Act applies to the use of this document. Nanyang Technological University Library

the CMP-surface leakage path through optimizing CMP conditions. These reliabilities are dominated by the extrinsic failure mode.

There are several models for the prediction and the assessment on TDDB lifetime through investigating the Cu ion diffusion-induced leakage and conduction modes. However, the leakage and conduction mechanism are unclear for extreme low k dielectric. It is arguable which model is suitable for TDDB lifetime prediction at low electrical field. More supporting data are needed. In addition, porosity of low k dielectric compromise between sustaining the robustness of low k dielectric process and enhancing circuit performance. Reliability assessment needs more understandings of failure mode and TDDB characterization, such as thermal activation energy and Weibull shape factor for dense and porous low k SiCO dielectric with length scaling.

K. Y. Yiang used a voltage ramp method in SiOC dielectric to investigate electrical conduction in carbon-doped silicon oxide [14]. The electric field was in the range of 0 MV/cm to the breakdown field at 300 K. At the electrical fields below 1.4 MV/cm, the dominant conduction mechanisms are the electron hopping at electrical fields less than 0.2 MV/cm) and the Schottky emission at electrical fields from 0.2 to 1.4 MV/cm. Poole–Frenkel emissions at electrical fields higher than 1.4 MV/cm demonstrates the presence of electron traps in the SiOC conduction. Close to breakdown field from 1.7 to 2.08 MV/cm, Fowler–Nordheim tunneling, which can cause dielectric breakdown in SiOC was observed. In an integrated Cu damascene structure, the effective dielectric constant of the SiOC was calculated from the experimental data and the emission modeling.

ATTENTION: The Singapore Copyright Act applies to the use of this document. Nanyang Technological University Library

J. M. Atkin used the conductance and capacitance probing techniques to study the charge trapping at the low k dielectric-silicon interface [15]. In porous low k dielectric thin films, trap states close to the interfaces affect interfacial barriers with contacts, creating electrical leakage and reliability issues. The investigation was done in metal/insulator/silicon capacitor structures, which composed of carbon-doped oxide low k dielectric films and gold electrodes. The measurements obtained the information on the charge state of the low k dielectrics. The estimated density of traps near the Si interface is $2\times10^{11}\ \mathrm{cm}^{-2}\ \mathrm{eV}^{-1}$, which is considerably greater than that in a typical SiO_2 film. He also studied the effect of annealing temperature.

1.3 Vibrational Spectroscopy of low k and ultra-low k dielectrics

Ultra-low k dielectrics can be fabricated with the spin-on or CVD process. Most of them are polymeric compounds. Their dielectric constants are dependent on both the chemistry of the materials and the porosity in the materials. The hardness and modulus properties are also related to the composition, the cross-linking, the stoichiometry, and cure temperature of the polymer.

Normally, a complementary analytical approach is used to determine the film chemistry. The complementary analytical techniques include hydrogen forward scattering (HFS) and Rutherford backscattering (RBS), time of flight secondary ion mass spectrometry (ToFSIMS) and Auger , Raman spectroscopy and Fourier transform infrared (FTIR).

ATTENTION: The Singapore Copyright Act applies to the use of this document. Nanyang Technological University Library

Raman and FTIR spectroscopy are spectroscopy techniques for complementary vibrational analysis, which can be used to obstain the molecular bonding and structure information of a material. FTIR provides straightforward quantitative analysis of molecular groups as the peak areas follows Beer's Law. Raman spectroscopy measures a scattering process from a material interacted with a laser with wavelength from UV to infrared. The spectrum measures the inelastic scattering.

Thus, both FTIR and Raman spectroscopy can be used to detect the molecular bonding and structure of a material. By coupling a microscope, both FTIR and Raman is workable in microprobing mode. FTIR microanalysis has a spatial resolution of 10 microns, while the Raman microprobe has a spatial resolution of 1 micron.

1.3.1 Raman Spectroscopy [16-19].

Raman spectroscopy is an important analytical and research tool. It has been widely used polymers, thin films, forensic science, pharmaceuticals, semiconductors, carbon nano-materials and fullerene structures.

Raman spectroscopy is to measure light scattering. The light scattering is a process of a photon interacting with a sample and it radiates light emission at different wavelengths.

Raman spectroscopy provides rich information on chemical identification, effects of bonding, stress on a sample, characterization of molecular structures, and environment).

The scattering process was established by Professor C.V Raman in 1928. At that time, NMR, UV-VIS, and FTIR, etc. were commonly used. For a long time, the Raman spectroscopy was not a common university courses. In the middle of 1990s, Raman

ATTENTION: The Singapore Copyright Act applies to the use of this document. Nanyang Technological University Library

spectroscopy became a important analytical techniques with the advancement in the techniques of laser, optics and light detectors.

In the light interaction with the sample, Reflection, absorption and scattering will happen in different manners. One of the light scattering is the Raman scattering, which tells people about the molecular structures of the materials.

In the spectrum of the light scattering, we can see both the Rayleigh scattering, which is at the incident light wavelength, and the Raman scattering. Raman scattering includes Stokes and Anti-Stokes Raman scattering. Only the scattered photon with shifted wavelength provides the chemical and structural information of the materials.

In a molecular system, the scattering frequency range covers the ranges related to vibrational, rotational, and electronic level transitions. The light scattering without a frequency change is called Rayleigh scattering. The same process was described by Lord Rayleigh. The light scattering with frequency changes is called Raman scattering.

1.3.2 Fourier Transform Infrared Spectrometry (FTIR) [16-19].

In order to overcome the limitations of dispersive instruments, FTIR spectrometry was developed. An IR dispersive instrument is a slow scanning process. It is challenging to measure all of the infrared frequencies at the same time and the old IR dispersive system can only perform individual measurement.

In order to resove this issue, FTIR technique was developed. FTIR uses an interferometer. The interferometer is a very simple optical device which can produce a unique type of signal to include all of the infrared frequencies. The interferometer signal can be measured at the order of one second or so. Thus, the measurement time per sample

ATTENTION: The Singapore Copyright Act applies to the use of this document. Nanyang Technological University Library

is reduced to a few seconds rather than several minutes. Most interferometers use a beamsplitter to take the incoming infrared beam and, then, to divide the beam into two optical beams. A flat mirror fixed in place reflects one of the two optical beams. Another flat mirror fixed on a movable mechanics reflects another beam reflects off. Reflecting off their respective mirrors, the two optical beams are recombined and meet at a beamsplitter. One optical beam travels at a fixed length and the other constantly changes its travel length with the moving mirror. The two optical beams interfere with each other after exiting the interferometer. The interfered optical beams are called an interferogram. The measured interferogram signal is not a frequency spectrum, which was required by analyst. To plot the intensity at each individual frequency, the Fourier transformation can decode the individual frequencies.

1.3.3 Vibrational spectroscopy on low k dielectrics

In the past 10 years, many research activities focused on low k materials because of the potential application in the semiconductor industry. These materials can effectively reduce the parasitic capacitance of ILD [1]. They are very promising candidates as ILD and ILD in the leading edge ultra-large-scale integrated (ULSIs) IC devices. Among these the low k dielectrics, SiOC dielectric materials attracted people much interest as they have good mechanical strength and thermal stability [20].

Fluorine-incorporated silicon oxide (SiOF) and SiOC films can be prepared by plasma enhanced chemical vapor deposition. Their bonding characteristics were investigated by FTIR. With the increase of fluorine incorporation, the frequency of Si–O stretching vibration mode in SiOF films shifted to higher wave number, blueshift. With the carbon content increased, the Si-O stretching vibration mode in SiOC films shifted to

ATTENTION: The Singapore Copyright Act applies to the use of this document. Nanyang Technological University Library

lower wave number, redshift, the Si–O stretching frequency in SiOC films annealed in N_2 environment slightly shifted to lower wave number. These phenomena observed in SiOF and SiOC films can be explained by the "bonding structure model", which is based on the electronegativity of an atom.

To incorporate doping elements such as hydrogen and carbon is crucial to lowering the value of SiO_2 dielectric constant. These elements are able to modify the local structures of the silicon oxide network and create a lower density material. To replace Si–O bonds with Si–CH 3 bonds will cause bulk porosity as nano-sized voids form in in the silicon oxide matrix [21]. In the study, the low k dielectric film of Carbon-doped silicon oxide (SiOC) was deposited on a p-type Si(100) substrate by inductively coupled plasma chemical vapor deposition (ICPCVD) with a mixture of oxygen and bis-trimethylsilylmethane (BTMSM) . At a low pressure less than 300 mTorr and a radio RF frequency with the power of approximately 300 W, Electron density of $\sim 10^{12}$ cm^{-3} with electron temperature of 1.6 eV were obtained. From the investigation of the bonding configurations, atomic concentrations, and porosity with FTIR spectroscopy and X-ray photoelectron spectroscopy (XPS), the increase of carbon content in films and decrease of the film density was observed after the films were annealed at 400 °C in vacuum. In the bonding structure of SiOC composite films, the Si-O-Si and Si-O-C bonds were separately identified. Enhanced porosity with caged SiO bonds exists in the film, which is deduced from the results. The pore density and relative carbon content determine the dielectric constant of the SiOC composite film . The calculated porosity is 68% and the dielectric constant is approximately 2.1.

ATTENTION: The Singapore Copyright Act applies to the use of this document. Nanyang Technological University Library

the study on the micro-structural of the SiOC:H system is critical to optimize the synthesis of low k thin films. From the fundamental point of view, people knew about the structural evolution of SiOC:H films annealed at temperature up to 450 ^{o}C, but the effects of those doping elements on the film microstructure with higher annealing temperature is unsure.

Brusa et al. [22]. reported the chemical and structural changes observed by nuclear reaction analyses and positron annihilation spectroscopy on SiOC:H samples. The films were deposited at 120 ^{o}C with a PECVD technique. A mixture of trimethyl-silane and ozone gas was use for PECVD. The films, then, annealed at fixed temperatures up to 900 ^{o}C. Their results suggested that, in order to get a SiOC:H films with substantial stabile structure and composition, the annealing temperature must be at least up to 600 ^{o}C. Those films have small size pores uniformly distributed within the films. With an important structural rearrangement of the amorphous matrix, hydrogen was progressive released in samples annealed at higher temperatures,. Annealed at 800 and 900 ^{o}C, the hydrogen content in the samples remained is about 1/3 of that in the preliminarily treated sample. The micro-structures were investigated with FT-IR and Raman spectroscopy [23]. To characterize the films with vibrational spectroscopy techniques is to understand more about its structural evolution at higher annealing temperatures and to study the thermal stability of SiOC:H system up to 600 ^{o}C . FT-IR absorption spectra can study the chemical arrangement in SiOC:H film and the breaking of hydrogen terminated bonds under the effects of thermal annealing. The FTIR analysis showed that the hydrogen in SiOC:H films released together with a structural rearrangement of the unsaturated carbon bonds. More detailed understanding on the film microstructure was reached with the

ATTENTION: The Singapore Copyright Act applies to the use of this document. Nanyang Technological University Library

study of its Raman scattering spectra. After thermal annealing at temperatures of 500 ^{o}C, the carbon domains within the amorphous matrix form. Pre-treated samples do not show any appreciable scattering related to the SiOC:H layer in its Raman spectra, but those Raman spectra from the samples annealed at 500 ^{o}C have clear signal of typical of sp2-hybridised carbon and exhibit both G and D bands.

The k value of organic polyphenylene polymers is about 2.1-2.6. Their specific chemistry and porosity make the difference in k value. The precursor materials contain a cross-linking agent of cyclopentadienone, aromatic acetylene which contains three or more acetylene moieties and optional polyfunctional compound which contains two aromatic acetylene moieties [24]. The precursor solution was spun onto the wafer. After soft baking, the material finally cured and a cross-linked polyphenylene product formed. The intermediate Diels-Alder cycloaddition reactions repeatedly consumed acetylene branches of the polyfunctional acetylene monomers. Raman spectroscopy is a very sensitive to the acetylene functional group. Raman spectroscope can be used to monitor the decrease of the acetylene groups which is at 2200 cm^{-1} and the aromatic ring stretching bands which is at 1600 cm^{-1}. However, the FTIR spectrum cannot detect the acetylene chemistry due to the selection rules of symmetry considerations which forbid the vibrational transition in this group. Spectroscopic ellipsometry measurements on inline refractive index match well in the with the peak intensity ratio of the Raman peaks at 2200 cm^{-1} to 1600 cm^{-1}.

The silsesquioxanes' generic formula is $(RSiO_{1.5})_n$. One hydrocarbon group (ane) and an average of one and a half (sesqui) oxygens is bound to each silicon atom. They can exist as polymers in the form of polycyclic oligomers. MSQ (methyl silsesquioxane,

ATTENTION: The Singapore Copyright Act applies to the use of this document. Nanyang Technological University Library

R=CH_3) and HSQ (hydrogen silsesquioxane, R=H) are typically ultra-low k dielectrics made from these materials. The silsesquioxane-based ULK materials fabricated with spin-on and CVD have the same general chemistry [25, 26]. Si-CH_3 groups and Si-O-Si linkages exist in Methyl silsesquioxanes. The detailed information of the molecular bonding in the film can be detected with FTIR spectroscopy. The stretching of the CH_3 functional groups is at around 2980 cm^{-1} and 2850 cm^{-1}, while its bending features is at around 1410 cm^{-1}. The $Si(CH_3)_x$ functionality is different from the Si-C stretching region, which is at around 880-750 cm^{-1}, and the bending region, which is at about 1275-1250 cm^{-1} [27]. The carbon content affects k values in dense silsesquioxane-based ULK materials, so lower dielectric constants is correlated to the increased methyl and Si-C functionality .

The Si-O-Si bonding with both ladder type and polycyclic structures exits in HSQ and MSQ films as a complex chemistry. In some cases, they also form as linear chains. The mechanical properties of hardness and modulus were affected by the relative amounts of network type bonding with cross-linked ladder and linear chain structures and cage type bonding of polyhedral. A higher modulus film has higher network type bonding. In the FTIR spectra, the peaks of the network structure and Si-O-Si cage fall in the 1200-1000 cm^{-1} region. They consist of overlapping bands from the distribution of bond angles and local bond types in the microstructure. Curve-fitting can help to have better understanding on this structure. In thermal oxide, the Si-O-Si bond angle of the tetrahedral SiO_2 is 144 degrees, and the peak position of Si-O asymmetric stretch is at 1080 cm^{-1}. The Si-O-Si bond angles of cage-like structures is at 150 degrees or greater,

ATTENTION: The Singapore Copyright Act applies to the use of this document. Nanyang Technological University Library

and the peak position of Si-O-Si shifts to higher frequency which is about1180 cm^{-1}. The bond angle of the network-like structures is less than 144 degrees and the peak position of Si-O shifts downward in energy of about 1030 cm^{-1}n [28, 29]. The frequency shift of SiO at x=1 is about 940 cm^{-1} [30].

The information of Plasma-damaged films can also be obtained from FTIR analysis. The Si-CH_3 groups oxidized by plasma form Si-OH groups. Both hydrogen-bonded and isolated silanol groups are can be observed. to the -OH stretching bands is at around 3750 cm^{-1} of isolated -OH and broad bands are in the region of 3500 cm^{-1} of hydrogen-bonded -OH. The Si-OH bending band at around 935 cm^{-1} is observed. Carbon depletion caused by plasma damage was detected as demethylation, which leads to intensity losses in the $Si(CH_3)_x$ and CH_3vibrations. FTIR spectroscopy can be used to monitor the repair of the damaged region in which was methyl functionality was restored through chemical treatments. The amount of bulk repair to the film chemistry can be assessed also. During the repair, the -OH bonds react with methyl and $Si(CH_3)x$ bonds reformation [31].

Introducing porosity into the structure into the ULK dielectric materials can further reduce the k value. In ULK materials deposited with CVD, an additional precursor component, a porogen, flows into the plasma mixture. A post deposition burnout process removes the porogen through a thermal treatment, Electron beam or photon exposure.

Sensitive outgassing analysis techniques, like thermal desorption mass spectrometry, can be used to determine the residual porogen. The bulk film chemistry changes can be determined with vibrational spectroscopy, while the compositional

ATTENTION: The Singapore Copyright Act applies to the use of this document. Nanyang Technological University Library

changes in the film after porogen burnout can be characterized with depth profiling techniques like ToFSIMS and Auger spectroscopy.

1.4 Summary and Conclusions

In summary, with device feature size scaling, especially into nano meter scale, Cu is used to replace Al as metal interconnects and low k dielectric was used to replace SiO_2 as ILD. Cu has a resistivity 36% lower than Al. The dielectric constant of SiO_2 is 3.9, while low k dielectrics have dielectric constant between 2 to 3. By introducing pores into low k dielectrics to form, ultra-low k dielectrics, the dielectric constant can be reduced to a value less than 2.

However, the material strength of low k and ultra-low k dielectrics is weakened in the process and Cu drift leading to LER is a severe issue for Cu/low k interconnects. From fabrication point of view, this is one of the sources for leakage and breakdown properties. Hence, leakage and breakdown properties became important selection criteria for low k dielectrics.

TDDB is a commonly used low k dielectric reliability test methodology. Most TDDB studies focus on a wide range of area and electrical fields to investigate the mechanism of TDDB failures. In recent years, the simulation and modeling are widely investigated.

Low k dielectric can be characterized with a complementary analytical technique, like RBS and HFS, Auger or ToFSIMS, and FTIR and Raman spectroscopy. Other characterization techniques include Nuclear magnetic resonance (NMR), High resolution TEM (HRTEM), Surface acoustical wave spectroscopy (SAWS), Ellipsometric porosimetry (EP), specular X-ray, and Brillouin light scattering (BLS).

ATTENTION: The Singapore Copyright Act applies to the use of this document. Nanyang Technological University Library

Among these characterization techniques, FTIR and Raman spectroscopy are favorable because of their abilities to provide valuable information on chemical bonding at low cost.

The complementary vibrational spectroscopy of FTIR and Raman spectroscopy techniques can be used to analysis the molecular structures and bondings in low k dielectrics. Raman spectrum is sensitive to inelastic scattering of the incident laser versus molecular vibrational energy. FTIR spectra can detect the absorption of infrared radiation by polychromatic at specific vibration energies of molecular groups. As the selection rules are different for Raman and FTIR techniques, they are sensitive to different molecular geometries and bonding.

However, in TDDB analysis, the mechanism is still arguable and damage on low k dielectric under TDDB test is uncertain. FTIR and Raman spectroscopy is believed to be the most promising techniques to analyze the change in chemical bonding dynamically during the TDDB test. Current FTIR and Raman techniques are widely used on thin film or bulk materials and no research on patterned wafers are reported. Another challenge resides in obtaining TDDB samples for FITR and Raman spectroscopy analysis because electrical overstress usually happens soon during dielectric breakdown.

In this project, Raman and FTIR were used as a complementary vibrational spectroscopy to investigate the change of the chemical bonding due to the TDDB test. This will lead to the in-depth understanding on the failure mechanism. In our investigation, one of the most advanced Raman systems with self-designed sample holding fixture was used to maximize the Raman signal collection. This enables us to be able to detect the weak Raman signal on the pattern wafer. This work was not published

ATTENTION: The Singapore Copyright Act applies to the use of this document. Nanyang Technological University Library

by other researchers. With the capability of detection of Raman spectroscopy on the patterned wafers, TDDB study with Raman and FTIR complementary vibrational spectroscopy becomes possible. This research demonstrated the first finding on Raman and FTIR on TDDB failing samples and it changes the conventional analytical methodology in semiconductor industrial on the TDDB failure, which mainly relies on physical analysis with cross section and delayering methodology with SEM and TEM after electrical measurements. This failure mechanism fits well to the TDDB “square E” model.

ATTENTION: The Singapore Copyright Act applies to the use of this document. Nanyang Technological University Library

Chapter 2 Experimental Setup

2.1 Introduction

As the leakage and breakdown properties become one of the important selection criteria for low k dielectric materials, effective methodologies and techniques are needed to understand the mechanism of low k reliability issues. The weak material strength and metal ion diffusions, we believe, have strong correlation to the intrinsic chemical bonding and its properties under electrical field. To obtain in-depth understanding of the change of the chemical bonding of low k and ultra-low k dielectrics, we propose to use the complementary vibrational spectroscopy with Raman and FTIR to investigate the reliability failure mechanism of the low k and ultra-low k dielectrics.

The TDDB test structures are fabricated with standard leading edge CMOS process. SiCOH is the choice for low k dielectric. In order to get significant Raman and FTIR signal, the system should have high sensitivity as the TDDB structures were patterned with spacing in the nanometer scale. When laser interacts with nanometer scale structures, the structures will induce light scattering and diffraction depending on the size and locations of the structure structures. Cu interconnects, will generate luminescence during Raman excitation and signal collection. In this project, the following technical challenges on TDDB analysis are investigated. Horiba T64000, a research Raman spectroscopy system is used. With a triple grating spectrometer system, tunable laser filtering and unique stray light rejection, Horiba T64000 has ultra-high spectral resolution. In this project, the following investigations were carried out on T64000.

1. Raman spectrum from TDDB structures at nanometer scales.

ATTENTION: The Singapore Copyright Act applies to the use of this document. Nanyang Technological University Library

2. Effect from different excitation laser wavelengths.
3. Reduction of luminescence signal from Cu.
4. Enhancement of FTIR spectrum from the TDDB structures.
5. Raman spectroscopy and FTIR of TDDB physical damage from electrical stress.

2.2 Fabrication of Cu/Ultra-low k dielectrics

The process flow of an IC can be classified into two categories: front end of line (FEOL) and back end of line (BEOL). FEOL consists of transistors and contact interface to BEOL. BEOL includes interconnecting metals to form an IC. BEOL also includes inter-metal-dielectric (IMD). In leading edge technologies, Cu and low k dielectric are introduced into IMD to reduce the RC delay. The resistance and capacitance arise from metal lines and IMD, respectively. In order to maintain strong mechanical strength at BEOL, upper IMD layers are formed with SiO_2 and wider metal lines. Figure 2.1 shows a cross section view of a device fabricated with a standard low k/Cu process. The Cu/low k layers of the BEOL was fabricated with single damascene at low k M1 layer and dual damascene process at low k M2 layer and above. In the damascene process, patterning was carried out before barrier layer and metal layer fabrication. After patterning the insulator layers for via and metal, a barrier layer of Ta/TaN layer with the thickness of several tens nanometers was deposited with physical deposition. The barrier layer can prevent the diffusion of Cu into the insulator material (IMD and ILD). On the barrier layer was deposited, a think seed layer of Cu was deposited with physical deposition. A

ATTENTION: The Singapore Copyright Act applies to the use of this document. Nanyang Technological University Library

thick Cu layer was deposited on the seed layer with electroplating. After the CMP, all the access Cu on the top the IMD was removed to form the patterned Cu interconnects.

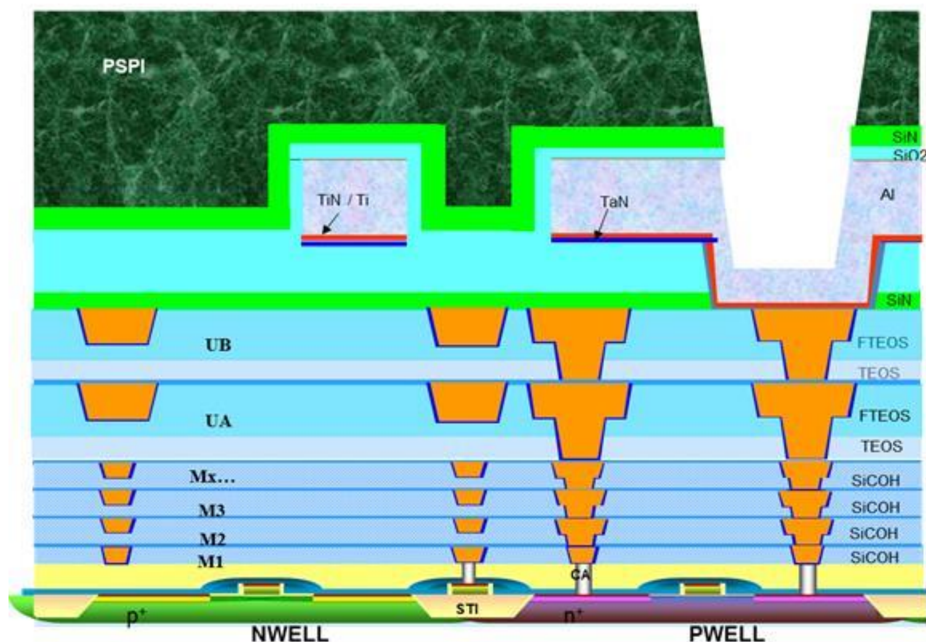

Figure 2.1 a cross section view of a device fabricated with a standard Cu/low k process.

From a historic point of view, semiconductor industrial is always looking for new low k and ultra-low k materials. Fundamental research and technology in has strong connection to develop new materials. A large variety of potential materials are widely investigated with detailed study. Many research reports were published in the past decade, the selection of the most promising materials for a given technology node was decided from the integration point of view. Table 1.2 shows the low k dielectric candidates for IC application.

Organic polymers are good candidates of low k and ultra-low k dielectrics. However, the properties of organic polymers, such as, thermal properties, mechanical strength and interface mismatch, is incompatible to have compatible electrical and

ATTENTION: The Singapore Copyright Act applies to the use of this document. Nanyang Technological University Library

mechanical properties to those of SiO_2, which is well established as the insulating material of reference.

To integrate the low k materials in the BEOL process, the silicon network was chemically modification by introduction of fluorine and, later, the addition of carbon. To modify the silicon network is a low risk solution, so Silicates and organosilicates become the dominant candidates. Both spin-on and CVD processes can be used to deposit the films. However, the final thin-film properties depend on the film chemical structure, which is a result of both the deposition process and the precursor or resin chemistry. Since 1997, plasma-enhanced CVD (PECVD) was chosen for the deposition of silicon dioxide (SiO_2), SiCOHF- SiO_2, and porous SiCOH. SiCOH thin films deposited by PECVD were successfully implemented in the 90 nm (k = 3.0) and 65 nm (k = 2.7) technology nodes for IBM microprocessors. The k value is 3.0 for 90nm nodes and 2.7 for 65 nm nodes. In 1997, IBM ramped up the first high volume manufacturing in 2008 with PECVD deposited porous p-SiCOH, with which the IBM make real technology node/dielectric constant relationship with significant difference to the NTRS proposed targets . This shows that predicting dielectric targets cannot be solely based on engineering designs with a new material which is not fully developed. The challenge to design dielectric insulators is to meet all the BEOL requirements in terms of electrical, thermal and mechanical properties. For the leading edge technologies, in order to get the k value of 2.4 and beyond, it is necessary to add porosity at higher levels, which created integration issues with the damage and the decrease in material mechanical properties. Serious concerns for the reliability were raised for these advanced structures.

2.3 Process integration of Low k/Cu interconnects

ATTENTION: The Singapore Copyright Act applies to the use of this document. Nanyang Technological University Library

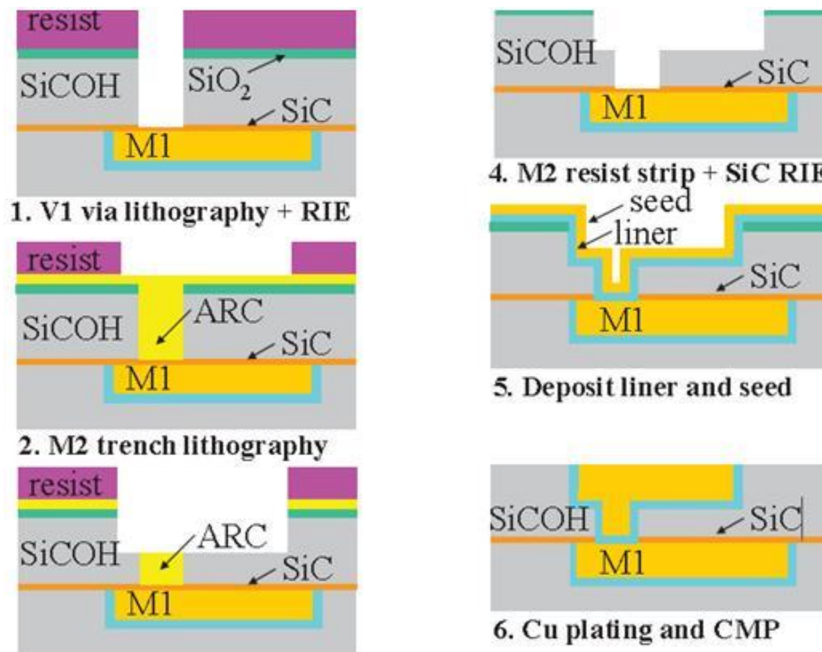

Figure 2.2 Schematic diagram of a Cu/low k dual damascence process

In our process, single damascence was applied to metal layer 1 and dual damascence was applied to metal layer 2 and above for low k/Cu interconnects. The schematic of the process flow was illustrated in Figure 2.2.

In the single damascence process of the metal layer 1, the metal trench is patterned and formed by plasma etch. A barrier metal is deposited to prevent Cu diffusion into the low k or porous low k dielectrics. After seed layer deposition with physical deposition, Cu is deposited onto the seed layer with electroplating. CMP removes the excess Cu, seed layer, and barrier metal, terminating after the hard mask is fully removed.

In the dual damascence process, additional via patterning is carried out before trench patterning. Cu electroplating fills both via and trench at the same time. The rest of process steps for single damascence are the same as described above.

A TEM cross-section view was shown in Figure 2.3.

ATTENTION: The Singapore Copyright Act applies to the use of this document. Nanyang Technological University Library

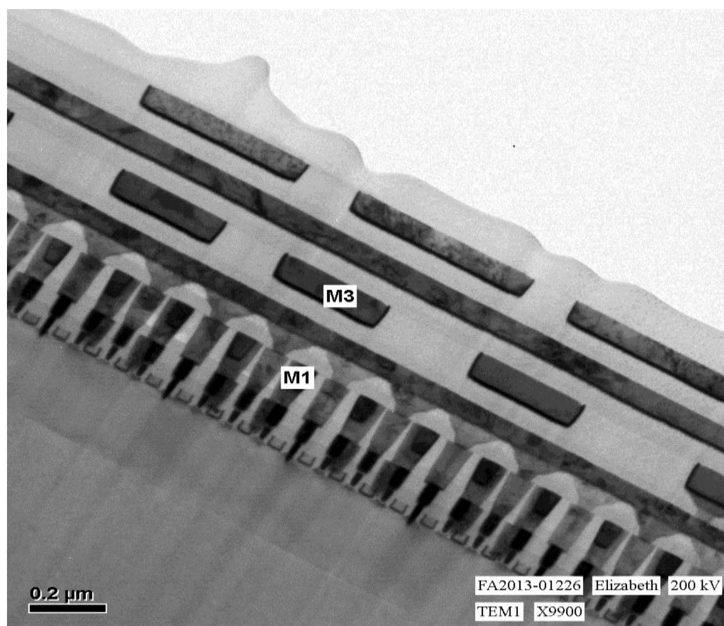

Figure 2.3 XTEM image on a 20 nm IC device

2.4 Process tools and their configurations

The process flow integrated lithography, thin film deposition, etching, Cu plating, and CMP, etc. Each key process will be described in greater detail.

a. PECVD

PECVD was used for the thin film deposition of low k dielectrics, linear or cap layers after Cu CMP and annealing. In the device fabrication, we used Applied Producer, enhanced High Aspect Ratio Process (eHARP). It is a non-plasma based CVD oxide film. The eHARP can meet the stringent gap fill requirements, such as for shallow trench isolation (STI) processes in the leading edge technologies In the eHARP deposition process, water vapor was introduce into the TEOS/ozone chemistry. Comparing to the first-generation HARP, the film quality and capability were improved with tightly packed

ATTENTION: The Singapore Copyright Act applies to the use of this document. Nanyang Technological University Library

and denser film deposition. It enables void-free and seamless gap fill in features with aspect ratios greater than 12:1. eHARP is proven for 32 nm logic gap fill and applications in 4X nm devices. Complex 3D island features can be used for to design vertical profiles. 4X nm flash meomory devices used eHARP as the first CVD solution for STI fill. The TEOS/ozone based processes of eHARP can also deposit strain inducing films which can enhance the transistor performance. In a logic device, a strain inducing film can significantly increase transistor drive current, and, in a memory device, it can minimize the integration complexity or cost. The Producer platform of the Applied eHARP has three Twin Chambers with the capability of high-throughput to process up to six wafers at the same time. It was proved in production.

b. Etching

Etching tools are used for both via and metal trench patterning. The dielectric etch product family of Lam 2300 Flex continuously evolutes the etching productivity and performance with densified fluid cleaning (DFC) technology. The product of Exelan Flex45 and beyond, a multi-frequency confined design was applied to DFC technology. It provides additional process tuning capability. These advanced system design is to meet the more demanding requirements on uniformity and profile for the applications of the 50 nm technology node and beyond for memory device and the 45 nm technology node and beyond for logic device. By With a broad process window, a single chamber design in the Flex family can be used in a wide range of applications for multiple technology generations. In the BEOL applications, they can be used for the etch process of dual damascene of oxide, low k, and porous-low k, and they also have the capability of etch-stop-layer removal and in situ photoresist strip. In critical FEOL applications, they can be

ATTENTION: The Singapore Copyright Act applies to the use of this document. Nanyang Technological University Library

used to etch high aspect ratio contact, capacitor cell, self-aligned contact, and borderless contact. Besides, the systems are also be used to etch mask-open and amorphous carbon hardmasks.

c. Cu Electroplating

Electroplating is applied for Cu deposition on the seed layers. SABRE® Excel is one of the latest models of the SABRE platform. The SABRE was designed for manufacturing copper damascene interconnects. For the 22 nm technology node and beyond, it enhanced its capability and performance in superior fill and defect density. With the company's patented IRISCell™ technology, a new deposition module was used to control the current modulation at the initial stages of the plating process to achieve consistent feature fill. Additionally, Multiwave™ wafer bath entry of SABRE Excel improves the plating results on the thin PVD seeds.

d. CMP

CMP is applied to remove the excess Cu, seed layers, and the barrier metal in the non-metal region. In our process, an Applied Reflexion LK CMP was used. The Applied Reflexion LK CMP was a proven product with good planarization solutions. I can be applied for CMP applications on shallow trench isolation (STI), polysilicon, copper damascene, oxide, and tungsten. It has high-speed planarizing platens and multi-zone polishing heads to ensure superior uniformity and efficiency.

The Applied Reflexion LK CMP was integrated with a post-CMP Desica cleaner. The cleaner uses the vapor drying technology of full-immersion Marangoni and it can greatly reduce particle contamination and eliminate watermark defects. The CMP wafer after cleaning has only 0.3 acres remaining contaminants.

ATTENTION: The Singapore Copyright Act applies to the use of this document. Nanyang Technological University Library

A full suite of endpoint methods, such as in-line metrology and advanced process control capabilities, were equipped into the Applied LK Reflexion CMP system. Those endpoint methods provide good control and repeatability within the wafer and from wafer to wafer.

2.5 TDDB test setup

Our TDDB test setup on MPS150 cascade probe station is shown in Figure 2.4. A semiconductor parameter analyzer, Keithly 4200-SCS, is used to stress the device. Leakage and voltage applied are measured. It follows the latest industrial standard on TDDB test.

MPS150 is a very cost-effective and easy to use solution for TDDB test. It can support microprobing on a substrate or wafer up to 8” It can be used for a wide variety of applications such as I-V, C-V, RF, sub-THz measurements, mm-Wave, failure analysis (FA), device characterization, MEMS, submicron probing, optoelectronic engineering tests, and etc. The platen can support up to sixteen positioners.

Figure 2.4 Cascade Probe Station MPS150.

ATTENTION: The Singapore Copyright Act applies to the use of this document. Nanyang Technological University Library

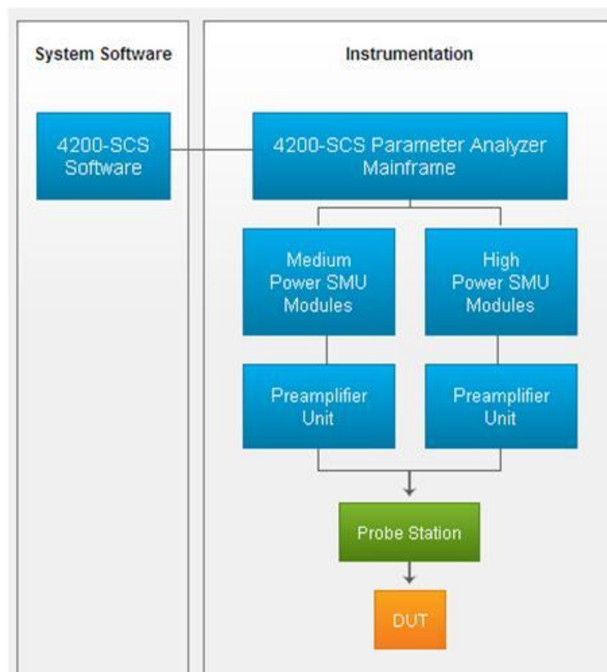

Figure 2.5 Keithly 4200-SCS semiconductor parameter analyzer

A modular and fully integrated parameter analyzer, Keithly 4200-SCS, was used for TDDB test and measurements. Keithly 4200-SCS performs electrical characterization and measurement of semiconductor devices, materials, and processes. It can be applied to basic I-V and C-V measurement, including advanced ultra-fast pulsed I-V, transient I-V measurements, and waveform capture. DC I-V measurements are the most critical to device and material characterization. The Source Measure Units (SMU) of the 4200-SCS are very precise and accurate to source current or voltage and, at the same time, to measure current and voltage. The 4200-SCS can also be applied for the measurements of sub-ρA leakage measurements and μΩ resistance.

2.6 Raman Spectroscopy System

ATTENTION: The Singapore Copyright Act applies to the use of this document. Nanyang Technological University Library

In recent years there, the application of Raman spectroscopy increased greatly in research and industry. For easy to use, small bench-top spectrometer systems have been introduced and certainly raised great interest to researchers in the fields of study with even more demanding applications.

Hence, the bench-top systems was implemented a variety of cutting edge technology to meet the requirements of the advanced Research and that of higher performance required for more challenging analysis on the special samples.

In our study, a T64000 Raman system from Horiba was used. The T64000 system integrated with a triple spectrometer design to achieve better optical stability. Its confocal LabRAM Raman microprobe provides rigid and stable mechanical coupling. It has efficient optical coupling is and fast throughput.

Holographic notch filter technology can achieve very good solution to laser rejection in the region of visible light, which is being used for in many applications. However, it has limitations to the use of the Holographic notch filter when the interested Raman peaks are closed to the laser line. Even the special low frequency accessories are still impossible to get reliable data at 30 cm^{-1} or below.

In order to resolve the issue of the holographic notch filter, the T64000 was implemented with double subtractive configuration enable it possible to detect spectrum very close to the laser line. The subtractive mode was successfully applied to study the detail of crystal lattice modes and longitudinal acoustic (LA) modes in polymer systems.

ATTENTION: The Singapore Copyright Act applies to the use of this document. Nanyang Technological University Library

The study on the Spectrum of a SiGe material showed that it is possible to observe spectral bands at the wavernumbers as low as 4 cm^{-1}.

Another important advanced of T64000 Raman microscope is to use a ultra-high resolution triple additive configuration. The triple additive solution makes it possible to achieve very accurate study on the Raman band positions. The triple additive configuration was successfully used to measure the stress in semiconductor materials, like SiC, GaN, and diamond. The stress induced shifts are in the order of 0.1 cm^{-1}. The high resolution improves the level of accuracy, which was required for the certification and authentication of materials for Raman analysis.

The system also has a final mode of operation with the direct spectrograph entrance. This operation mode can be used as a more conventional single spectrometer based system with holographic notch filter technology. Thus Raman mapping can be achieved by the high throughput spectrum detection. Raman spectral imaging (or mapping) is a method for generating detailed chemical images based on a sample's Raman spectrum. A complete spectrum is acquired at each and every pixel of the image, and then interrogated to generate false colour images based on material composition and structure: (1) Raman peak intensity yields images of material concentration and distribution; (2) Raman peak position yields images of molecular structure and phase, and material stress/strain; (3) Raman peak width yields images of crystallinity and phase. A typical experiment uses sequential sample movement and spectrum acquisition, repeated hundreds, thousands or even millions of times, to collect data from the user defined image area. Raman spectral images can be collected in two and three dimensions, to yield

ATTENTION: The Singapore Copyright Act applies to the use of this document. Nanyang Technological University Library

XY images, XZ and YZ slices, and XYZ datacubes. Raman spectral imaging is an invaluable technique for scientists in many varied fields, since it allows chemical distribution to be viewed which is invisible by standard optical microscopy.In Figure 2.6, Strain enhanced Si peak density yield was mapped cross the sample. From the mapping image, we can see the area with high strain in the Si.

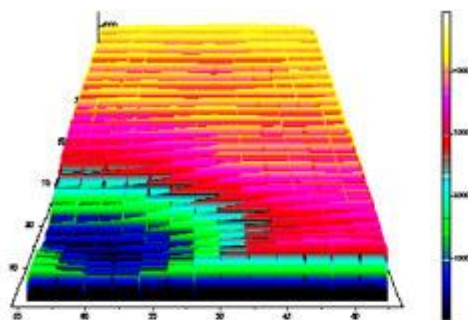

Figure 2.6 A Raman mapped image of a stressed Silicon interface by T64000.

The T64000 can also be applied for the measurement in deep UV region Its high stray light rejection can detect the Raman bands below 100cm^{-1} at the deep UV wavelength of 244 nm. With the tune-ability of the double filter stage, T664000 can be used for various deep UV frequencies, e,g., from 227 to 290 nm.T64000 was widely used in the field of thin films, solid state materials and devices, and biological chemistry. T64000 provides the techniques of UV, PL resonance Raman, and laser fluorescence.

ATTENTION: The Singapore Copyright Act applies to the use of this document. Nanyang Technological University Library

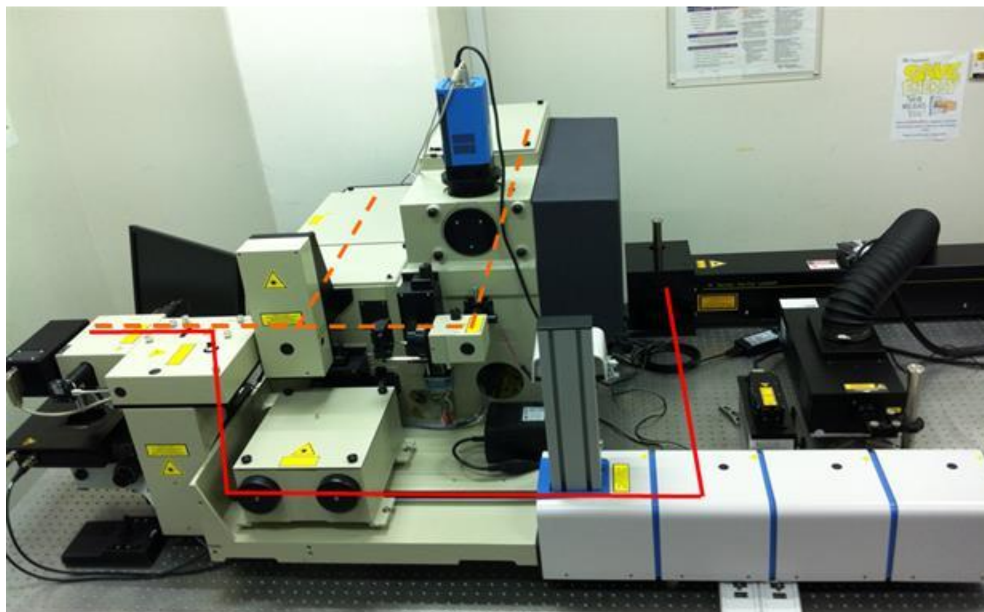

Figure 2.7 The T64000 Raman spectroscopy system

While there are many studies on low k dielectric characterization, these works are less commonly performed on real patterned wafers and IC devices. Due to the small thickness of the low k IMD layer and complicated mixed structures and materials in the IC device, the vibrational spectroscopy detection needs a detailed analysis to extract low k dielectric signals from the mixed structures in spectroscopy. In our previous studies, Raman and FTIR vibrational microscopy was has successfully been used to characterize the low k dielectric property as well as the Cu/low k degradation behavior, which is helpful for us to clearly understand the low k related reliability failure mechanism.

During the Raman experiment, an incident laser beam is shone onto the low k IMD layer and the reflected beam is then collected with its spectrum analyzed. A long spectrum acquisition time would require the incident beam to be continuously focused onto the low k material for a long period of time, resulting in undesirable laser-induced degradation during the characterization process. In this invention, a setup is designed to

ATTENTION: The Singapore Copyright Act applies to the use of this document. Nanyang Technological University Library

increase the signal detection efficiency, which could in turn shorten the spectrum acquisition time and reduce the laser-induced degradation on the device under test (DUT). However, the small number of atoms present in the lower dimensional systems turns out to be the main measurement obstacle. To address the challenge, the electromagnetic field enhancement mechanism is proposed for increasing Raman scattering on nanometer scaled Cu/low k integration.

One prominent method is surface enhanced Raman scattering (SERS). SERS employs rough metallic surfaces (silver, gold, copper, etc.) formed by different nanostructures (nanoparticle dimmers, nanoparticles aggregates, regular arrays of nanospheriods, aligned nanowire bundles, scratched metal surface, etc.) to achieve the highest Raman enhancement on the analytes absorbed on SERS-active substrates [8-10]. The mechanism behind the enhancement is mostly explained by surface plasmon (SP) excitation induced by rough metallic surfaces. The concentrated electric field from SP resonances is responsible for the enhanced Raman signals. Since the SERS is a SP-mediated phenomenon, the magnitude of the effect is strongly dependent on the excitation conditions and the morphology of the metal surface. For isolated nanoparticle aggregates or small arrays, the stronger polarized SERS signals appear along the long axis of the nanoparticles. While for the aligned of high-aspect-ratio nanowires or nanorods, the maximum SERS intensity observed is in the polarization direction perpendicular to the long axis of the wires/rods. This means that each of these substrates presents its own specific advantages and disadvantages in terms of reproductivity, sensitivity and detection limit. However, many of these nanostructures are expensive and

ATTENTION: The Singapore Copyright Act applies to the use of this document. Nanyang Technological University Library

fail to produce reproducible substrates so that the SERS effect will vary dramatically across the sample.

The other effective method is tip-enhanced Raman scattering (TERS) where Raman spectroscopy is combined with a scanning near-field optical microscope (SNOM). In a SNOM setup, light is focused on a metallic tip of a scanning tunneling or of an atomic force microscope, and the localized strong fields underneath the tip is used for probing the sample to understand its surface properties [11]. Actually, TERS is originated from SERS. If an individual silver nanoparticle can induce surface plasmons, it is natural that a silver tip with a sufficiently small apex may have the same effects. In addition to surface plasmons, lightning rod effect also contributes to the field enhancement due to geometry singularity of the tip apex [12]. In our previous studies, it has been demonstrated that the metallic tip is an effective nanostructure and can be used to trigger a very strong local-field around its tip apex [13, 14]. However, the highly-localized strongly-enhanced electric field is evanescent, degrading rapidly along the light propagation direction and only exists in a nanometer range. It needs a precise distance control for the field enhancement by the utilization of scanning probe microscope.

In nano IC devices, the nanometer scaled Cu metallization can be directly used as SERS-active substrate for the field enhancement. It is expected to tune the activity behavior of the anisotropic Cu nanostructure to increase the low k Raman signals in Cu/low k interconnect. However, the light scattering from a nano structure has polarity and the adjustment of the light incident angle is needed to achieve the strongest scattering signal.

ATTENTION: The Singapore Copyright Act applies to the use of this document. Nanyang Technological University Library

In this setup, a 3-D rotational stage was integrated on the microscope of Raman system. An overview of the 3-D rotational stage is shown in Fig. 2.8. It indicates that the rotational stage was fixed on the stand of microscope and can be moved in the vertical direction by adjusting the focusing knob of microscope. The tilt platform was made of stainless steel. The detailed components of the tilt platform are shown in Fig. 2.9. The tilt platform consists of three main parts, namely 1) tilted body, 2) movement sheet and 3) mounting sheet. The tilted body has a rotational rod covered by a colophony coating. This rod can rotate along its long axis by rotating the knob (a) at the one end of the rod. At the other end of the rod, it is connected with a sample holder (b). The rotation range of the rod is 0~90o, and the resolution is 1o where the rotation can be controlled by a protractor. The rod will be fixed by a screw (c) after it has rotated to the intended angle. There is also a screw (d) to clamp the sample holder to the rotational rod and also keep to maintain the leveling of the sample holder. The sample (e) is then fixed on the sample holder surface where the sample can be tilted by rotating the rod. The tilted body is fixed on the movement sheet by four screws (f), and the movement sheet is connected with the mounting sheet. Between the sheets (2) and (3), there are tracks for the sheet (2) movement in X and Y directions. The sheet's movement is controlled by rotating the knobs (g) and (h). Finally, the tilt platform is mounted on the stand of microscope via the rabbet (j) with a screw (k) at the end of the L shape arm (i). In this tilt platform, the sample can move in X, Y and Z directions and rotate along X direction.

ATTENTION: The Singapore Copyright Act applies to the use of this document. Nanyang Technological University Library

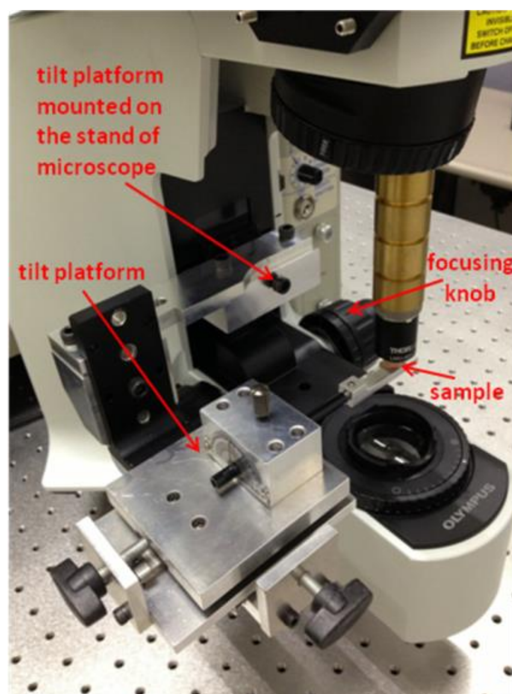

Figure 2.8. A photograph of the precision tilt platform.

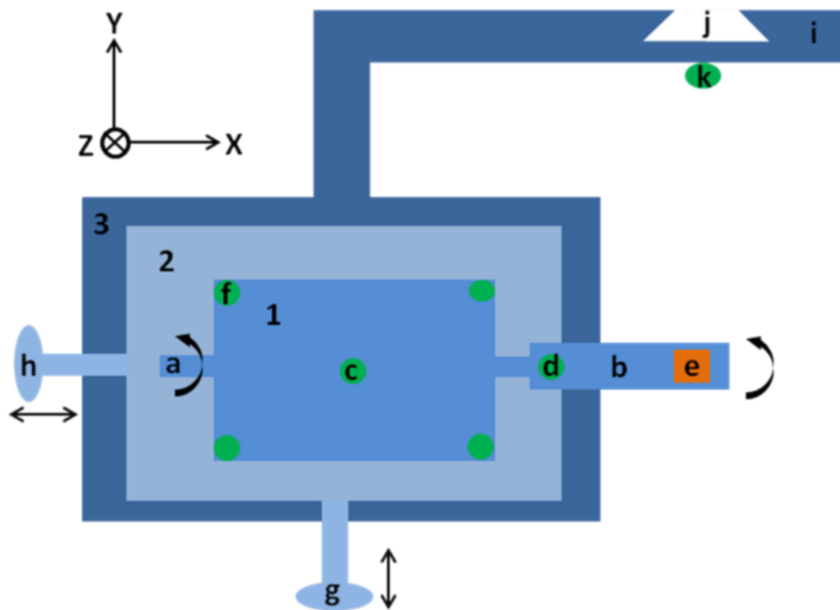

Figure 2.9. The schematic of the tilt platform.

In the Raman system, a 325 nm air-cooled Helium-Cadmium CW laser was used as excitation source and the laser beam was p-polarized. The spectrometer model is JY Horiba T64000. A 40x near ultra-violet (NUV) microscope lens with a N.A. value of 0.43

ATTENTION: The Singapore Copyright Act applies to the use of this document. Nanyang Technological University Library

was used to focus the laser on the samples and it also to collect the Raman signal from the samples. The laser incidence was consistent along the normal direction of sample surface. A small laser focal spot size of 500nm could be obtained with this equipment configuration.

Raman measurement was carried out at the same point on the metal one (M1) layer in a block area of 40 nm technology node SRAM device. Two spectra were captured for the SRAM device with the sample tilted at 0o (no-tilt) and 15°, respectively. The same parameters were set for the two spectra acquisition. In Fig. 2.10, it can be seen that low k information from Cu/low k interconnect can be obtained from the two measurements. The low k bonding are assigned as Si-O-Si symmetric stretch band at 470 cm-1, Si-O-Si asymmetric stretch band at 940 cm-1, Si(CH)x stretch bands around 780 cm-1, Si-H band at 2170 cm-1, C-Hx stretch band around 2920 cm-1. However, it is obvious that the intensities of low k bands in the curve of 15° are much stronger than that of tilt 0°.

ATTENTION: The Singapore Copyright Act applies to the use of this document. Nanyang Technological University Library

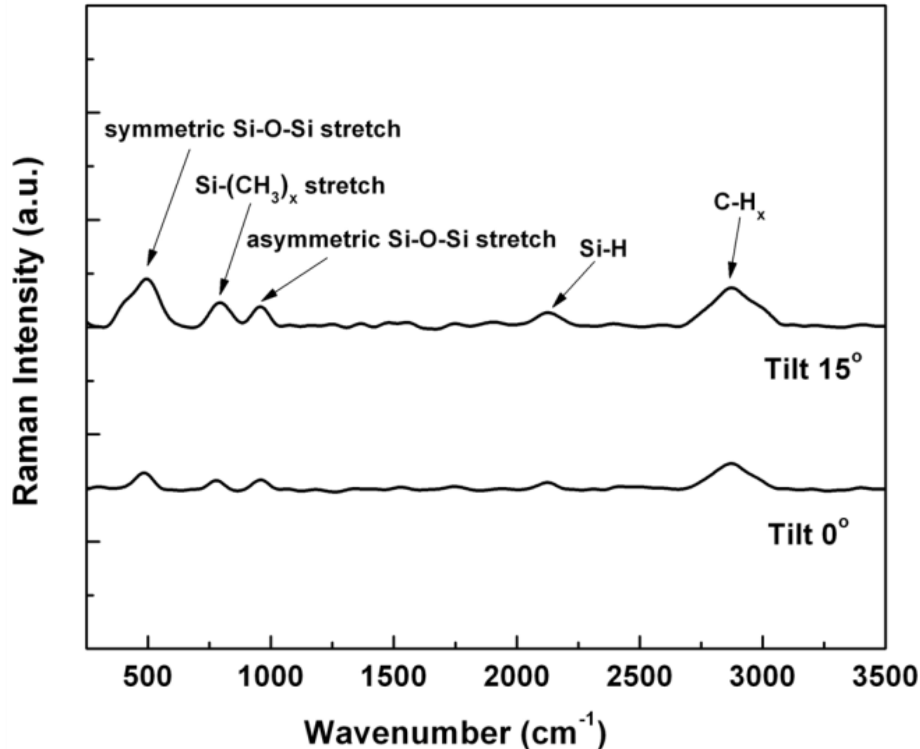

Figure 2.10. Raman spectra captured for the SRAM sample with tilt 0° (no-tilt) and tilt 15°, respectively.

Figure 2.11 shows the mechanism for the Raman scattering enhancement on nanometer scaled Cu/low k interconnects. The simplified cross-section structure of metal one layer of the SRAM sample is shown in Fig. 2.11(a). The Cu metallization can be considered as small nanoparticles array. It is known that the strong field enhancement generally appears at the cavity or junction of the nanostructures [11]. As shown in Fig. 2.11(a), there is an enhanced filed around each Cu nanoparticle. When laser beam source is incident on the Cu nanoparticles, plasmonic evanescent waves are generated. The evanescent waves propagating towards each other are constructively interfered and the fields within two neighbor Cu nanoparticles are enhanced as a result. The enhanced field could be further strengthened if the size of the Cu nanoparticle is small. To emulate a reduction in Cu nanoparticle, the sample can be tilted in such a way that only the tip of

ATTENTION: The Singapore Copyright Act applies to the use of this document. Nanyang Technological University Library

Cu nanoparticle is protuberant as shown in Fig. 2.11(b). These tilted Cu nanoparticles can be visualized as tip-shaped nanostructures as shown as in Fig. 2.11 (c) and these structures are capable of inducing very strong field. There are two factors which will impact the field enhancement, namely the apex of tip-shaped Cu nanoparticles and the cavity formed between neighbor Cu nanoparticles. This explains why more Raman signals induced in the tilted sample can be seen compared to the non-tilted sample. More importantly, this nanostructure, in the form of tip-shaped nanoparticles array, has high potential to be an effective SERS-active substrate.

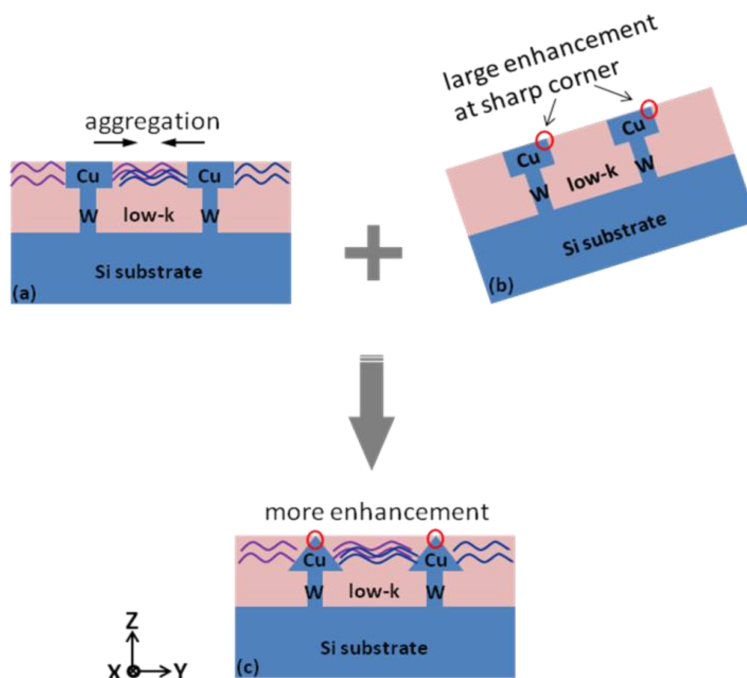

Figure 2.11. The schematic for enhanced Raman scattering on nanometer scaled Cu/low k interconnect.

In this project, we proposed to use a precision tilt platform to adjust the orientation of the nanometer scale of Cu metallization on sample surface to the incident laser. As the sample surface progressively tilts, the edge and corner of Cu nanostructure will become more protuberant. This tip-shape topography of Cu nanostructure will induce

ATTENTION: The Singapore Copyright Act applies to the use of this document. Nanyang Technological University Library

enhanced electromagnetic field for increasing Raman scattering on the low k IMD layer. As a result, a high quality of Raman spectrum with a better signal to background ratio is obtained. This enhancement will be useful for the detection of weak low k information in much smaller technology device. As weak signal could be more efficiently collected using this setup, there is a lesser need for averaging to be performed on the collected signal and overall data acquisition time could be shortened as a result. The shorter characterization time could translate to higher throughput as more samples could be analyzed within the same allocated machine time. This method can be used for other patterns of Cu metallization for enhanced Raman scattering on low k IMD.

2.7 Fourier Transform Infrared (FTIR) spectrometry

In our analysis, a Nicolet 6700 FTIR system with Continuum microscope as shown in figure 2.12 is used. It is a conventional methodology and technique for FTIR spectroscopy.

A schematic to summary the principle of FTIR spectrometry is as shown in figure 2.13.

ATTENTION: The Singapore Copyright Act applies to the use of this document. Nanyang Technological University Library

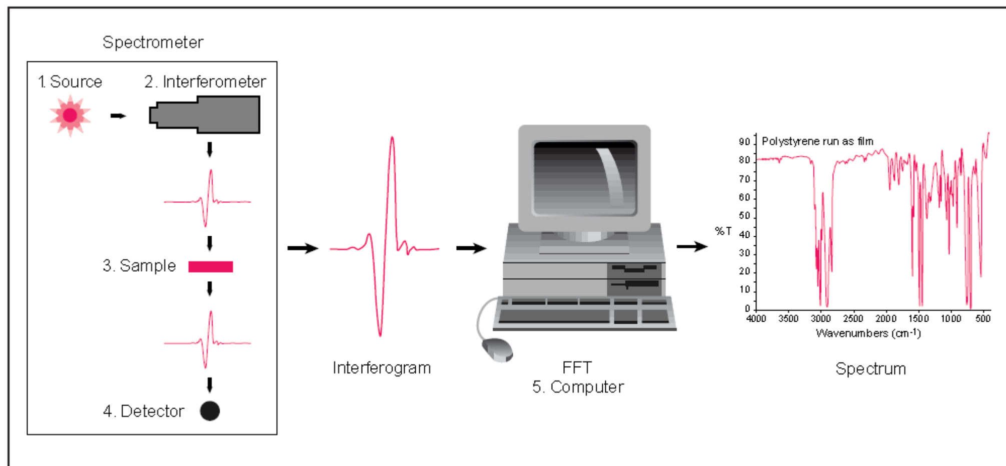

Figure 2.12 FITR principle

The Nicolet 6700 FTIR system in our investigation includes:

- DLaTGS detector with Ge coated KBr beamsplitter
- Gold optics and passport
- MCT-A detector
- 10X , 15X , 32X objectives
- ATR Ge tip slider for microscope
- Motorised stage with Atlus software control
- OMNIC software with standard data processing tools completes with PC preloaded with Win XP Pro or Win 7

ATTENTION: The Singapore Copyright Act applies to the use of this document. Nanyang Technological University Library

Figure 2.13 the Nicolet 6700 FTIR system

ATTENTION: The Singapore Copyright Act applies to the use of this document. Nanyang Technological University Library

Chapter 3 Vibrational spectroscopy of low k/ultra-low k dielectrics on patterned wafers

3.1 Introduction

Since low k dielectric was incorporated into IC devices, much effort has been devoted to the development of low k dielectric materials. With the technology moving to 45 nm and beyond, porous low k dielectric was introduced into IC technologies to reduce the dielectric constant of low k dielectrics down to 2 and below. Low k dielectrics and ultra-low k dielectrics were deposited with either spin-on or CVD process, widely reported in the literature [1–4]. The dielectric constant is dependent upon both chemistry and porosity. With the decrease of the metal line spacing due to the shrinkage of the device dimension, the reliability of low k dielectrics, especially porous low k dielectrics, has become one of the most challenging issues for current leading edge semiconductor technologies. In reliability studies of the low k dielectric IMD, the leakage current will increase due to the degradation of the low k/Cu interconnects, which will finally result in dielectric related failure. In Fig. 3.1, a TEM cross section image showed the low k dielectric breakdown during a reliability test, the infant mortality (IM) test, for 168 h. The IM 168 test was carried out at temperature of 140°C. DUT was fixed on a testing board in burn-in oven. During the reliability test, DUT was driven by IM test pattern at bias of 1.40 V. The failing criterion of IM test is 168 hours. Recent research [5, 6]. has shown that the leakage issues could be Cu diffusion into the low k dielectric. However, there is

ATTENTION: The Singapore Copyright Act applies to the use of this document. Nanyang Technological University Library

no detailed research to address the methodology of the analysis on the chemical property degradation of the low k dielectric during the reliability test on an IC device.

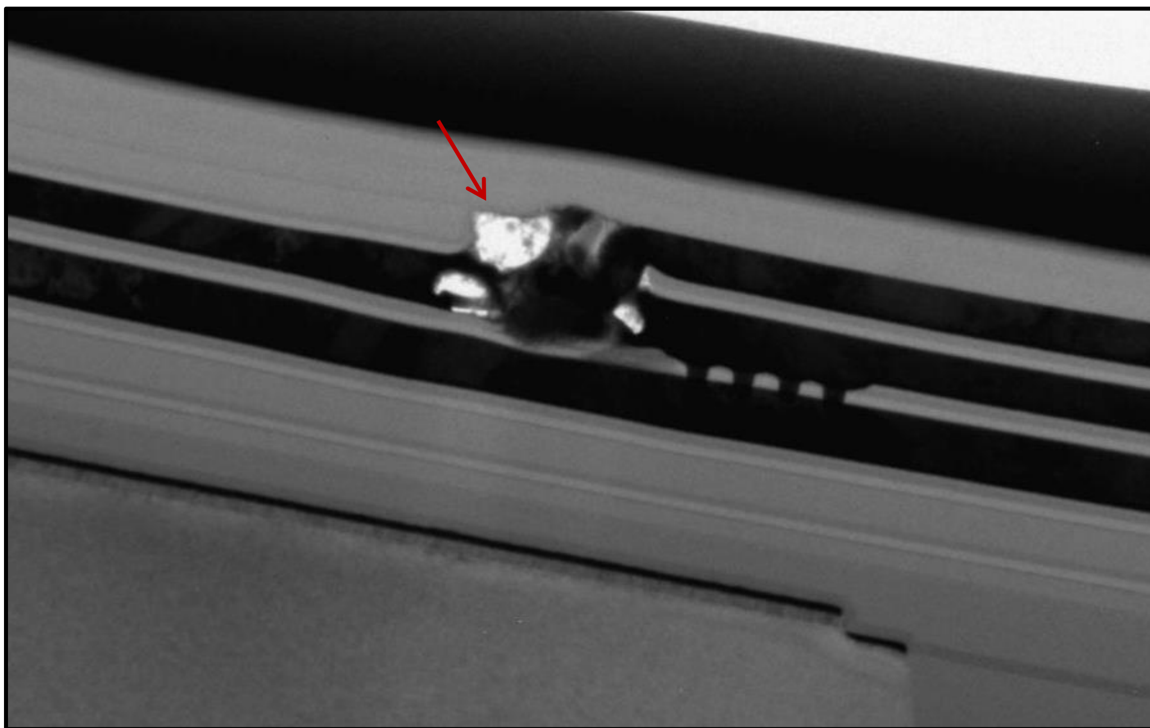

Figure 3.1 Low k dielectric breakdown (indicated by the arrow) during the reliability test, IM 168 hours.

With the development of low k dielectrics, material characterization and analysis techniques have been widely investigated with great interest. Rutherford backscattering and hydrogen forward scattering were used for atomic composition [7]. X-ray photoelectron spectroscopy, auger electron spectroscopy, and time of flight secondary ion mass spectroscopy were used to detect the elemental composition uniformity from the top to bottom of the film [8–12]. Nuclear magnetic resonance can also be used to characterize the structure of low k dielectrics regarding chemical composition and bond polarity [13]. There are also other techniques, like high resolution transmission electron microscope (TEM), ellipsometry porosimetry, and specular x-ray reflectivity to investigate the

ATTENTION: The Singapore Copyright Act applies to the use of this document. Nanyang Technological University Library

porosity and density of the low k dielectrics [14]. Another one of the most common characterization tools is the complementary vibrational spectroscopy with Raman and FTIR. It can identify the chemical bonds of materials. Hence, Raman and FTIR spectroscopy are widely used to analyze the organosilicon materials with the organic group attached to silicon [15–19].

While there are many studies on low k dielectric characterization, there are fewer on real patterned wafers and IC devices [20]. In current process development efforts, material has been developed and characterized on Si substrates or other substrates. With the developed process, the low k dielectric was deposited on patterned wafer with the damascene technique. Material was annealed to form stable low k dielectrics. The process margin is critical to make accurate control of the anneal time and temperature. On a patterned wafer, the metal layout below the as-deposited layers will contribute to the actual temperature distribution cross the chip or the wafer. For example, in an IC device, the input and output circuitry is normally built with large components and has a loose structure and memory cell area and the logic circuitry area has a very dense layout. The different metal trace distribution will make the temperature variation cross the chip. Over a whole wafer, the chip was arranged with scribe line for dicing. Many electrical test (ET) structures are fabricated within the scribe line for process monitoring. In the vertical structure of an IC device, the intermetal dielectric (IMD) at different layers took different annealing time and temperature because of the subsequent layer process.

Due to the small thickness of the low k IMD layer and complicated mixed structures and materials in the IC device, the vibrational spectroscopy detection will be very challenging and a detailed analysis is needed to extract low k dielectric signals from

ATTENTION: The Singapore Copyright Act applies to the use of this document. Nanyang Technological University Library

the mixed structures in spectroscopy. In this paper, Raman with high resolution and various laser sources have been employed intensively to characterize patterned wafers with SiCOH as the low k/ultra-low k dielectrics. FTIR was also used as a complement to investigate the chemical composition of SiCOH low k dielectrics. The effect of spectroscopy at different SiCOH densities was studied. Furthermore, the analysis of spectroscopy on SiCOH/Cu with different pattern layouts was studied in details.

3.2 Experiments

In our experiments, patterned low k/Cu wafers were used for the Raman spectroscopy study. The patterned wafers were fabricated with a standard CMOS process. Figure 3.2 shows a typical cross-section TEM of an IC device with low k/Cu CMOS process. The SiCOH was used as low k IMD deposited with a CVD process and Cu was used as the metal interconnects fabricated with conventional dualdamascene process. With physical sputtering, a Ta layer was deposited as a barrier layer between the Cu interconnects and the surrounding low k IMD. And a SiN_x N-block layer between the SiCOH low k dielectrics was used to provide mechanical support to the low k/Cu interconnects construction. The SiCOH low k dielectric, Ta barrier layer, and SiN_x N-block layer have a thickness of 200, 10, and 50 nm, respectively.

The vibrational spectroscopy study on conventional SiCOH thin films was carried out on two completed CMOS IC devices. One sample has dense low k SiCOH while the other has porous ultra-low k SiCOH. The dielectric constants and optical properties of the low k and ultra-low k SiCOH were listed in the Table 3.1. The optical properties of low k materials at different k values were measured with a Refractive Index and Extinction

ATTENTION: The Singapore Copyright Act applies to the use of this document. Nanyang Technological University Library

Coefficient Analyzer at two different laser wavelength of 532 nm and 325 nm respectively. The thin film thickness of the low k dielectrics is 250 nm. The samples were polished to the interested layers, and the low k/ultra-low k micro regions were characterized by vibrational spectroscopy. The conventional mechanical polishing avoided chemical reaction which could result in damage or change on the chemical bonding of the low k/ultra-low k dielectrics.

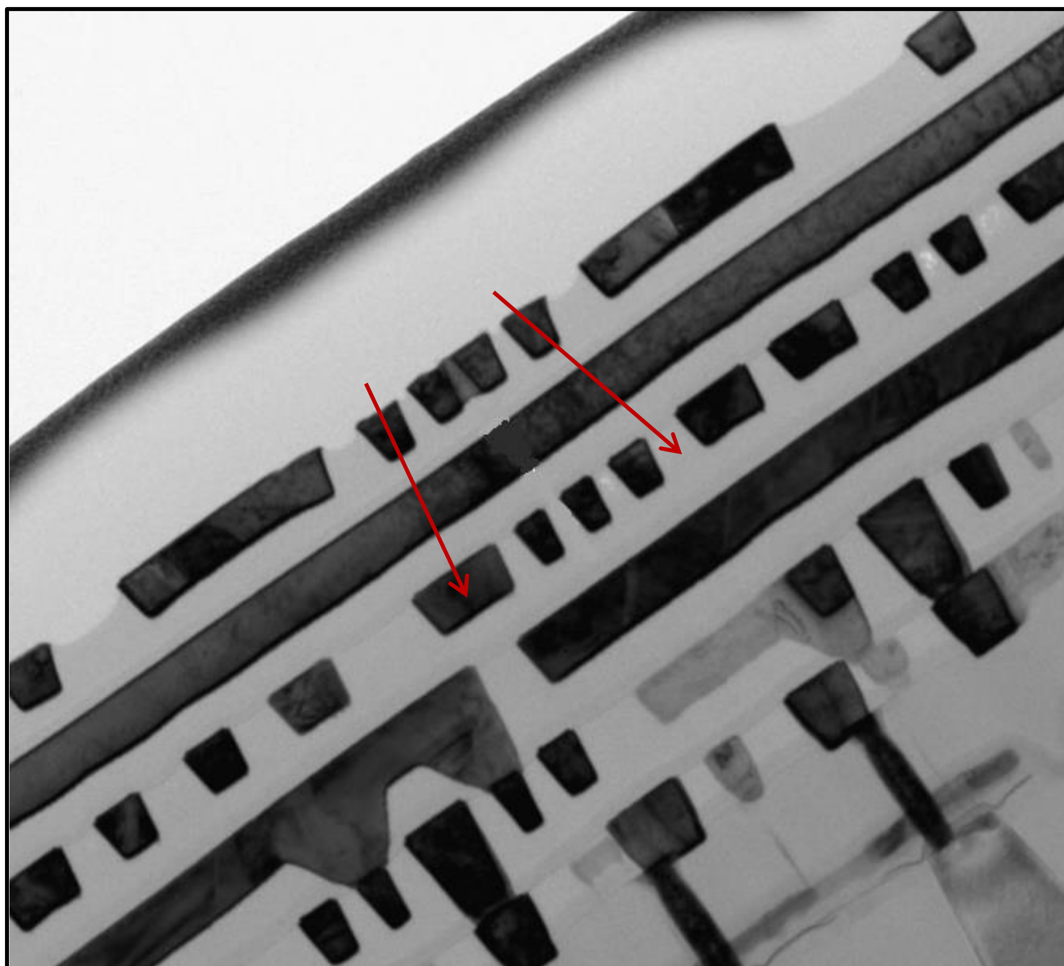

Figure 3.2 A typical cross-section TEM of an IC device with low k/Cu CMOS process.

Raman spectra were measured at room temperature by a JY-LabRam HR spectrometer attached to a microscope. The 532 nm Nd: YAG laser and 325 nm air-cooled heliumcadmium CW laser were used as excitation sources. A holographic notch

ATTENTION: The Singapore Copyright Act applies to the use of this document. Nanyang Technological University Library

filter was used as both a beam splitter and a notch filter. A 100x objective lens for 532 nm laser and a 40x near ultraviolet (NUV) lens for 325 nm laser were used to focus the laser on the samples and it also collects the Raman signal from the samples. The laser beam was vertically irradiated on the sample surface to realize maximum incident. The beam spot could be focused about 1 μm under both 532 and 325 nm lasers. For the 325 nm laser, an additional Duoscan mode was used to limit the laser power below 4 mW to avoid thermal effect. FTIR spectra were recorded on a Nicolet 6700 Analytical FTIR spectrometer coupled with a Nicolet Continuum infrared microscope. A 10 μm IR beam spot size was available. A MCT detector and a KBr beam splitter were used for the data collection in the mid-IR range from 4000 to 400 cm^{-1}. The resolution is 4 cm^{-1}. The attenuated total reflectance (ATR) collection mode was used in our experiments.

Table 3.1 k value and optical properties of low k and ultra-low k SiCOH

	K value	Refractive index at 532 nm	Extinction coefficient at 532 nm	Refractive index at 325 nm	Extinction coefficient at 325 nm
Low-k	2.8	1.46	0.010	1.49	0.013
Ultra-low-k	2.3	1.19	0.001	1.23	0.005

3.3 Results and Discussion

3.3.1. Vibrational spectroscopy on SiCOH low k dielectric on patterned wafer

Raman spectroscopy was first used for characterizing dense SiCOH low k dielectric deposited on the second metal layer in the first CMOS IC device. A point measurement was captured on the surface of pure low k area inside an inner guard ring surrounding the memory circuit patterns. Figure 3.3 shows the Raman spectrum excited by a 532 nm

ATTENTION: The Singapore Copyright Act applies to the use of this document. Nanyang Technological University Library

laser. The characteristic bands in the spectrum can be assigned based on findings from previous research [21, 22]. The bands located at about 1430, 2180, 2910, and 2970 cm^{-1} can be attributed to the C–H3 symmetric bending, Si–H, C–H3 symmetric stretching, and C–H3 asymmetric stretching modes, respectively. For the vibrational modes of Si–O–Si, no bands are expected either in the spectral region between 450 and 550 cm^{-1} for the symmetric stretching mode or in the region between 1000 and 1130–1 for the asymmetric mode [15]. Additionally, three bands at 308, 520, and 960 cm^{-1} with high intensities are observed. These bands can be attributed to the characteristic vibrational modes of Si–Si. The results suggest that 532 nm laser only managed to detect partial bands of SiCOH low k dielectric on the patterned wafer. Meanwhile, the Si Raman signals were simultaneously collected in the SiCOH spectrum, because the 532 nm laser penetrated the SiCOH low k dielectrics and reached the bulk Si substrate. For 532 nm laser, the penetration depth of Si could reach about 700 nm, resulting in strong Si Raman signals the SiCOH spectrum. In contrast, the SiCOH low k dielectrics had poor Raman signals due to its highly transparent of optical property in both visible and UV range, as shown in Table 3.1. As a result, longer acquisition time was needed for SiCOH measurement in order to enhance its Raman signals. Unfortunately, the strong intensity of Si band quickly led to Raman signals saturation so that no more signals from SiCOH can be recorded. Therefore, the SiCOH-related bands could not completely appear in the spectrum in Fig. 3.3.

In order to understand the bonding structures of the SiCOH low k dielectric on a patterned wafer, we use 325 nm lasers as the excitation source for further Raman characterization. Because the UV laser has much less penetration depth (10 nm) than that

ATTENTION: The Singapore Copyright Act applies to the use of this document. Nanyang Technological University Library

of 532 nm laser in Si wafer, and its higher sensitivity is helpful to detect the SiCOH chemical information.

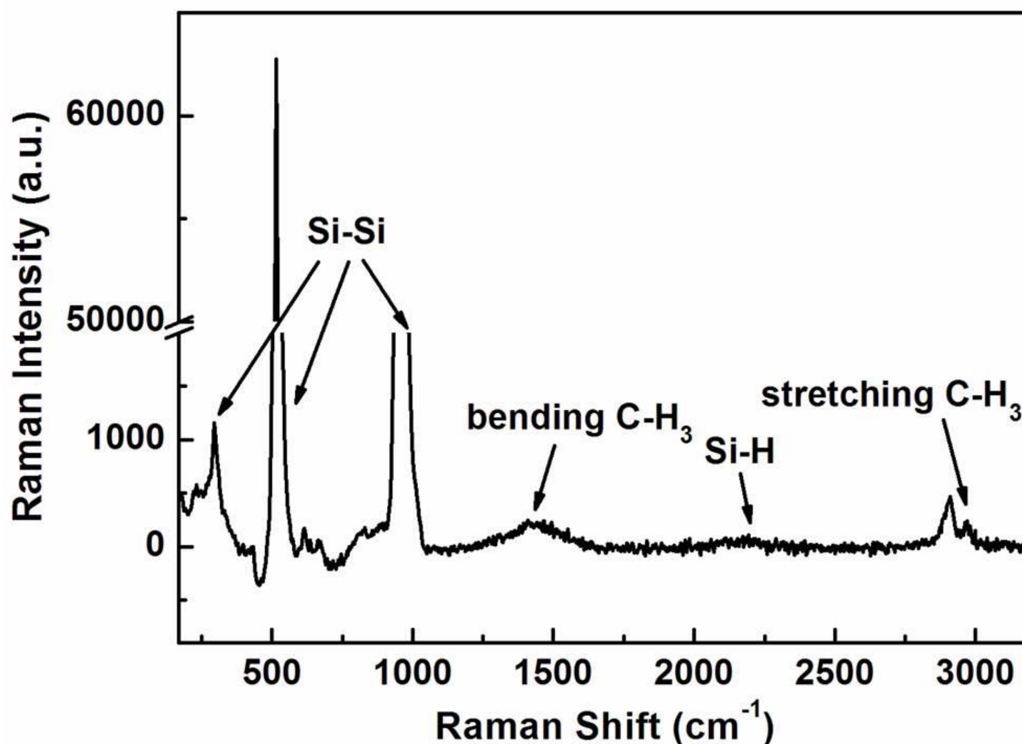

Figure 3.3 Raman spectrum excited by 532 nm laser of the dense SiCOH low k dielectric deposited on the second via in the first IC device.

The Raman spectrum of dense SiCOH low k dielectric at the same location under 325 nm laser excitation is shown in Fig. 3.4. Comparing with Fig. 3.3, it is obvious that the spectra measured at different wavelengths are very dissimilar. First, much lower intensities of Si bands were observed in the spectrum and the intensities of the C–H3 and Si–H bands of the SiCOH were dramatically increased. Two new bands were found, which were located at 240 and 790 cm^{-1}. These bands were assigned to the asymmetric deformation mode of Si–C3 [15]. and the stretching mode of the Si–CH3, respectively. Meanwhile, the symmetric stretching mode of the Si–O–Si was suspected to overlap with Si band at 520 cm^{-1}. The reason will be discussed later in Sec. III C. Comparing the 532

ATTENTION: The Singapore Copyright Act applies to the use of this document. Nanyang Technological University Library

nm and UV laser Raman spectra provided more information on the SiCOH and less Raman signal from Si substrate, due to its high resolution, high sensitivity and less penetration depth in the thin layer.

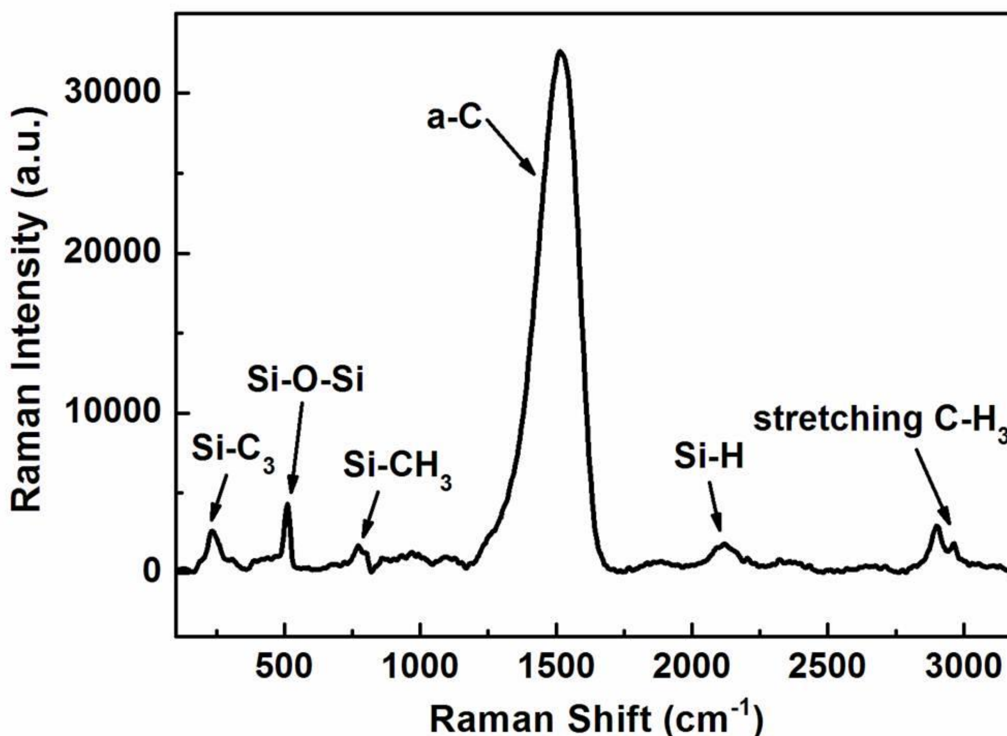

Figure 3.4 Raman spectrum excited by 325 nm laser of the porous SiCOH ultra-low k dielectric deposited on the second via in the second IC device.

The second notable difference is that the spectrum has a very strong and broad band at the range of 1300–1700 cm^{-1}, which had not been observed in the 532 nm spectrum. This band was a typical amorphous carbon (a-C). By fitting the curve with Gaussian functions, D and G bands can be revealed at the position of approximately 1380 and 1560 cm^{-1}. The two band positions are typical disordered graphite [23]. That is to say, an appreciable formation of sp2-carbon clusters in the SiOCH film accompanied the release of hydrogen. The possibilities for breaking of H-terminated bonds are (1) low

ATTENTION: The Singapore Copyright Act applies to the use of this document. Nanyang Technological University Library

k/process interaction-induced material modification or (2) UV laser thermal or photoenergy-induced damage.

In order to better understand the origin of the formation of a-C, FTIR spectroscopy was carried out. Since the IR source has a lower spatial resolution compared to Raman, the FTIR measurement was taken in a 20 μm x 20 μm area around the inner guard ring. This area was away from the Raman testing point to avoid the Raman radiation effect on the sample surface. In Fig. 3.5, the peak around 1600 cm^{-1} is the characteristic of the sp2-carbon bond vibration, indicating that the graphitelike phase is from the SiCOH [24]. It suggested that SiCOH low k dielectric was modified by the process. The sp2-carbon will increase the dielectric constant and weak the dielectric electrical property.

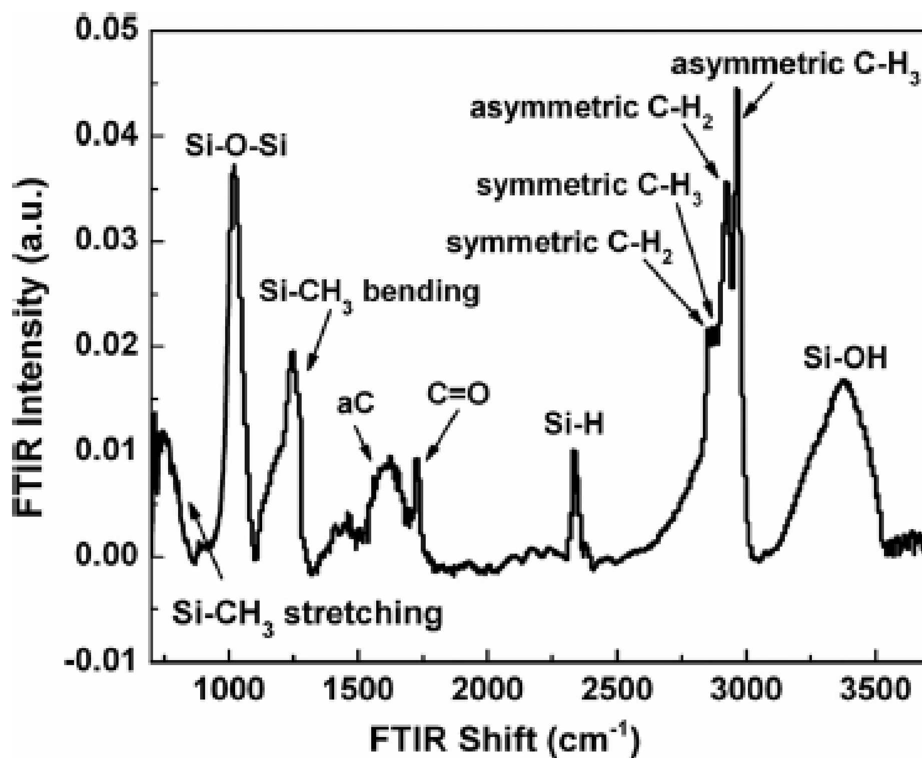

ATTENTION: The Singapore Copyright Act applies to the use of this document. Nanyang Technological University Library

Figure. 3.5 FTIR spectrum of the dense SiCOH low k dielectric at the same location corresponding to the Fig. 3.3.

In the FTIR spectrum, several SiCOH intrinsic bands were observed which corresponded to those appearing in the Raman spectrum. There are Si–O–Si network bands at 1027 cm^{-1}, the stretching mode of Si–CH3 at 760 cm^{-1}, the bending mode of the Si–CH3 band 1250 cm^{-1}, the Si–H band at 2300 cm^{-1}, the symmetric and asymmetric stretching modes of the C–H3 band at 2880 and 2970 cm^{-1}, and symmetric and asymmetric stretching modes of the C–H2 band at 2860 and 2920 cm^{-1}. Moreover, the band of C¼O centered at 1720 cm^{-1} and a broad band of Si–OH centered at 3400 cm^{-1} indicate that the SiCOH low k was oxidized and the Si–CH3 bands were partly broke, which is the result of plasma damage during the process [22].

3.3.2 Vibrational spectroscopy on SiCOH ultra-low k dielectric on patterned wafer

Both Raman and FTIR spectrum were also performed on porous SiCOH ultra-low k dielectric deposited in the second metal layer in the second COMS IC device. A point measurement was also taken inside the inner guard ring surrounding the memory circuit patterns. Figure 3.6 is the Raman spectroscopy with 325 nm lasers. The Si–O–Si band and Si–Si band overlapped at 520 cm–1, the Si–CH3 at 790 cm^{-1} and C–H3 at 2910 and 2970 cm^{-1} were still observed. However, the Si–H band at 2180 cm^{-1} and the Si–C3 band at 240 cm^{-1} could not be observed due to the weak signals. Moreover, three new bands of 254, 320, and 870–1100 cm^{-1}, appeared in the spectrum. The band at 870–1100 cm^{-1} corresponded to the Si–N band observed in the literature [25]. The Si–N band signal originates from the amorphous SiN_x layer between the SiCOH dielectric. The amorphous Si (a-Si) bands occur in the spectral range of 50–500 cm^{-1}, at 254 and 320 cm^{-1} in this case.

ATTENTION: The Singapore Copyright Act applies to the use of this document. Nanyang Technological University Library

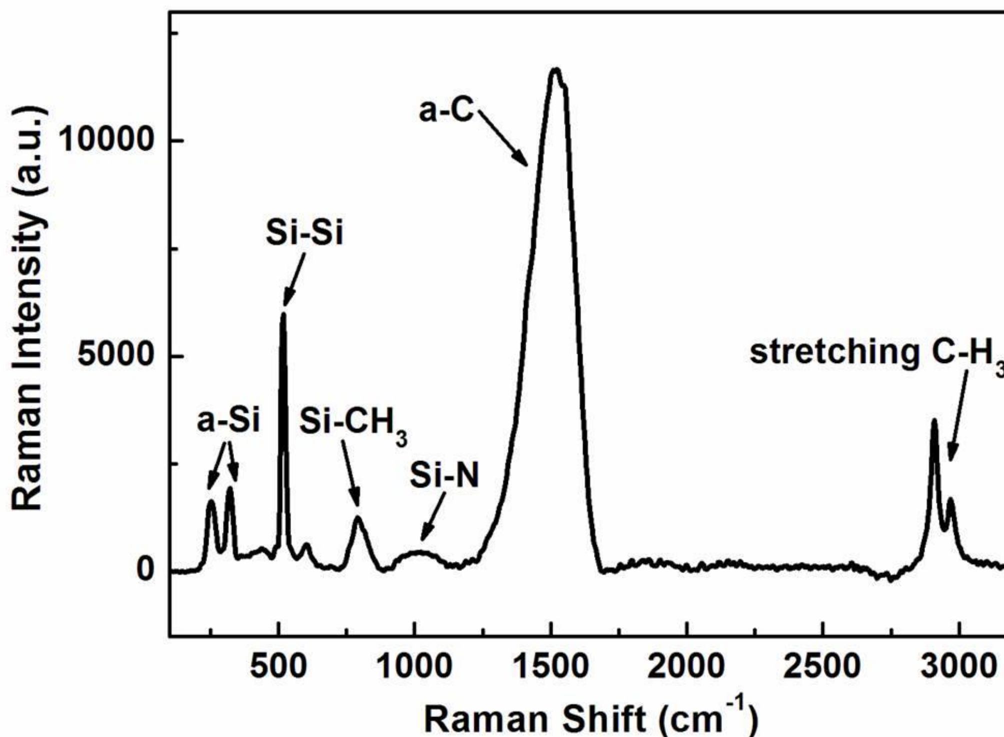

Figure 3.6 Raman spectrum excited by 325 nm laser of the porous SiCOH ultra-low k dielectric deposited on the second via in the second IC device.

The Raman results showed an obvious change in chemical compositions in the SiCOH matrix from the dense to the porous. It can be ascribed as that organic precursor was incorporated in the porous SiCOH matrix for increasing porosity and reducing the dielectric constant. The organic precursor incorporated in the SiCOH film preferentially occurred at the Si–H sites, inducing the broken of the Si–H band and forming porous networked structure. Therefore low Si–H signals are detected in the porous SiCOH spectrum. In the latter, the organic precursor and CHx bands in the matrix will be removed at low k during the curing process after deposition. The study from Verdonck et al. [26, 27]. showed that, after removing CH2 groups, the porosity increases and hence the dielectric constant decreases, while, after removing the CH3 groups, the cross-linking increases and hence the porosity and increases mechanical strength probably decreases.

ATTENTION: The Singapore Copyright Act applies to the use of this document. Nanyang Technological University Library

Figure 3.7 shows the distribution of CHx bands in both dense and porous SiCOH in the range of 2700–3200 cm^{-1}. It is shown that many fewer CH2 bands were observed in the porous SiCOH (top curve), which contrasts with the fact that the higher intensity CH2 bands still remained in the dense SiCOH (bottom curve). The result is consistent with the porosity formation mechanism in ultra-low k SiCOH.

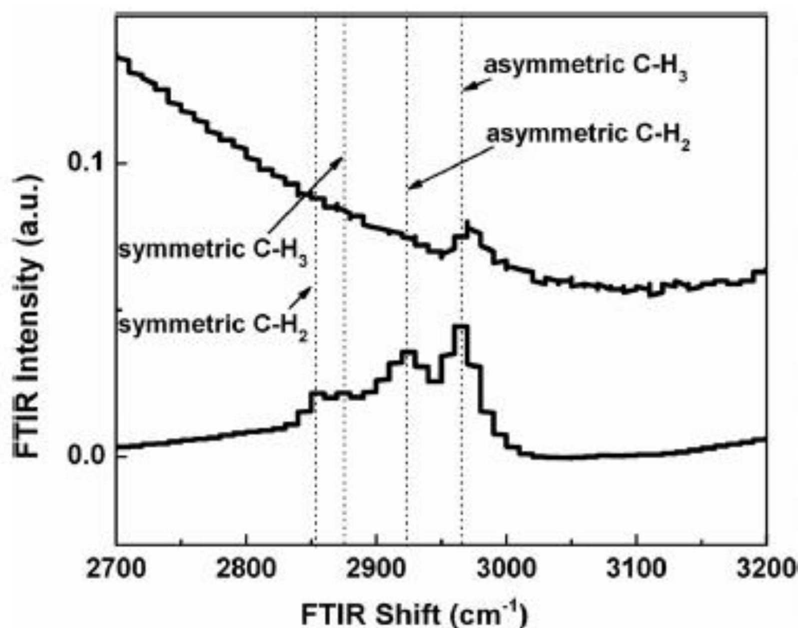

FIG. 3.7 Comparison of FTIR spectra, in a range of 2700–3200 cm^{-1}, between the dense (bottom curve) and porous SiCOH (top curve) dielectrics in the two IC devices, respectively.

3.3.3 Vibrational spectroscopy on SiCOH/Cu mixed structure on patterned wafer

As devices become smaller with device scaling, it is becoming a challenge to isolate the signals from copper and SiCOH low k/ultra-low k dielectrics by spectroscopy. More importantly, one is expected to monitor and localize the lowk degradation and breakdown in the low k/Cu reliability analysis, as in low k/Cu TDDB studies. Therefore, it is essential to characterize a mixed spectrum in a nanometer-scaled low k/Cu structure

ATTENTION: The Singapore Copyright Act applies to the use of this document. Nanyang Technological University Library

to overcome the limitations in spectroscopy. In this experiment, Raman spectroscopy with a higher resolution was carried out on two kinds of layout in the ultra-low k CMOS IC device. First, an ET comb structure with a size of 30 µm_40 µm for TDDB testing in the scribe line in the second metal layer was characterized. For the comb structure, the nominal linewidth and the nominal line-to-line spacing both were 70 nm. It was noted that there is a Cu plate with the same size beneath the measure ET comb structure. Namely, the Cu plate was deposited in the first metal layer and had a thickness of 200 nm. The Cu plate can effectively avoid the disturbance of Si wafer signal in the low k Raman spectroscopy. It is because both the visible and UV laser only has a penetration depth of tens of nanometers in Cu [28]. The comb structure is comprised of ultralow-k/Ta/Cu. The Raman spectrum was captured in a region of 2 µm_2 µm using both 532 and 325 nm lasers, as shown in Fig. 3.8. For 532 nm curve, we can see the signals (top curve) from Cu and SiCOH ultra-low k dielectric being masked by very strong fluorescence from Cu from 1000 to 3000 cm^{-1}. In order to reduce this fluorescence effect, we replace the excitation source using a 325 nm laser (bottom curve). It is found that the fluorescence can be significantly separated from the Raman signals of SiCOH and spectrum resolution enhanced. The 325 nm spectrum is very similar with what is shown in Fig. 3.4. It is confirmed that the symmetric stretching mode of Si–O–Si is really located at 520 cm^{-1} in our sample. The ultra-low k on patterned wafer shows an obvious blueshift in the Raman spectrum compared to generally blanket ultra-low k dielectrics. It may relate with the stress induced by chemical mechanical polish process.

ATTENTION: The Singapore Copyright Act applies to the use of this document. Nanyang Technological University Library

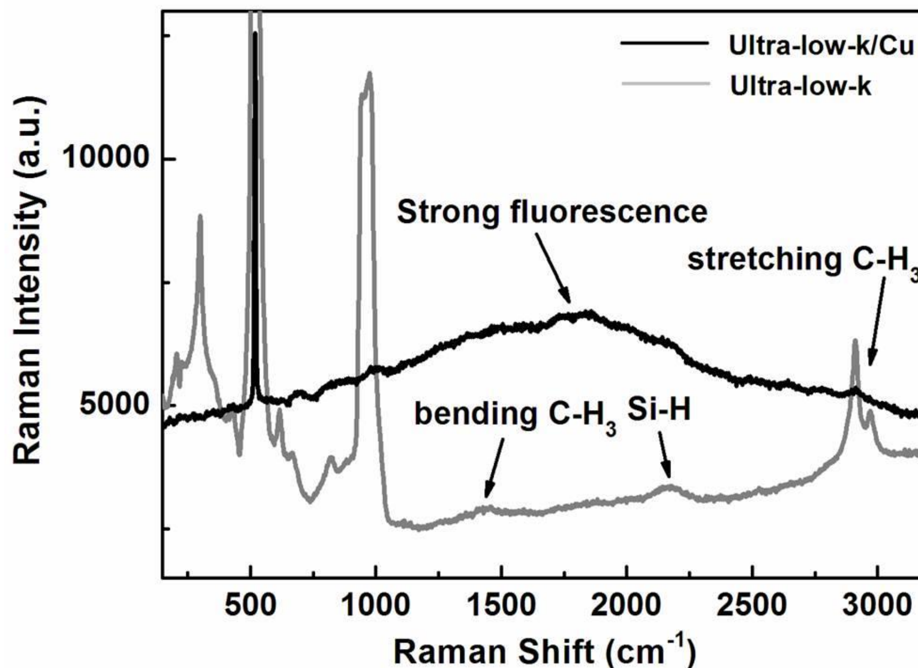

Figure 3.8 Raman spectra excited by 532 nm laser of the individual SiCOH ultra-low k dielectric and the ultra-low k/Cu mixed structure in the second IC device.

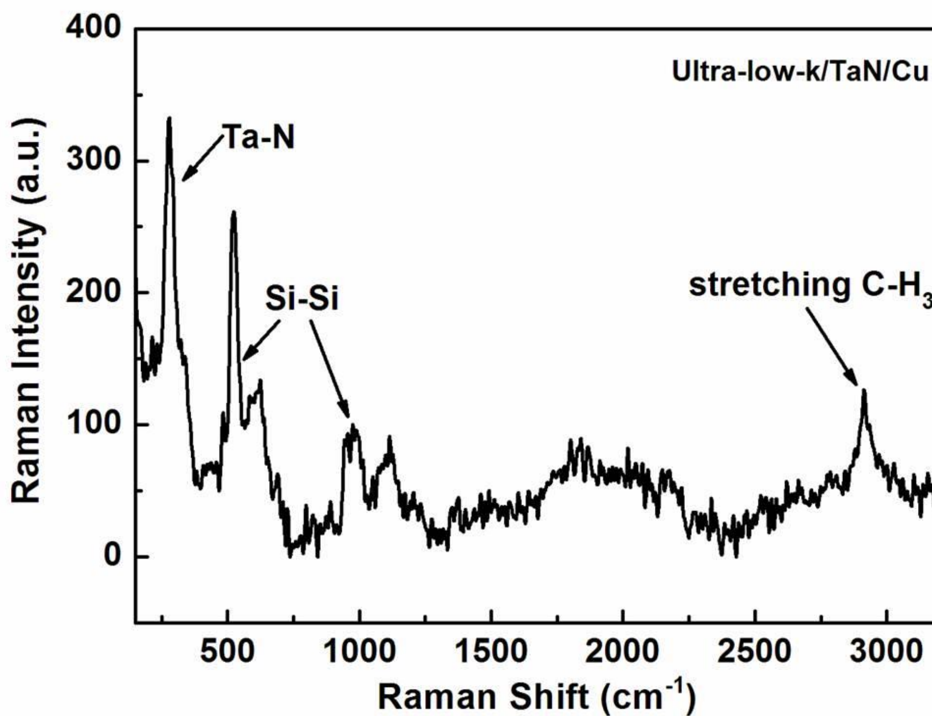

Figure 3.9 Raman spectrum excited by 532 nm laser of the ultra-low k/TaN/Cu mixed structure in the second IC device.

ATTENTION: The Singapore Copyright Act applies to the use of this document. Nanyang Technological University Library

Secondly, a bond pad in the second metal layer in the scribe line was characterized. It was intentionally deprocessed to the barrier layer of Ta on the top surface of the bond pad. It was aimed at analyzing the barrier effect on the Raman spectrum of the SiCOH/low k structure. Figure 3.9 shows the spectrum excited by a 532 nm laser. It is believed that the Ta layer deposited on Cu is capable to absorb most of the laser power to reduce the Cu fluorescence. This is evident by the new band at 278 cm^{-1}, which is likely related to Ta [29].

3.4 Summary and Conclusions

SiCOH low k/ultra-low k dielectric thin films on patterned wafers have been characterized by Raman spectroscopy. The results show that the Raman spectra vary significantly under various laser sources, in particular 532 and 325 nm wavelength lasers used in this work. With the visible laser, the SiCOH dielectric on patterned wafers was partially characterized and the Si signals are simultaneously collected in the SiCOH spectrum. Compared to the visible laser, the UV laser had an advantage for measuring a few tens of nanometers from the SiCOH surface, and the SiCOH spectrum was more complete. Meanwhile, the FTIR spectrum was an effective complementary tool for characterizing SiCOH on patterned wafers. There are also significant differences in the Raman and FTIR spectra between low k and ultra-low k dielectrics due to their different deposition processes. Finally, the individual SiCOH Raman signal has been successfully extracted from the ultra-low k/Cu mixed structure at nanometer-scale sizes.

ATTENTION: The Singapore Copyright Act applies to the use of this document. Nanyang Technological University Library

Chapter 4 FTIR Spectroscopy of Ultra-Low k dielectric on Patterned Wafers

4.1 Introduction

Vibrational spectroscopy technique can identify the chemical bonds of materials. And one of the complementary vibrational spectroscopy technique, the Raman and FTIR spectroscopy, is sensitive to the organic group attached to SiliconTherefore, they are widely used to identify the organosilicon materials [1, 2].

With the shrinkage of the IC device dimension, Cu and low k dielectric were introduced into IC device to reduce the RC delay. In the past decade, many research and application effort make the Cu and low k dielectric technology to be the main stream of the backend of line (BEOL) of the leading edge IC process. Since low k dielectric was incorporated into IC devices, there are a lot of researches done on the development of the low k dielectrics. With the technology moving to 45 nm and below, porous low k dielectric was introduce into the IC technology to further reduce the dielectric Constance of low k dielectric down to 2 and below, so the problem of cross-talk and power dissipation can be minimized largely. Low k dielectrics are polymeric compounds deposited with either spin-on or CVD process. The dielectric constant is dependent upon both the thin film chemistry and porosity. Due to the decrease of the metal spacing required by the shrinkage of the device dimension, the reliability of low k dielectric, especially porous low k dielectric, becomes one of the most challenging issues for the current leading edge semiconductor technologies. In the reliability study of the low k

ATTENTION: The Singapore Copyright Act applies to the use of this document. Nanyang Technological University Library

dielectric, the leakage current will increase due to the degradation of the low k/Cu interconnects, which will finally result in the dielectric related failure. Recent research [3,4]. showed that the leakage issues could be Cu diffusion into the low k dielectric. However, there is no detailed research to address the methodology of analysis on the chemical property degradation of the low k dielectric during the reliability test on an IC device.

Although a lot of studies on low k dielectric characterization have been done, there is a lack of investigation on real patterned wafers and IC devices. In current process development activity, material was developed and characterized on Si substrates or other substrates. With developed process, the material was deposited on patterned wafer with the damascene technique. Material was annealed to form stable low k dielectrics. The process margin is critical to achieve accurate control of the anneal time and temperature. On a patterned wafer, the metal layout below the as-deposited layers will contribute to the actual temperature distribution cross the chip or the wafer. For example, in an IC device, the input and output (IO) circuitry is normally built with large components and has a lose structure but the memory block and logic circuitry area have very dense layout. The difference in metal trace distribution will cause the variation of temperature field across the chip in 2-D and 3-D space. Over a whole wafer, chips are arranged with scribe lines for dicing. Many electrical test (ET) structures are fabricated within the scribe lines for process monitoring. In the vertical structure of an IC device, the IMD at different layers underwent different annealing time and temperature because of their different subsequent layer processes. All these will affect the uniformity of IMD within same layer and across layers to some extent.

ATTENTION: The Singapore Copyright Act applies to the use of this document. Nanyang Technological University Library

Moreover, due to the small thickness of low k IMD layer and complicated mixed structures and materials in the IC device, the FTIR spectroscopy detection will be very challenging and detailed analysis is needed to extract the FTIR signal of low k dielectric from the mixed FTIR spectroscopy. In this paper, we will apply the FTIR spectroscopy techniques on patterned wafers with SiCOH as the low k dielectrics. The effectiveness of different FTIR spectroscopy collection modes will be discussed.

4.2 Experiments

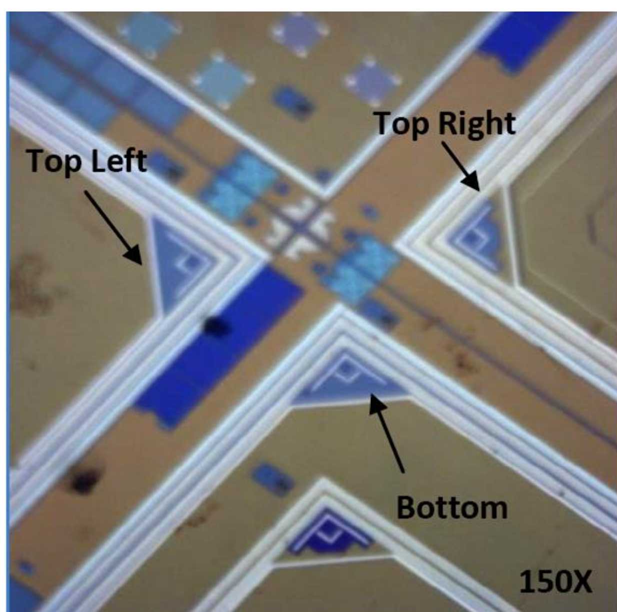

Figure 4.1 Optical micrograph of a pattern wafer with low k dielectric. Areas of interest are indicated on the graph.

IR spectra were recorded on a Nicolet 6700 Analytical FTIR spectrometer coupled with a Nicolet Contiuμm infrared microscope. MCT detector and KBr beam splitter were used for mid-IR (4000-400 cm^{-1}) data collection with a resolution of 4 cm^{-1}. Three collection modes: reflection, attenuated total reflectance (ATR) and X-Y mapping mode were used in our experiments (the resolution is 16 cm^{-1} for the mapping mode).

ATTENTION: The Singapore Copyright Act applies to the use of this document. Nanyang Technological University Library

The FTIR spectra were captured to study the properties of low k dielectric within mixed structures in an IC device. The optical image of an IC device was shown in Figure 4.1. The IC device was fabricated with a standard Cu/low k process. SiCOH was used as the low k dielectric for IMD. Cu is used as the metal interconnects and low k dielectric was used as the inter-metal dielectrics. A 50nm thick SiN_x layer on top of each Cu layer is used as the N-block layer between low k dielectric layers and it also provides mechanical support to the Cu/low k interconnects construction. TaN is used to form a 10nm thick barrier layer to prevent Cu diffusion into the low k dielectrics. The thickness of low k dielectric layer is 250 nm. In our experiments, the sample was polished to the layer of interest for FTIR spectroscopy by conventional method. The conventional mechanical polishing method can avoid chemical reaction, which could result in damage or change on the chemical bonding of the low k dielectrics.

4.3 Results and Discussion

4.3.1 FTIR Spectroscopy on low k dielectric on patterned wafers: reflection mode

Figure 4.1 shows the optical micrograph of the area of interest for FTIR spectrum collection. There are three areas of interest: top left, top right and bottom as indicated in the graph. Figure 4.2 illustrates the FTIR spectra of the three locations under reflection mode. Peak assignments are based on Ref 5 to 13. Small peaks around 2980 cm^{-1} are characteristic of C-H stretching in CH_3 present in the low k dielectric. The peaks around 1275 cm^{-1} revealed the Si-CH_3 bending [5-13]. Si-O-Si cage-like stretching can be seen from the peaks around 1135 cm^{-1}. The broad peaks between 800 to 1100 cm^{-1} can be

ATTENTION: The Singapore Copyright Act applies to the use of this document. Nanyang Technological University Library

hydrogen bond absorption or overlapped with Si-Ethyl group absorption. Figure 4.3 also shows the Si-$(CH_3)_2$ stretching mode centered at above 780 cm^{-1} [5-13]. It can be seen from this figure that the three areas of interest showed identical FTIR spectrum under reflection collection mode and the major bonds within the SiCOH network structure can be detected.

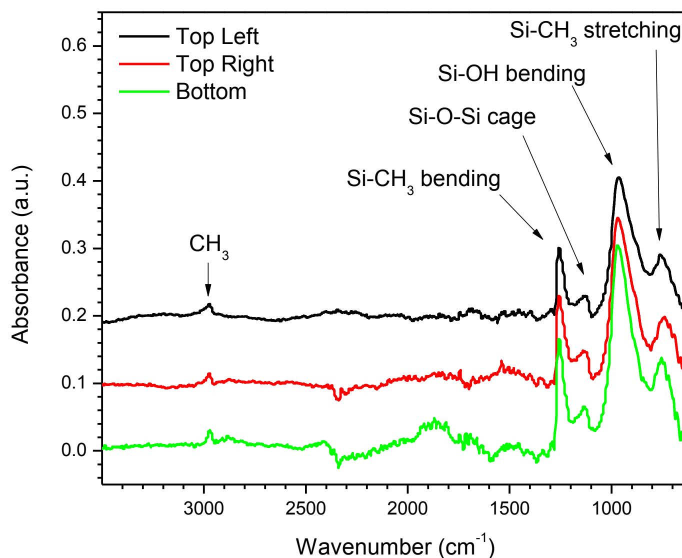

Figure 4.2 FTIR spectra of SiCOH layer structure from the patterned wafer recorded under reflection mode.

Ushio *et al.* [15]. reported that the most probable chemical reactions of porous low k SiCOH materials during the UV curing process are the two reactions:

I: $O_3Si\text{-}CH_3 + H_2 \rightarrow O_3Si\text{-}H + CH_4$

II: $O_3Si\text{-}CH_3 + OH\text{-}SiO_3 \rightarrow O_3Si\text{-}O\text{-}SiO_3 + CH_4$

The results in Figure 4 tally with the structure modification of low k dielectrics during UV irradiation. CH Huang *et al.* [12]. also reported a detailed study on the UV irradiation process and concluded that both reaction I and II occurred during the UV

ATTENTION: The Singapore Copyright Act applies to the use of this document. Nanyang Technological University Library

curing process. The Si-O-Si case-like stretching peak in Figure 4.3 also illustrates the formation of O-Si-O network structures, which derive from the reactions between cage-like structure and O_3Si-CH_3 bonds [12, 14].

4.3.2 FTIR Spectroscopy on low k dielectric on patterned wafers: ATR mode

In attenuated total reflectance (ATR) mode, the infrared beam incidents, at a certain angle, onto an optically dense crystal which has a high refractive index to ensure total reflection inside the crystal. An evanescent wave created by the internal reflectance extends beyond the crystal surface into the sample which contacts the crystal surface. The evanescent wave can only enter a few microns into the sample beyond the crystal surface. The evanescent wave will be attenuated due to the absorption of the IR energy by the sample. Then, the attenuated IR energy reflects back from the sample surface and is collected by an IR detector in the spectrometer.

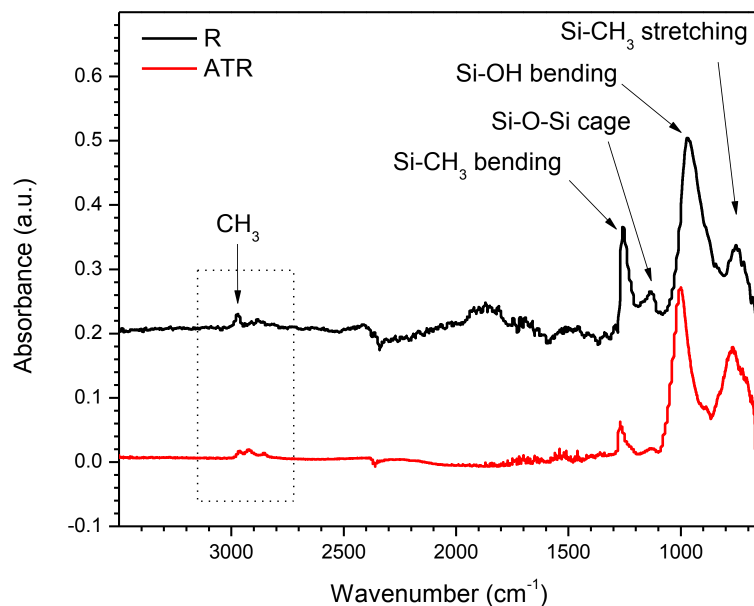

ATTENTION: The Singapore Copyright Act applies to the use of this document. Nanyang Technological University Library

Figure 4.3 Comparison of FTIR spectra recorded by reflection and ATR mode from the same area of interest on the patterned wafer.

Figure 4.3 shows the comparison between reflection and ATR mode for spectrum collected over the same area. These two spectra showed identical characteristics: the CH_3 stretching, Si-CH_3 bending, Si-O-Si cage-like stretching, Si-OH bending and Si-CH_3 stretching peaks can be seen from both spectra, except that the intensity for each peak varies. However, the spectrum collected under ATR mode showed a higher sensitivity in the CH_3 stretching band over the range of 2825 to 3025 cm^{-1}. The CH_x band over this range comprises four hydrocarbon peaks: the CH_3 asymmetric (2970 cm^{-1}), CH_2 asymmetric (2926 cm^{-1}), CH_3 symmetric (2888 cm^{-1}) and CH2 symmetric (2878cm^{-1}) vibrations. [8]. It can be seen from Figure 4.3 that the ATR spectrum showed more small peaks over this CH_x band, while the reflection spectrum only showed a major peak around 2970 cm^{-1} (CH_3 asymmetric). If we take a closer look over this range and compare all the collected spectra from area of interests, as shown in Figure 4.4, the spectra from ATR mode showed distinguished peaks for CH_3 asymmetric, CH_2 asymmetric and CH_2 symmetric vibrations (the lower three spectra in Figure 4.4), while those from reflection mode (the upper three spectra in Figure 4.4), can hardly show the vibrations other than CH_3 asymmetric vibration. Some spectra showed a possible CH_3 symmetric vibration but the signal to noise ratio is not so good.

ATTENTION: The Singapore Copyright Act applies to the use of this document. Nanyang Technological University Library

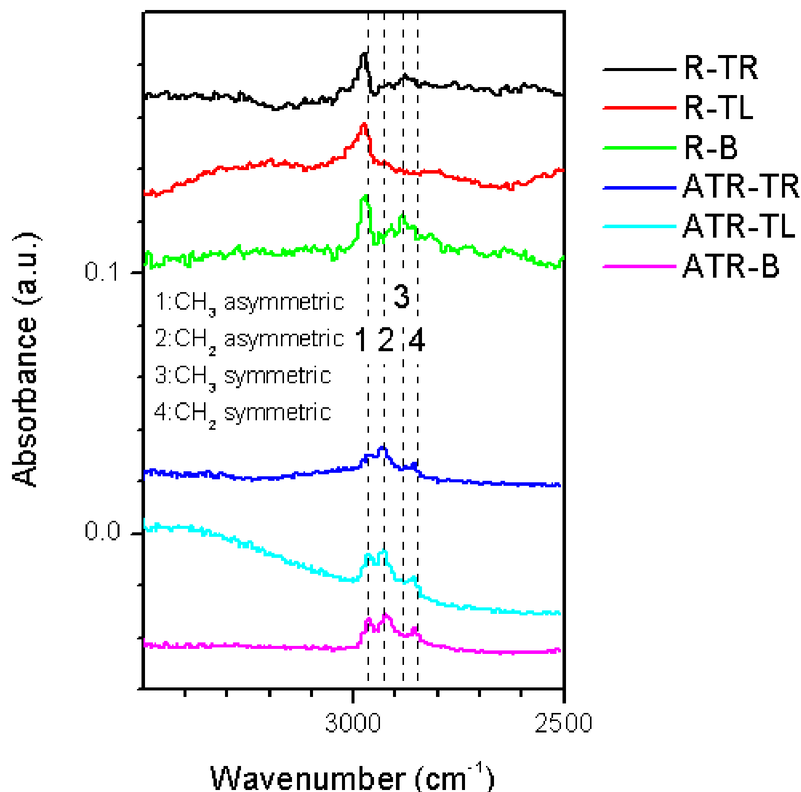

Figure 4.4 Comparison of FTIR spectra recorded by reflection and ATR mode over CH_x band.

The CH_2 groups in the porogen material are easily removed from the film with UV curing, creating the porous structure in the material. The study from Verdonck *et al.* [7, 15]. showed that, after removing CH_2 groups, the porosity increases and hence the dielectric constant decreases, while, after removing the CH_3 groups, the cross-linking increases and hence the porosity and increases mechanical strength probably decreases. Therefore, the CH_x peaks can be used to monitor the removal of the CH_x fragments in the precursor mixture and it is of essential importance to have the ability to detect and resolve the peaks within the CH_x band for process monitoring. ATR mode has been reported to have high sensitivity to thin dielectrics on silicon by Sayan *et al.*, [16]. based on the results in Figure 4.3 and Figure 4.4, it can be concluded that ATR mode is suitable for CH_x band studies on patterned wafer.

ATTENTION: The Singapore Copyright Act applies to the use of this document. Nanyang Technological University Library

4.3.3 FTIR Signal Analysis on Mixed FTIR Spectroscopy: mapping mode

For real applications on patterned wafer, it is necessary to identify the abnormal sites over a relatively large area and mapping mode will be ideal to reveal the sites of interests provided that it can differentiate the component materials (Cu, low k dielectric etc.) of the patterned wafer. FTIR mapping mode was used to collect the spectra over a rectangle area (940μm × 550μm) and the results are illustrated in Figure 4.5. From the Chemigram in Figure 4.5, it can be seen that the mapping mode clearly showed the Cu metal lines (blue) and the areas low k dielectric exposed (yellow to orange). This mapping result was done collecting 20979 spectra with reflection model. The sampling interval was 0.1 second. By adjusting the collecting parameters such as sampling interval, integration time, record mode and mapping peak position, it should be able to investigate areas with more complicated components inside. This will be addressed in our next studies.

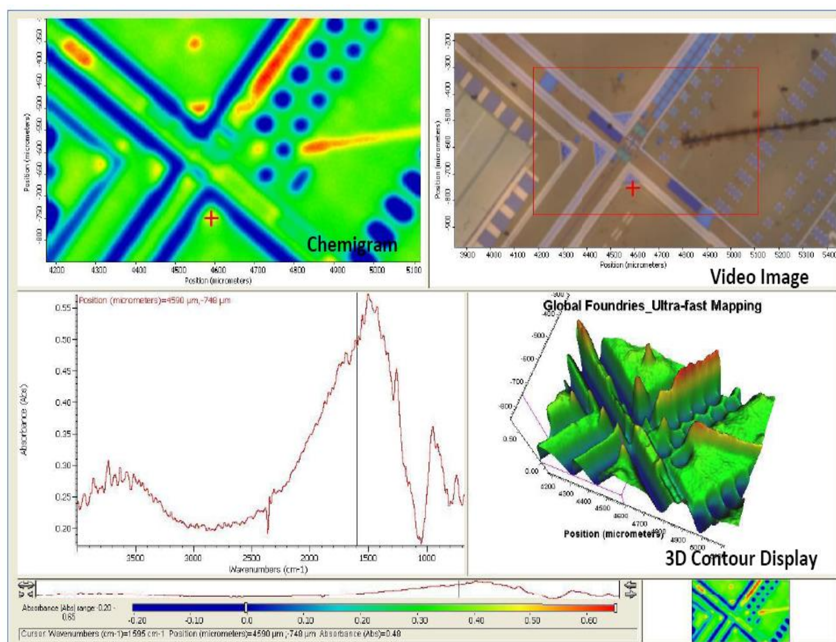

Figure 4.5 FTIR mapping over a rectangular area on a patterned wafer.

ATTENTION: The Singapore Copyright Act applies to the use of this document. Nanyang Technological University Library

4.4 Summary and Conclusions

In summary, we have shown that FTIR spectroscopy can be used to investigate the low k dielectrics on patterned wafers, all three modes used in this investigation showed satisfactory results. Our study suggests that:

1). ATR mode is more suitable for monitoring the UV curing due to its higher sensitivity on CH_x band over reflection mode;

2). It is possible to pinpoint the failure sites over large area by mapping mode.

Our current study is mainly focused on X-Y 2-D analysis. Investigation for the Z-direction resolution across different thin layers remains to be challenging and we will extend the current study into that scope in the future.

ATTENTION: The Singapore Copyright Act applies to the use of this document. Nanyang Technological University Library

Chapter 5 Ultra-Low k Dielectric TDDB Failure

5.1 Introduction

Cu and low k or ultra-low k dielectrics have been widely used as interconnects in current leading edge semiconductor technologies. Damascene and dual-damascene processes were applied to form IC interconnects to achieve significant reduction in RC delays. However, due to the weak strength of ultra-low k dielectric materials, inter-metal-dielectric (IMD) reliability becomes a big concern [1]. Time-dependent dielectric breakdown (TDDB) is one of the most common IMD reliability tests [2]. A significant amount of studies on electric field dependence of the TDDB time to failure (TTF) have been conducted. The TDDB E and square root E models have been proposed and are currently being used by most researchers for fitting TDDB plots. Theoretical support to the TDDB models is mainly based on the assumption that weak bonds in the dielectric can be broken, or the Cu ions can diffuse out and drift either into the dielectric or along the dielectric/barrier interfaces [3-5]. The factors such as Cu CMP, post CMP annealing, fine line effect and line edge roughness, could affect the Cu/ultra-low k interconnects TDDB lifetime model, have also been reported [6,7].

Of equal importance to the TDDB lifetime model is the breakdown mechanism. In recent years, the TDDB behaviors of the ultra-low k have been studied from different dielectric materials, failure-dominated factors and process effects [8]. Degradation and

ATTENTION: The Singapore Copyright Act applies to the use of this document. Nanyang Technological University Library

breakdown of the ultra-low k dielectrics have been studied by many research groups and a common approach involves the investigation of the conduction mechanism and leakage path in the dielectrics. K. Y. Yiang used a voltage ramp method to investigate the electrical conduction in carbon-doped silicon oxide (SiOC). The electrical conduction in the SiOC was studied over an electric field range of 0 MV/cm to the breakdown field at 300 K [9]. In his results, the dominant current conduction mechanisms were identified by fitting slopes for various conduction mechanisms at the different ranges of electric field. J. M. Atkin studied the charge trapping mechanisms at the ultra-low k dielectric-silicon interface by using the conductance and capacitance techniques [10]. Trap states close to the interfaces in thin films of porous ultra-low k dielectrics are expected to affect interfacial barriers with contacts and consequently results in electrical leakage and reliability issues in these materials. L. C. Chen reported his observation of the space charge limited current (SCLC) induced by injection of Cu ion into porous ultra-low k dielectrics [11]. It was suggested that the charge limited current (CLC), characterized by the momentary rise and fall of current with time, was found in all Cu interconnects having defective Ta barrier while it was absent in the interconnects with intact barrier.

Direct evidence and clear understanding on the cause and effect of the sources of TDDB failure are still lacking in most of the current investigations. It is well known that the complementary application of Raman and FTIR vibrational spectroscopy is one of the most common characterization tools and methodology for low k and ultra-low k material analyses and characterization [12-16]. Due to the challenges of capturing Raman and FTIR spectrum on the patterned wafers, as far as we know of, there has been no publication on Raman and FTIR analyses for TDDB failure. Recent progress of the

ATTENTION: The Singapore Copyright Act applies to the use of this document. Nanyang Technological University Library

complementary Raman and FTIR vibrational spectroscopy on nanometer-scaled structures on patterned wafers allows for the application of these techniques for TDDB analysis [17]. In this letter, we will present our investigation on the application of complementary vibrational spectroscopy on alternating interconnect nanostructures and the evidence of dielectric's degradation of the ultra-low k materials. This investigation provides a new methodology to study the breakdown mechanism on low k and ultra-low k dielectrics during a reliability test. Our study details observations on degradation behavior found in Cu/ultra-low k damascene structures and discusses their implication for ultra-low k technology.

5.2 Experiments

The combination of vibrational spectroscopy of in-situ micro-FTIR with micro-Raman was carried out to characterize the ultra-low k dielectric degradation in TDDB tests. The experiments were conducted on the planar comb capacitor structures consisting of 300 Cu lines with a length of 40 μm. These test structures were made using standard dual-damascene Cu interconnect process. The ultra-low k material used in this study was a porous plasma-enhanced chemical vapor deposition (PECVD) SiCOH film fabricated with the pore volume close to 20%, pore size of about 2 nm and k ~ 2.7. In the Cu/ultra-low k integration process, 10 nm Ta/TaN barrier bi-layer and 50 nm SiN capping layer were formed.

In order to investigate the degradation process before the structure is destroyed by TDDB tests, all measurements were performed at room temperature under an electrical field ranging from 1.3 to 2.6 MV/cm. The Cu line trench has a sloped profile with a top Cu line-to-line spacing of 50nm and a bottom line-to-line spacing of 70 nm. The local

ATTENTION: The Singapore Copyright Act applies to the use of this document. Nanyang Technological University Library

field at the upper interface is hence higher than the local field at the lower interface by at least 1.4 times. The calculation of applied electric field was based on the smaller line-to-line spacing of 50 nm. Computer-controlled Keithley 4200 semiconductor parameter analyzer was used to stress and then measure the current at selected intervals. During the TDDB tests, in-situ FTIR spectra were acquired on the whole area of the comb capacitor structures. The FTIR spectra were recorded using reflection mode on a Nicolet 6700 Analytical FTIR spectrometer where the spectrometer was coupled with a Nicolet Continuum infrared microscope. MCT/A detector and KBr beam splitter, with a spectra resolution of 4 cm^{-1}, were used for mid-IR (700 - 4000 cm^{-1}) data collection. On the Raman setup, the equipment has a 325 nm air-cooled Helium-Cadmium CW laser as excitation source and the spectra were measured by JY Horiba T64000 spectrometer. The Raman spectra were captured on the comb capacitor structures before and after the TDDB tests. The "duoscan" capture mode was used in order to avoid UV laser thermal effect on the ultra-low k film. For the FTIR and Raman spectroscopes, the spatial resolutions were 15 μm and 0.5 μm, respectively. At the end of the experiments, transmission electron microscopy (TEM) and energy-dispersive X-ray spectroscopy (EDX) analyses were carried out at the cross section of the Cu line comb structure. The TEM sample was milled and thinned by focused ion beam (FIB) under a beam energy of 30 KeV and a beam current of 80 pA. The prepared lamella was in-situ lifted in Helio 450 FIB and then examined using FEI Titan TEM at 200 KeV.

5.3 Results and Discussion

Figure 5.1 shows the typical curve of leakage current versus stress time at the early stage of the TDDB test on the comb capacitor structures. All samples were found to

ATTENTION: The Singapore Copyright Act applies to the use of this document. Nanyang Technological University Library

follow the general conduction behavior of the ultra-low k dielectric, that is, upon the application of the electric field, the current flow was initially high, but decayed exponentially until it reached the saturation level, indicated in the first stress period of AB. The quick initial current decrease is believed to be caused by electron trapping, which thickened the electron tunneling barrier from the cathode into dielectric conduction band. Generally, this conduction mechanism of dielectric is independent of extrinsic factors, such as out-diffusion of Cu ions. However, for the increasing current with increased stressing time, during the second stress period of BC, the dependence of leakage on Cu diffusion is still debated in the published researches.

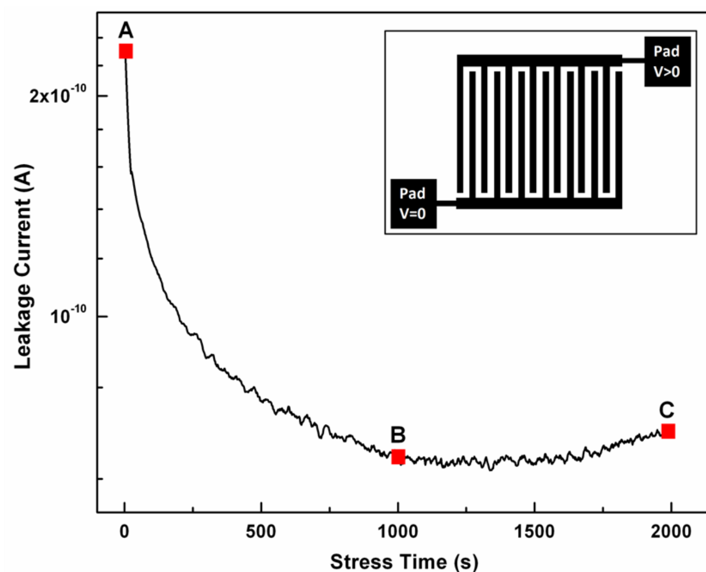

Figure 5.1 a plot showing the leakage current as a function of time in Cu/ultra-low k comb structure. The insert shows the top-down schematics of the comb structure used in the study.

Figure 5.2 is the result of in-situ FTIR spectra captured on the comb capacitor structure during TDDB test. It shows the chemical bonding evolution in ultra-low k dielectric from the stress status A to C as indicated in Fig.1. On the original sample at status A, it can clearly show the ultra-low k chemical bonding including the network Si-

ATTENTION: The Singapore Copyright Act applies to the use of this document. Nanyang Technological University Library

O-Si band at 1027 cm^{-1}, the caged Si-O-Si band at 1035 cm^{-1}, the bending mode of Si-CH_3 band at 1250 cm^{-1}, the Si-H band at 2300 cm^{-1} and the C-H group bands consisting of the symmetric and asymmetric stretching modes of C-H_3 band at 2880 cm^{-1} and 2970 cm^{-1}, as well as the symmetric and asymmetric stretching modes of C-H_2 band at 2860 cm^{-1} and 2920 cm^{-1}. After the ultra-low k dielectric experienced the initial period of leakage decay to a saturation level at status B, its chemical bonding intensity decreased, indicating an occurrence of intrinsic degradation in ultra-low k dielectric since no extrinsic factors were introduced in this stress period. The result suggests that the injected electrons from cathode have enough energy to break the chemical bonding of ultra-low k dielectric and the degradation is more severe for the network Si-O-Si bands at 1027 cm^{-1}. When the leakage begins to increase after continued stress (status C), the intensities of chemical bonding of ultra-low k decrease further. Additionally, a peak shift towards the higher wave frequency vibration is observed for the Si-O-Si network band. It is a combination of effects from both stress and strain on the ultra-low k dielectric. The formation of strain is due to an additional force on the ultra-low k bonding breakage from bigger size species (compared to electrons) such as metal ions, injected from the anode. The metal ions migration is expected to have caused an increase in the leakage current in the dielectric.

ATTENTION: The Singapore Copyright Act applies to the use of this document. Nanyang Technological University Library

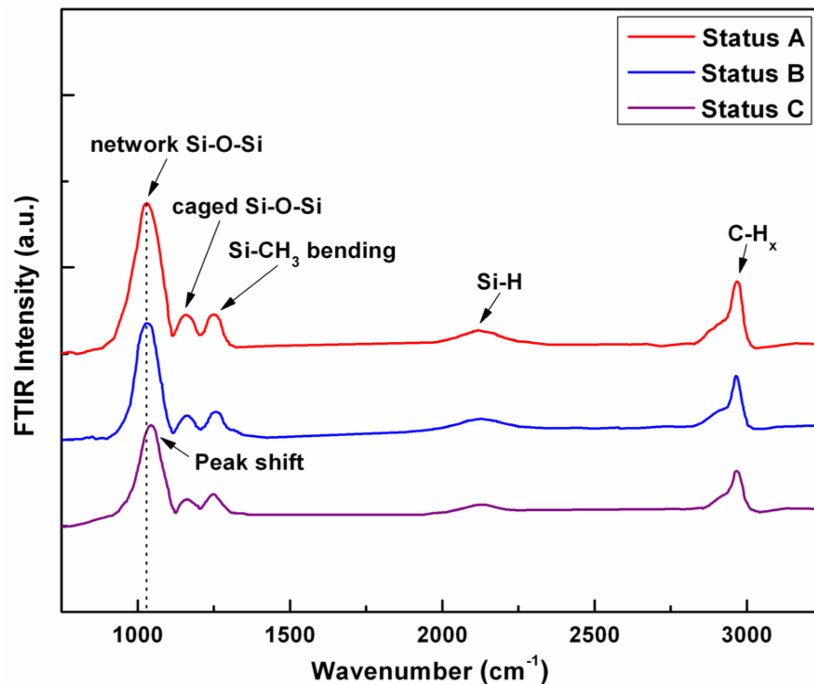

Figure 5.2 In-situ FTIR spectroscopy on the Cu/ultra-low k comb structure at different stress status.

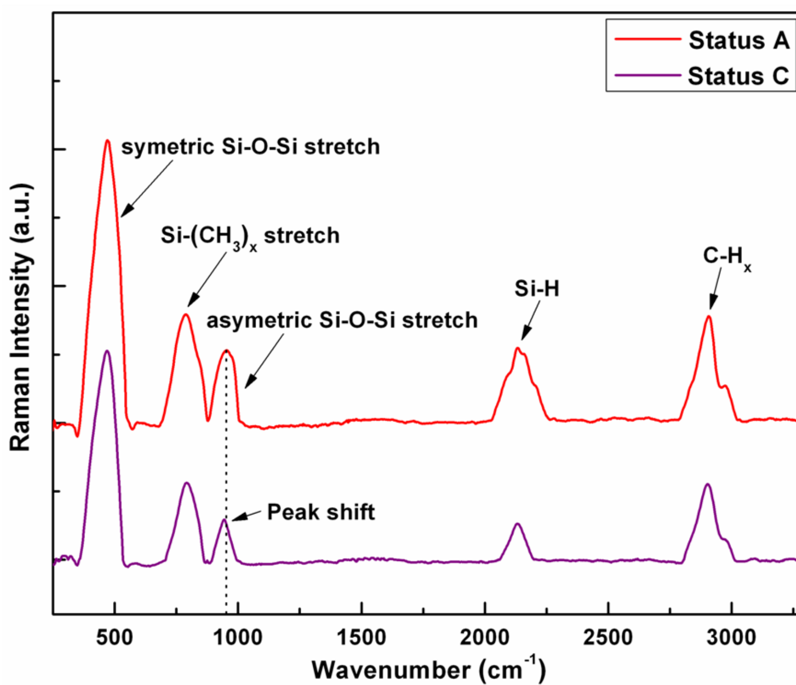

Figure 5.3 Raman spectroscopy on the Cu/ultra-low k comb structure at different stress status.

ATTENTION: The Singapore Copyright Act applies to the use of this document. Nanyang Technological University Library

Raman measurement was carried out after the TDDB test for verification of degradation in the ultra-low k structure. Figure 5.3 shows the Raman spectra captured on the comb capacitor structure before and after stress. The chemical bonding include Si-O-Si symmetric stretch band at 470 cm^{-1}, Si-O-Si asymmetric stretch band at 940 cm^{-1}, $Si(CH)_x$ stretch bands around 780 cm^{-1}, Si-H band at 2170 cm^{-1}, $C\text{-}H_3$ symmetric stretch band at 2920 cm^{-1} and $C\text{-}H_3$ asymmetric stretch band at 2960 cm^{-1}. Compared to the original sample, all the ultra-low k bands (especially the Si-O-Si stretch bands) are obviously degraded after stress. More importantly, a shift towards the lower wave frequency for the asymmetric stretch band of Si-O-Si is observed. This left band shift in the Raman spectra is generally caused by strain, confirming that band damage has occurred in the dielectric during and after the TDDB test.

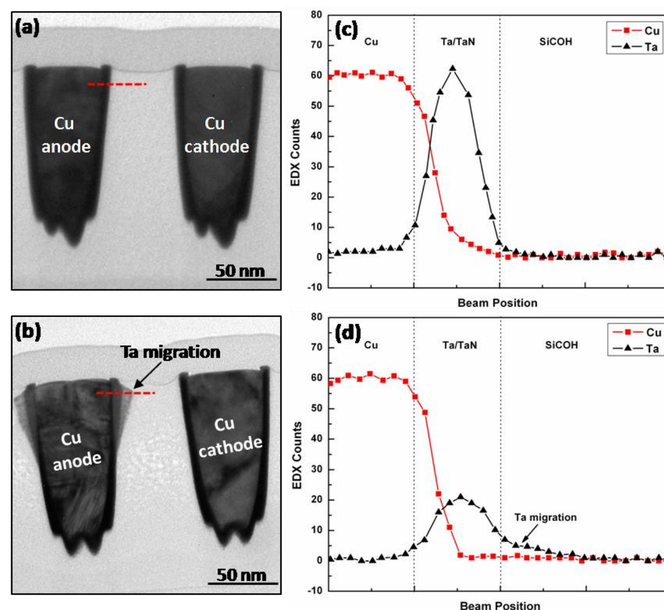

Figure 5.4 TEM cross-section images of the Cu/ultra-low k comb structure for the original sample before stress (a) and the sample with a certain time of stress with leakage current (b). EDX line profile of the Ta migration along the interface of Cu/Ta/TaN/SiCOH before stress (c) and after stress (d), respectively.

ATTENTION: The Singapore Copyright Act applies to the use of this document. Nanyang Technological University Library

In order to have a clear understanding of the effect of the leakage current on the ultra-low k dielectric degradation in TDDB test, high resolution TEM and EDX were used to investigate the possible damage information within ultra-low k dielectric. Figure 5.4(a) shows the cross-section image of the comb structure before the application of stress and no abnormality is observed in the original sample. However, Fig. 5.4(b) shows a severe degradation in ultra-low k of the comb structure at the stress status C indicated in Fig. 1. It is seen that Ta/TaN barrier bi-layer was decomposed and only a weakened Ta layer was left to cover the Cu lines. EDX line scans along the interface of Cu/Ta/TaN/SiCOH at the anode for both two samples were conducted. Figures 4(c) and (d) illustrate that there was no Cu diffusion out of Ta/TaN bilayer in both positions. Comparing with the position shown in the original sample, the Ta/TaN liner peak maximum is much reduced and the width is increased, which confirms that the Ta ions out-migration occurs during TDDB test, but the Ta/TaN bi-layer is sufficient to stop Cu out-diffusion in this condition. This explains the result that the strain measured in vibrational spectra was induced by out-diffused metal ions, which resulted in more damage in ultra-low k dielectric, manifested by increased leakage current. When the Ta ions drifted into ultra-low k dielectric, it occurred at a location that was a distance away beneath the capping layer, as shown in Fig. 4(b). This is because the capping layer had a stronger dielectric strength than the ultra-low k so that the capping layer could push the out-migrating Ta ions into the ultra-low k volume. Meanwhile, the ultra-low k dielectric was degraded due to the effect of the electrical field. As a result, migrating Ta ions preferred the path along the weakened ultra-low k dielectric. The Ta ions diffusion inside ultra-low k dielectric shows a non-uniform distribution due to the gradient local electrical

ATTENTION: The Singapore Copyright Act applies to the use of this document. Nanyang Technological University Library

field formed between Cu lines from upper to lower interface of dielectric and barrier. The highest local electrical field is formed at the upper interface with the smallest Cu line-to-line spacing. Ta ions diffusion reduced the dielectric gap between Cu lines and thus enhanced the local electrical field, which resulted in an acceleration of ultra-low k degradation to breakdown.

5.4 Summary and Conclusion

In conclusion, we observed the ultra-low k dielectric degradation in TDDB test by the complementary application of Raman and FTIR vibrational spectroscopy. It was found that the intrinsic degradation of the ultra-low k dielectric would first occur under the applied electrical field, Ta ions would then migrate into ultra-low k along the weakened interface of Cu/Ta/TaN/SiCOH, causing a more severe damage to the ultra-low k dielectric. The Ta ions inside the ultra-low k induced an increased local electrical field between Cu electrodes and thus accelerated the ultra-low k degradation to final breakdown. In our investigation on the Cu/Ta/TaN/SiCOH structures, no out-diffusion of Cu ions was observed.

ATTENTION: The Singapore Copyright Act applies to the use of this document. Nanyang Technological University Library

Chapter 6 A Model Analysis and the Process Improvement for Ultra-Low k Dielectric TDDB Failure

6.1 Introduction

In summary, to replace Al with Cu and to replace SiO_2 with low k dielectrics [1-5]. and ultra-low k dielectrics [6-10]., IC device performance can be greatly improved due to reduction of RC delay. However, low k and ultra-low k dielectrics have to face the challenge of reliability issues due to their weak material strength and Cu drift [11]. Hence, leakage and breakdown properties became important selection criteria for low k dielectrics [12, 13].

TDDB is commonly used low k dielectric reliability test. Many TDDB studies on a wide range of area and electrical fields were carried out to reveal the mechanism of TDDB failure of low k dielectrics. And simulation and modeling become a hot research topic in recent years. FTIR and Raman spectroscopy are complementary vibrational spectroscopy techniques that help elucidate the molecular bonding and molecular structure in low k dielectrics.

To understand the mechanism of TDDB failure of low k and ultra-low k dielectrics, we proposed to use FTIR and Raman spectroscopy identify the chemical bonding change during the TDDB test. Current FTIR and Raman techniques were widely

ATTENTION: The Singapore Copyright Act applies to the use of this document. Nanyang Technological University Library

used on thin film or bulk materials and no research on patterned wafers were reported. And how to get suitable TDDB samples for FITR and Raman spectroscopy is another challenging as electric overstress was always out of control after dielectric breakdown.

In our preliminary study on Raman spectroscopy and FTIR spectroscopy, we successfully detected the signal on patterned wafers by experiments with different laser wafer length [14]. With these, we can move forward to apply Raman and FTIR into the TDDB analysis [15].

With the advance of device scaling, The copper (Cu) and the Low k dielectrics are essential for the reduction of Resistance–Capacitance (RC) delays, cross talk noise minimization, and power dissipation reduction. However the long term reliability is also a critical criteria from the technology qualification point of view. Low k time-dependent dielectric breakdown (TDDB) is commonly used as an important reliability test to test the IMD reliability [16].

Because the low k dielectrics generally has weaker intrinsic breakdown strength than traditional SiO_2 dielectrics, the degradation of inter-metal dielectrics (IMD), especially with low k and ultra-low k material, causes backend-of-the-line (BEOL) reliability issue for the leading edge semiconductor technologies. Many studies have been published to understand the mechanism of ultra-low k TDDB failure. With the hypothesis of the Cu diffusion or the suspected possible degradation or damage on the low k materials, there are some of models were proposed with 1/E [17, 18].or $1/\sqrt{E}$ [17]. models. The first TDDB model could be occurred as a result of electric field induced breakage of weak chemical bonds in the dielectric network so that new defects called traps are generated [18]. The other electronfluence-driven Cu-catalyzed SiCOH TDDB

ATTENTION: The Singapore Copyright Act applies to the use of this document. Nanyang Technological University Library

model was proposed by Chen [19]. This links to the breakdown model during the electrons transport across the dielectric. In recent research, the material degradation was detected by Raman and FTIR spectroscopy and Ta migration into the IMD was revealed with TEM analysis after Raman and FTIR spectroscopy analysis. Due to the difference to the prior models based on the hypothesis of Cu diffusion or the suspected IMD degradation or damage.

In this chapter, we will discuss the results of the TDDB reliability qualification on ultra-low k dielectric of the leading edge technologies and setup a model to fit the latest finding on the TDDB failure mechanism of ultra low k degradation and barrier metal (Ta) migration. DOE lots were designed to explore the line-edge-roughness (LER) effect to TDDB failure.

6.2 EXPERIMENTAL DETAILS

A. Ta Migration caused TDDB

The experiments were conducted with a Cu/ultra low k technology node fabricated with a dual damascene process. The ultra low k dielectrics are a porous SiCOH low k dielectric. In the Cu/ultra-low k integration process, 10 nm Ta/TaN barrier bi-layer and 50nm SiN capping layer were formed as shown in Figure 6.1. A properly deposited TaN/Ta stack forms a low resistivity α-Ta phase. The Ta/TaN barrier is also needed to avoid Cu corrodes & migration. The test structures used for our experiments are planar comb capacitor structures consisting of 300 Cu lines with a length of 40 um as shown in Figure 6.2. The Cu line trench has a sloped profile with a top Cu line-to-line spacing of 50 nm and a bottom line-to-line spacing of 70 nm.

ATTENTION: The Singapore Copyright Act applies to the use of this document. Nanyang Technological University Library

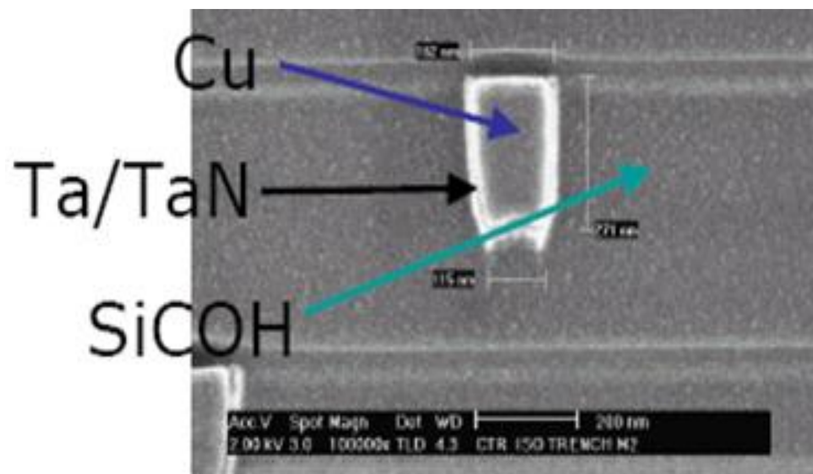

Figure 6.1 Cu/Ta/TaN/Low k SiCOH Damascene structure

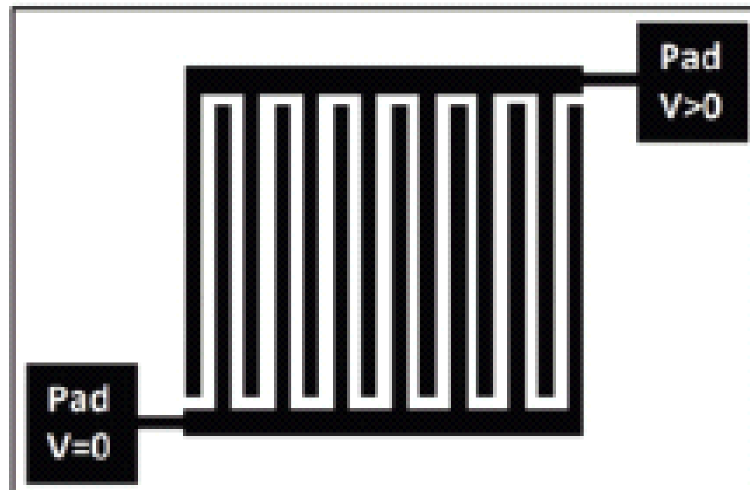

Figure 6.2 TDDB Test Structure

Figure 6.3 shows the TDDB distribution over the different electrical field stress (4.8, 5.1 & 5.4mV/cm) on the test structure. The Electrical field strength (E) in this study is calculated by the applied stress voltage divided by the smallest distance between metal lines which in this case is top Cu line-to-line spacing of 50 nm. A Weibull distribution is established with this data. It is obvious that the higher stress voltage applied, the shorter dielectric breakdown time was observed on the same wafer and same test structure. The TDDB is modulated by electrical field; however, the electrical field doesn't affect the

ATTENTION: The Singapore Copyright Act applies to the use of this document. Nanyang Technological University Library

TDDB distribution which suggests it should be an intrinsic degradation due to process weakness.

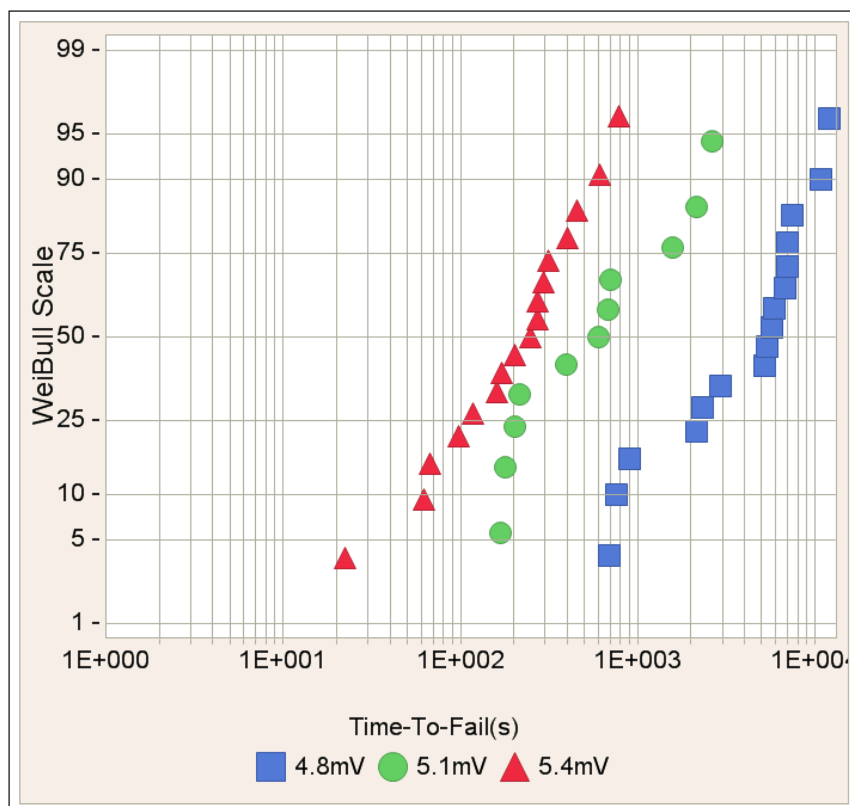

Figure 6.3 Measured TDDB on POR wafers under different stress Fields

ATTENTION: The Singapore Copyright Act applies to the use of this document. Nanyang Technological University Library

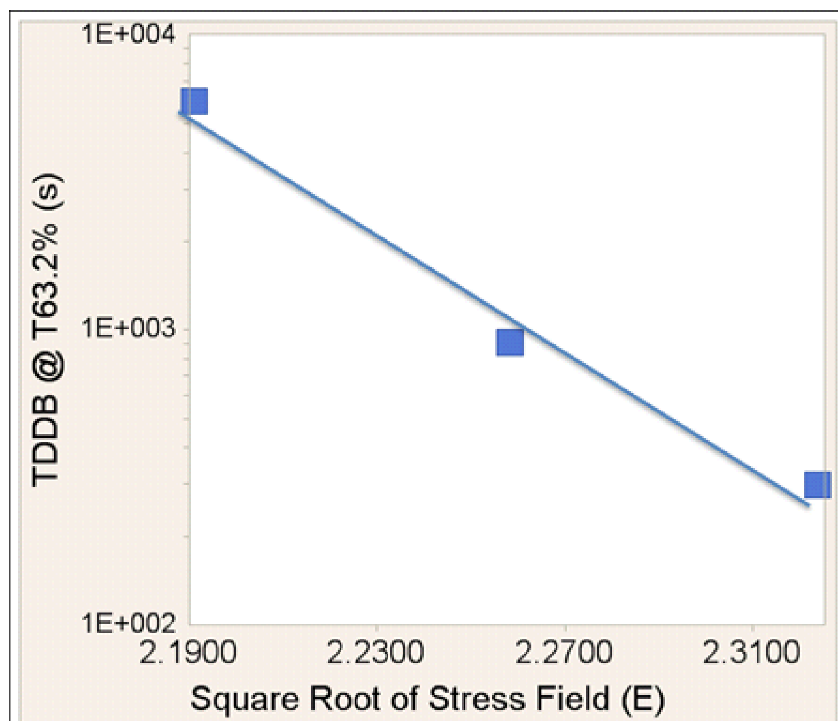

Figure 6.4 Measured TDDB @ T63.2(s) shows consistent with Square Root E Model for Ta Migration wafer

The Weibull characteristic failure percentages (t63.2%) at different square root of electrical stress field are further plotted on the log scale. In Figure 4, The "square root of E" (√E) dependence was found of which traditionally involves migration of Cu into the low k dielectric prior to breakdown at SiCOH–Cap interface [1, 2]. In order to know the mechanism of this TDDB failure, the FA was conducted on the samples before and after the stress. From the (Transmission electron microscopy) TEM and (Energy-dispersive X-ray) EDX analysis, a Ta migration is observed distance away from the capping layer as shown in the Figure 5.4. Based on this finding, a new failure mechanism of Ta migration for TDDB failure was found. The √E-model can be universal curve for different failure mechanisms at different technology node with different integration schemes.

ATTENTION: The Singapore Copyright Act applies to the use of this document. Nanyang Technological University Library

In our experiments, the TaN migration only happened at upper corner of the Copper trench. This can be explained by the following. First there's higher electrical field at top due to closer space from the sloped etch profile [21, 22]. Second, the corner of Cu trench is angular; the electric field is more likely to concentrate there. It is illustrated in Figure 6.5 by the simulation.

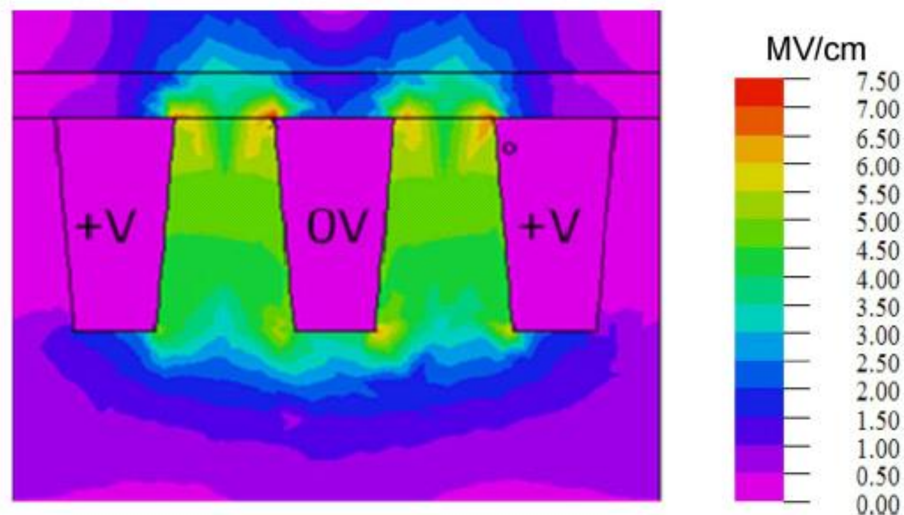

Figure 6.5 Simulation of the electric field distribution on a E-test comb structure [19].

Although Ta/TaN barrier metal provides better migration resistance than Copper [23]., the problem is that the pores in ultralow k materials can be highly connected and provide migration paths for processing gases and moistures [24]. That path is similar to capping layer which normally observed from Copper migration [25]. As shown in Figure 6.6, TDDB occurred when Ta ions accumulated near the cathode over a critical concentration. Since the top trench has higher electrical field and the capping layer had a stronger dielectric strength than the ultra-low k, the migrating Ta ions preferred the path along the weakened ultra-low k dielectric which some distance away from capping layer.

ATTENTION: The Singapore Copyright Act applies to the use of this document. Nanyang Technological University Library

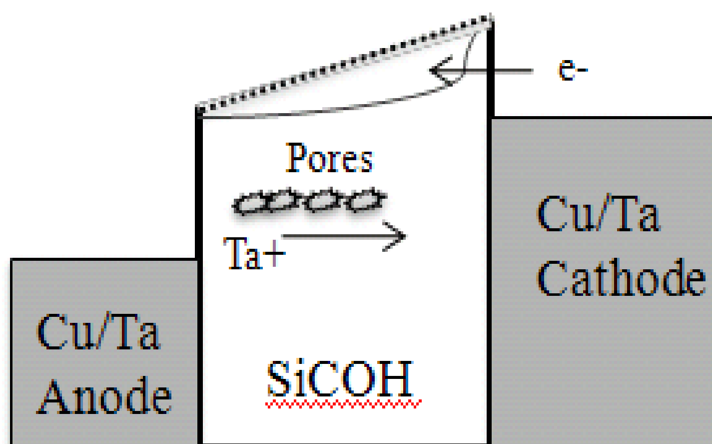

Figure 6.6 bond diagram for Ta Migration

For the Ta migration, the standard quantitative expression for the Poole–Frenkel effect is:

$$n_i \propto n_0 \exp\left[\frac{q}{k_B T}\sqrt{\frac{qE}{\pi\varepsilon_0 k}}\right]. \qquad (1)$$

The time to failure is therefore given by: [1, 7].

$$TTF \propto \frac{1}{E}\exp\left[-\frac{q}{k_B T}\left(\frac{q}{\pi\epsilon_0 k}\right)^{1/2}\sqrt{E}\right]. \qquad (2)$$

This aligns our previous observation that the Ta migration induced Time to Failure can fit to “square root of E” models.

B. line-edge-roughness (LER) effect on DOE lots

In order to explore the LER effect on TDDB, a further experiment was done to use Reactive Ion Etch (RIE) metal etch recipe to carefully control the metal edge roughness as shown in Figure 6.7. On the other hand, studying the LER effect from RIE recipe is very important for TDDB qualification on the process development.

ATTENTION: The Singapore Copyright Act applies to the use of this document. Nanyang Technological University Library

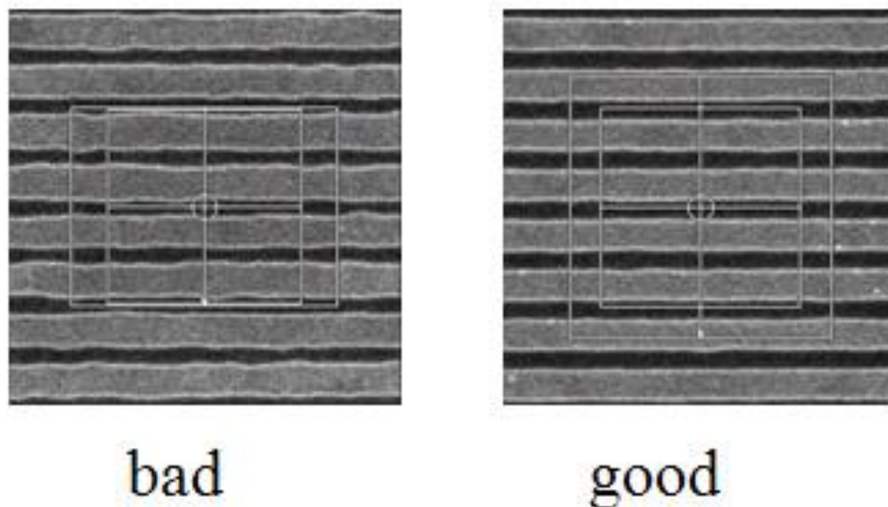

Figure 6.7 Metal Profile after Metal RIE & CMP for split wafers

Figure 6.8 shows the TDDB of the good and bad LER wafers at different Stress Field (4, 4.5 & 5mV/cm). The good LER wafers not only exhibits a better TDDB performance, but also the bad LER wafer has more sloped distribution on the higher electrical field which suggests the line edge roughness can accelerate the Cu or Ta migration.

ATTENTION: The Singapore Copyright Act applies to the use of this document. Nanyang Technological University Library

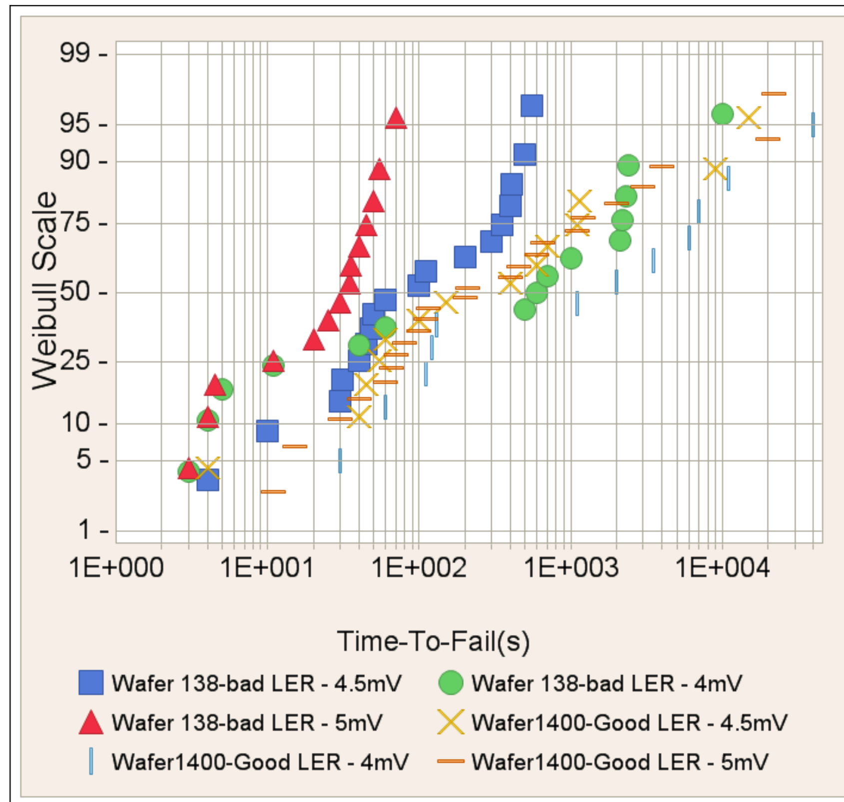

Figure 6.8 Tbd of bad LER Wafer(138) & Good LER Wafer(1400)

The 63.2% percentile of Weibull Tbd distribution should be mainly determined by LER and can be modeled by "square root of E" ($\sqrt{\mathrm{E}}$) model as shown in Figure 6.9. From this plot, it once again proves the good LER wafer not only has longer TDDB, but also a better slope of TDDB characteristic than bad wafer. For the bad wafer, rough line sidewalls will produce a non-uniform field which can be explained by field factor $\sqrt{\mathrm{E}} = \sqrt{\mathrm{V}}/\sqrt{\mathrm{S}}$, a small spacing variation could result in a large electrical field variation. This may produce some localized high field region which can increase the leakage current & weaken the TDDB strength. To prevent the Cu/Ta diffusing into dielectric, it's very essential to have an optimized lithograph, etch and chemical mechanical planarization

ATTENTION: The Singapore Copyright Act applies to the use of this document. Nanyang Technological University Library

(CMP) process to create a better metal profile to improve the TDDB performance in 40nm technology.

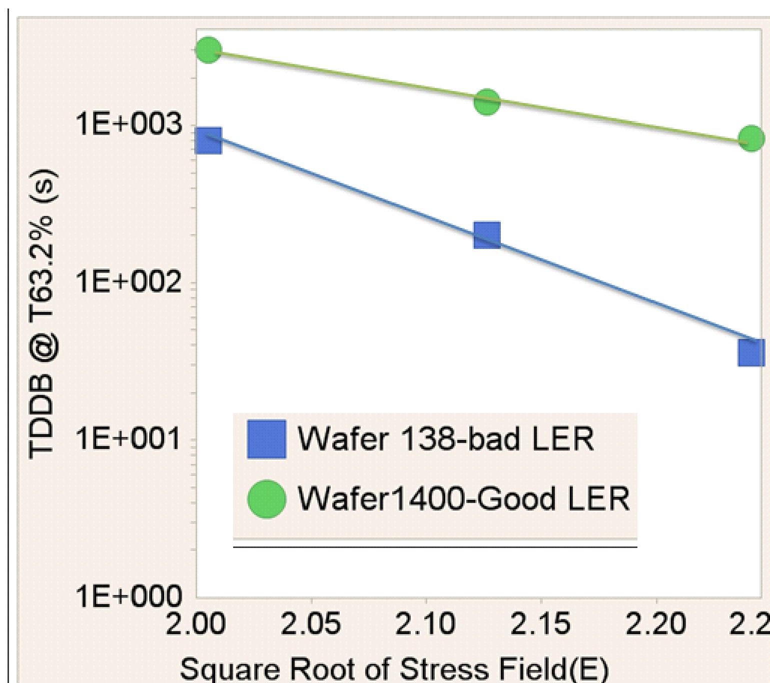

Fig.6.9 Measured TDDB @ T63.2(s) shows consistent with Square Root E Model, the bad LER wafer shows degradation on the TDDB.

5.3 Conclusion

In conclusion, 2 key issues for Cu/Ultra-Low k dielectric TDDB failures are discussed in this paper. For the first time, a new TDDB failure mechanism based on Ta/TaN barrier metal migration which occurred some distance away from capping layers is proposed. The pores in ultra-low k materials were degraded under high electrical field, resulting in the Ta ionic migration into the degraded IMD. This failure mechanism fits well to the "square root of E" √(E)model. Additionally, a DOE lot with RIE etch splits was designed to explore the LER effect on TDDB. A unified model and understanding for the spacing variations was established. In summary, we can see that more dense Ultra-

ATTENTION: The Singapore Copyright Act applies to the use of this document. Nanyang Technological University Library

Low k dielectric material, a better slopped trench/Via profile and more tightened control on metal roughness are needed for a robust ultra-low k TDDB performance.

ATTENTION: The Singapore Copyright Act applies to the use of this document. Nanyang Technological University Library

Chapter 7 Conclusion and Future Work

7.1 Conclusion

In order to reduce RC delay to meet IC performance required in leading edge technologies, Cu and ultra-low k dielectric are introduce to replace Al and SiO_2 as metal interconnects and IMD, respectively. Cu has a resistivity 36% lower than Al. The dielectric constant of SiO_2 is 3.9, while low k dielectrics have dielectric constant between 2 to 3. With the introduction ofpores into low k dielectrics, the dielectric constants of ultra-low k dielectrics can be reduced to a value less than 2.

However, low k dielectric reliability becomes challenging due to the weak mechanical strength and chemical bonding characteristics of ultra-low k dielectrics. As a result of a weakened material strength, Cu drift becomes a serious concern for Cu/low k interconnects. From IC fabrication point of view, LER is one of the important factors of leakage and breakdown properties. This explains why leakage and breakdown properties are important selection criteria for low k dielectrics.

TDDB is commonly used for low k dielectric reliability test. Many TDDB studies on a wide range of area and electrical fields are carried out to reveal the mechanism of TDDB failure of low k dielectrics. Simulation and modeling are also widely studied in recent years.

However, in TDDB analysis, the process and damage mechanism of low k dielectric in TDDB test is uncertain. FTIR and Raman spectroscopy are the most promising techniques to identify the chemical bonding change during the TDDB test.

ATTENTION: The Singapore Copyright Act applies to the use of this document. Nanyang Technological University Library

Current FTIR and Raman techniques are widely used on thin film or bulk materials and no research on patterned wafers is reported. Obtaining suitable TDDB samples for FITR and Raman spectroscopy is another challenging aspect of this project as electrical overstress usually occursoon after dielectric breakdown.

SiCOH low k/ultra-low k dielectric thin films on patterned wafers have been characterized by Raman spectroscopy. It is found that the Raman spectra vary significantly under influence from various laser sources, in specific 532 and 325 nm wavelength lasers. With visible laser, the SiCOH dielectric on patterned wafers is partially characterized and Si signals are simultaneously collected in the SiCOH spectrum. Compared to the visible laser, UV laser has an advantage for measuring a few tens of nanometers from the SiCOH surface, and hence, its spectrum is more complete. Meanwhile, FTIR spectrum is an effective complementary tool for characterizing SiCOH on patterned wafers. There are also significant differences in the Raman and FTIR spectra between low k and ultra-low k dielectrics due to their different deposition processes. Finally, individual SiCOH Raman signal has been successfully extracted from the ultra-low k/Cu mixed structure at nanometer-scale sizes.

We have shown that FTIR spectroscopy can be used to investigate the low k dielectrics on patterned wafers, all three modes used in this investigation showed satisfactory results. Our study suggests that:

1). ATR mode is more suitable for monitoring the UV curing due to its higher sensitivity on CH_x band over reflection mode;

2). It is possible to pinpoint the failure sites over large area by mapping mode.

ATTENTION: The Singapore Copyright Act applies to the use of this document. Nanyang Technological University Library

Our current study is mainly focused on X-Y 2-D analysis. Investigation for the Z-direction resolution across different thin layers remains challenging challenge and we will extend the current study into that scope as part of future work.

We observed ultra-low k dielectric degradation in TDDB test using the complementary application of Raman and FTIR vibrational spectroscopy. Under the applied electrical field, he intrinsic degradation of the ultra-low k dielectric would first occur and Ta ions would then migrate into ultra-low k along the weakened interface of Cu/Ta/TaN/SiCOH, causing a more severe damage to the ultra-low k dielectric. The Ta ions inside the ultra-low k induced an increased local electrical field between Cu electrodes and thus accelerated ultra-low k degradation to final breakdown. In our investigation on the Cu/Ta/TaN/SiCOH structures, no out-diffusion of Cu ions is observed.

For the first time, a new TDDB failure mechanism based on Ta/TaN barrier metal migration which occurred some distance away from capping layers is proposed. The pores in ultra-low k materials are degraded under high electrical field, resulting in Ta ionic migration into the degraded IMD. This failure mechanism fits well to the "square root of E" $\sqrt{(E)}$ model. Additionally, wafers with RIE etch splits are designed to explore LER effect on TDDB. A unified model and understanding for the spacing variations is established. In summary, we can see that more dense Ultralow k dielectric material will lead to a better slopped trench/Via profile and more tightened control on metal roughness are needed for a robust ultra-low k TDDB performance.

7.2 Future Work

ATTENTION: The Singapore Copyright Act applies to the use of this document. Nanyang Technological University Library

Our analysis methodology opens a new direction for TDDB analysis on low k/Cu IC technology. It provides the root cause for TDDB failure. Moving forward, to get the methodology and analytical technique practical to industry, further investigation and development will be needed and we will continue to work on the following investigation for industrial implementations:

1. Improving the sensitivity based on the light scattering from nano structures in the patterned IC devices.
2. Develop a low electrical field TDDB hardware or software at low cost. Low electrical field TDDB test usually require a long stress time of up to months. Our current setup costs about USD 100 k.
3. Automatic control on the stress test. In current industrial practice, the test was monitored with data recording. However, the overstress will cause some unexpected damage on the device. The evidence for TDDB failure mechanism could be destroyed by the overstress.
4. Real time Raman and FTIR monitoring will help us to understand how the TDDB damage developed during the stress.
5. Measure optical spectra connecting to accelerated lifetest. Large sample size for data collection was needed the analysis. TDDB is a low process up to months for a device under test (DUT) at low voltage stress below the breakdown field, at which the Flowler-Nordheim tunneling occurs.
6. Time-dependent Raman and FTIR. Technology challenges need to be resolved on the laser beam or spot shift on the sample at long time intervals as the TDDB test is a long testing process.

ATTENTION: The Singapore Copyright Act applies to the use of this document. Nanyang Technological University Library

ATTENTION: The Singapore Copyright Act applies to the use of this document. Nanyang Technological University Library

References

Chapter 1

1. International Technology Roadmap for Semiconductors: 2010 Update.
2. B. Lee, W. Oh, Y. Hwang, Y.-H. Park, J. Yoon, K. S. Jin, K. Heo, J. Kim, K.-W. Kim, M. Ree, Imprinting Well-Controlled Nanopores in Organosilicate Dielectric Films: Triethoxysilyl-Modified Six-Armed Poly(-caprolactone) and Its Chemical Hybridization with an Organosilicate Precursor, Advanced Materials, 17(6), 696-701 (2005).
3. Mihail P. Petkov, Low k Dielectric Technology, March 2003, NASA Electronic Parts and Packaging, Jet Propulsion Laboratory.
4. Gaddi S. Haase, Ennis T. Ogawa, and Joe W. McPherson, Reliability analysis method for low k interconnect dielectrics breakdown in integrated circuits, JOURNAL OF APPLIED PHYSICS 98, 034503 (2005).
5. Low-k dielectric reliability. http://www.imec.be/ScientificReport/SR2010/2010/1159201.html.
6. Fen Chen and Mike Shinosky, Addressing Cu/Low k Dielectric TDDB-Reliability Challenges for Advanced CMOS Technologies, IEEE TRANSACTIONS ON ELECTRON DEVICES, 56 (1), 2-12 (2009).
7. J. R. Lloyd et al., "Role of CU in TDDB of low k dielectrics," in Proc. 45th Annu. IEEE IRPS, 410–411 (2007).

ATTENTION: The Singapore Copyright Act applies to the use of this document. Nanyang Technological University Library

8. A. T. Kimet al., “Line edge roughness of metal lines and time-dependent dielectric breakdown characteristics of low k interconnect dielectrics,” in Proc. IEEE IITC, 155–157 (2007).
9. McPherson, J.; Reddy, V.; Banerjee, K.; Huy Le; Comparison of E and 1/E TDDB models for SiO_2 under long-term/low-field test conditions Electron Devices Meeting, 1998. IEDM '98 Technical Digest., International 06 Dec 1998 - 09 Dec 1998. Location: San Francisco, CA , USA. 171 – 174.
10. Time Dependent Dielectric Breakdown Characteristics of Low k Dielectric (SiOC) Over a Wide Range of Test Areas and Electric Fields, Jinyoung Kim Ogawa, E.T. McPherson, J.W. Silicon Technol. Dev., Reliability physics symposium, 2007. proceedings. 45th annual. ieee international, 15-19 April 2007. 399 – 404.
11. A Comprehensive LER-Aware TDDB Lifetime Model for Advanced Cu Interconnects, Stucchi, M.; Roussel, P.J.; Tokei, Z.; Demuynck, S.; Groeseneken, G.; , IEEE Transactions on Device and Materials Reliability, 11 (2), 278 – 289 (2011).
12. J. Noguchi "Dominant factors in TDDB degradation of Cu interconnects", IEEE Trans. Electron Devices, vol. 52, no. 8, 2005, 1743 - 1750.
13. Study on Factors in Time-Dependent Dielectric Breakdown Degradation of Cu/Low k Integration Related to Cu Chemical–Mechanical Polishing, Yohei Yamada, Nobuhiro Konishi, Junji Noguchi, Tomoko Jimbo1, Syuhei Kurokawa, and Toshiro Doi, Jpn. J. Appl. Phys. 47, 4469-4474 (2008).

ATTENTION: The Singapore Copyright Act applies to the use of this document. Nanyang Technological University Library

14. Investigation of electrical conduction in carbon-doped silicon oxide using a voltage ramp method , K. Y. Yiang1, W. J. Yoo1, Q. Guo2, and Ahila Krishnamoorthy Appl. Phys. Lett. 93, 122902 (2008).
15. Charge trapping at the low k dielectric-silicon interface probed by the conductance and capacitance techniques, J. M. Atkin1, E. Cartier2, T. M. Shaw2, R. B. Laibowitz3, and T. F. Heinz, Appl. Phys. Lett. 93, 122902 (2008). .
16. M. Benyoucef. Raman scattering and photoluminescence studies on Si/ SiO_2 superlattices. J. App. Phy. 89, 155–158 (2001).
17. Colin. N Banwell and Elaine. M McCash, editors. Fundamentals of Molecular Spectroscopy., McGraw-Hill PUblishing Company, Shoppenangers Road, Maidenhead, Berkshire, SL6 2QL, England, 1994.
18. N. B. Colthup. Introduction to infrared and raman spectroscopy. Academic Press, New York, 1964.
19. Introductory Raman Spectroscopy, Second Edition. Elsevier Science (USA), 2003.
20. Kim Y-H, Hwang MS, Kim HJ, Kim JY, Lee Y. Infrared spectroscopy study of low-dielectric-constant fluorine-incorporated and carbon-incorporated silicon oxide films, J. Appl. Phys. 90, 3367 (2001).
21. Yang CS, Yu Y-H, Lee K-M, Lee H-J, Choi CK. The influence of carbon content in carbon-doped silicon oxide film by thermal treatment. Thin Solid Films, 435-165 (2003).

ATTENTION: The Singapore Copyright Act applies to the use of this document. Nanyang Technological University Library

22. Brusa RS, Spagolla M, Karwasz GP, Zecca A, Ottaviani G, Corni F, Bacchetta M, Carollo E. Porosity in low dielectric constant SiOCH films depth profiled by positron annihilation spectroscopy. J Appl Phys 95, 2348 (2004).

23. Vibrational spectroscopy characterization of low-dielectric constant SiOC:H films prepared by PECVD technique, G. Das, G. Mariotto, A. Quaranta, Materials Science in Semiconductor Processing, 7, 295–300 (2004).

24. J.P. Godschalx, et.al., "Polyphenylene oligomers and polymers," United States Patent No. 5,965,679, October 1999.

25. J. D. Lichtenhan, "Silsesquioxane polymers," in Polymer Handbook, CRC Press, 1996, 7768 (1996).

26. N. P. Hacker, "Organic and inorganic spin-on polymers for low-dielectric constant applications," MRS Bulletin 22 (10), 33 (1997).

27. P. J. Launer, "Infrared analysis of organosilicon compounds: spectra-structure correlations," Silicone Compounds Register and Review, Ed. By B. Arkles, et al., 100 (1987).

28. G. Lucovsky, et.al., "Low-temperature growth of silicon dioxide films: a study of chemical bonding by ellipsometry and infrared spectroscopy," J. Vac. Sci. Technol. B 5(2), 530 (1987)

29. Y-H Kim, et.al., "Infrared spectroscopy study of low-dielectric-constant fluorine-incorporated and carbon-incorporated silicon oxide films," J. Appl. Phys. 90(7), 3367 (2001).

30. P.G. Pai, et.al., "Infrared spectroscopic study of SiOx films produced by plasma enhanced chemical vapor deposition," J. Vac. Sci. Technol. A 4(3), 689 (1986).

ATTENTION: The Singapore Copyright Act applies to the use of this document. Nanyang Technological University Library

31. Y.S. Mor, et.al., “Effective repair to ultra-low k dielectric (k~2.0) by hexamethyldisilazane treatment,” J. Vac. Sci. Technol. B 20(4), 1334 (2002).

Chapter 3

1. K. Maex, M. R. Baklanov, D. Shamiryan, F. Iacopi, S. H. Brongersma, and Z. S. Yanovitskaya, “Low dielectric constant materials for microelectronics”, J. Appl. Phys. 93, 8794 (2003).
2. W. Volksen, R. D. Miller, and G. Dubois, "Low Dielectric Constant Materials", Chem. Rev. 110, 56 (2010).
3. A. Grilla and V. Patel, “Ultralow k dielectrics prepared by plasma-enhanced chemical vapor deposition”, Appl. Phys. Lett. 79, 803 (2001).
4. Y. Q. Huang and J. Economy, “New high strength low k spin-on thin films for IC application”, Macromolecules 39, 1850 (2006).
5. M. He, S. Novak, L. Vanamurthy, H. Bakhru, J. Plawsky, and T. M. Liu, “Cu penetration into low k dielectric during deposition and bias-temperature stress”, Appl. Phys. Lett. 97, 252901 (2010).
6. J. R. Lioyd, C. E. Murray, S. Ponoth, S. Cohen, and E. Liniger, “The effect of Cu diffusion on the TDDB behavior in a low k interlevel dielectrics”, Microelectron. Reliab. 46, 1643 (2006).
7. K. Kohama, K. Ito, K. Mori, K. Maekawa, Y. Shirai, and M. Murakami, “Rutherford Backscattering Spectrometry Analysis of Self-Formed Ti-Rich Interface Layer Growth in Cu(Ti)/Low k Samples”, J. Electron. Mater. 38, 1913 (2009).

ATTENTION: The Singapore Copyright Act applies to the use of this document. Nanyang Technological University Library

8. E. Maatinez, N. Rochat, C. Guedj, C. Licitra, G. Imbert, and Y. L. Friec, “Influence of electron-beam and ultraviolet treatments on low k porous dielectrics”, J. Appl. Phys. 100, 124106 (2006).
9. N. Ghalichechian, A. Modafe, R. Ghodssi, P. Lazzeri, V. Micheli, and M. Anderte, “Integration of benzocyclobutene polymers and silicon micromachined structures using anisotropic wet etching”, J. Vac. Sci. Technol. B 22, 2439 (2004).
10. J. Bao, H. Shi, J. Liu, H. Huang, P. S. Ho, M. D. Goodner, M. Moinpour, and G. M. Kloster, “Mechanistic study of plasma damage of low k dielectric surfaces”, J. Vac. Sci. Technol. B 26, 219 (2008).
11. M. A. Worsley, S. F. Bent, N. C. M. Fuller, T. L. Tai, J. Doyle, M. Rothwell, and T. Dalton, “Effect of radical species density and ion bombardment during ashing of extreme ultralow kappa interlevel dielectric materials”, J. Appl. Phys. 101, 013305 (2007).
12. X. F. Hua, C. Stolz, G. S. Oehrlein, P. Lazzeri, N. Coghe, M. Anderle, C. K. Inoki, T. S. Kuan, and P. Jiang, “Plasma-surface interactions of nanoporous silica during plasma-based pattern transfer using C4F8 and C4F8/Ar gas mixtures”, J. Vac. Sci. Technol A 23, 151 (2005).
13. Q. Wu and K. Gleason, “Plasma-enhanced chemical vapor deposition of low k dielectric films using methylsilane, dimethylsilane, and trimethylsilane precursors”, J. Vac. Sci. Technol. A 21, 388 (2003).
14. H. W. Ro, H. Peng, K. Niihara, H. Lee, E. K. Lin, A. Karim, D. W. Gidley, H. Jinnal, D. Y. Yoon, and C. L. Soles, “Self-sealing of nanoporous low dielectric

ATTENTION: The Singapore Copyright Act applies to the use of this document. Nanyang Technological University Library

constant patterns fabricated by nanoimprint lithography”, Adv. Mater. 20, 1932 (2008).

15. C. Cartereta and A. Labrosseb, “Vibrational properties of polysiloxanes: from dimer to oligomers and polymers. 1. Structural and vibrational properties of hexamethyldisiloxane (CH(3))(3)SiOSi(CH(3))(3)”, J. Raman Spectrosc. 41, 996 (2010).
16. N. J. Trujillo, Q. Wu, and K. K. Gleason, “Ultralow Dielectric Constant Tetravinyltetramethylcyclotetrasiloxane Films Deposited by Initiated Chemical Vapor Deposition (iCVD)”, Adv. Funct. Mater. 20, 607 (2010).
17. A. Grill and D. A. Neumayer, “Structure of low dielectric constant to extreme low dielectric constant SiCOH films: Fourier transform infrared spectroscopy characterization”, J. Appl. Phys. 94, 6697 (2003).
18. H. L. Shi, J. J. Bao, J. J. Liu, H. Huang, P. S. Ho, M. D. Goodner, M. Moinpour, and G. M. Kloster, “Effect of CH4 plasma treatment on O2 plasma ashed organosilicate low k dielectrics”, Mater. Res. Soc. Symp. Proc. 990, 51 (2007).
19. H. L. Shi, J. Bao, R. S. Smith, H. Huang, J. Liu, P. S. Ho, M. L. Mcswiney, M. Moinpour, and G. M. Kloster, “Origin of dielectric loss induced by oxygen plasma on organo-silicate glass low k dielectrics”, Appl. Phys. Lett. 93, 192909 (2008).
20. J. Bao, H. L. Shi, J. Liu, H. Huang, P. S. Ho, M. D. Goodner, M. Moinpour, G. M. Kloster, and G. M. Kloster, “Mechanistic study of plasma damage of low k dielectric surfaces”, J. Vac. Sci. Technol. B 26, 219 (2008).

ATTENTION: The Singapore Copyright Act applies to the use of this document. Nanyang Technological University Library

21. B. C. Trasferetti, C. U. Davanzo, and M. A. Moraes, “Infrared and Raman studies on films of organosiloxane networks produced by PECVD”, Macromolecules 37, 459 (2004).

22. C. Doux, K. C. Aw, M. Niewoudt, and W. Gao, “Analysis of HSG-7000 silsesquioxane-based low k dielectric hot plate curing using Raman spectroscopy”, Microelectron. Eng. 83, 387 (2006).

23. F. Balon, V. Stolojan, S. R. P. Silva, M. Michalka, and A. Kromka, “Diamond-like carbon thin films for high-temperature applications prepared by filtered pulsed laser deposition”, Vacuum 80, 163 (2005).

24. W. Mroz, S. Burdynska, A. Prokopiuk, M. Jedynski, B. Budner, and M. L. Korwin, “Characteristics of Carbon Films Deposited by Magnetron Sputtering”, Acta. Phys. Pol. A 116, 120 (2009).

25. A. Morimoto, M. Kumeda, and T. Shimizu, J. “CRYSTALLIZATION PROCESS IN TETRAHEDRALLY BONDED BINARY AMORPHOUS-SEMICONDUCTORS”, Non-Cryst. Solids 59&60, 537 (1983).

26. P. Verdonck, D. De Roest, S. Kaneko, R. Caluwaerts, N. Tsuji, K. Matsushita, N. Kemeling, Y. Travaly, H. Sprey, M. Schaekers, and G. Beyer, “Characterization and optimization of porogen-based PECVD deposited extreme low k dielectrics as a function of UV-cure time”, Surf. Coat. Technol. 201, 9264 (2007).

27. L. Prager, P. Marsik, L. Wennrich, M. R. Baklanov, S. Naumov, L. Pistol, D. Schneider, J. W. Gerlach, P. Verdonck, and M. R. Buchmeiser, “Effect of pressure on efficiency of UV curing of CVD-derived low k dielectric at different wavelengths”, Microelectron. Eng. 85, 2094 (2008).

ATTENTION: The Singapore Copyright Act applies to the use of this document. Nanyang Technological University Library

28. H. Ehrenreich and H. R. Philippi, “Optical Properties of Ag and Cu”, Phys. Rev. 121, 1622 (1962).

29. S. Kondoju, C. Lucas, P. Raghavan, S. Fischer, P. Moinpour, and M. Oehler, “Feasibility of detecting barrier layer to low k transition in copper CMP using Raman spectroscopy”, Mater. Res. Soc. Symp. Proc. 867, 175-181 (2005).

Chapter 4

1. C. Carteret and A. Labrosse, “Vibrational properties of polysiloxanes: from dimer to oligomers and polymers. 1. Structural and vibrational properties of hexamethyldisiloxane (CH3)(3)SiOSi(CH3)(3)”, J. Raman Spectrosc. 41, 996 (2010).
2. A. D. Ross and K. K. Gleason, “Enhancement of mechanical properties of organosilicon thin films deposited from diethylsilane”, J. Vac. Sci. Technol. A 23, 465 (2005).
3. M. He, S. Novak, L. Vanamurthy, H. Bakhru, J. Plawsky and T. M. Lu, “Cu penetration into low k dielectric during deposition and bias-temperature stress”, Appl. Phys. Lett. 97, (2010).
4. J. R. Lloyd, C. E. Murray, S. Ponoth, S. Cohen and E. Liniger, “The effect of Cu diffusion on the TDDB behavior in a low k interlevel dielectrics”, Microelectron. Reliab. 46, 1643 (2006).
5. B. N. Joshi, M. A. More and A. M. Mahajan, “Growth and characterization of MMA/ SiO_2 hybrid low k thin films for interlayer dielectric applications”, Bull. Mat. Sci. 33, 197 (2010).

ATTENTION: The Singapore Copyright Act applies to the use of this document. Nanyang Technological University Library

6. N. Posseme, T. Chevolleau, T. David, M. Darnon, O. Louveau and O. Joubert, “Mechanisms of porous dielectric film modification induced by reducing and oxidizing ash plasmas”, J. Vac. Sci. Technol. B 25, 1928 (2007).
7. P. Verdonck, D. De Roest, S. Kaneko, R. Caluwaerts, N. Tsuji, K. Matsushita, N. Kemeling, Y. Travaly, H. Sprey, M. Schaekers and G. Beyer, “Characterization and optimization of porogen-based PECVD deposited extreme low k dielectrics as a function of UV-cure time”, Surf. Coat. Technol. 201, 9264 (2007).
8. S. Lee, J. Yang, S. Yeo, J. Lee, D. Jung, J. H. Boo, H. Kim and H. Chae, “Effect of annealing temperature on dielectric constant and bonding structure of low k SiCOH thin films deposited by plasma enhanced chemical vapor deposition”, Jpn. J. Appl. Phys. Part 1 - Regul. Pap. Brief Commun. Rev. Pap. 46, 536 (2007).
9. A. L. Smith, “INFRARED SPECTRA-STRUCTURE CORRELATIONS FOR ORGANOSILICON COMPOUNDS”, Spectrochimica Acta 16, 87 (1960).
10. V. Jousseaume, L. Favennec, A. Zenasni and O. Gourhant, “Porous ultra-low k deposited by PECVD: From deposition to material properties”, Surf. Coat. Technol. 201, 9248 (2007).
11. Y. Shioya, T. Ohdaira, R. Suzuki, Y. Seino and K. Omote, “Effect of UV anneal on plasma CVD low k film”, J. Non-Cryst. Solids 354, 2973 (2008).
12. C. H. Huang, H. L. Huang, C. I. Hung, N. F. Wang, Y. H. Wang and M. P. Houng, “Bond structure in porous SiOCH low k film fabricated by ultraviolet irradiation”, Jpn. J. Appl. Phys. 47, 1532 (2008).

ATTENTION: The Singapore Copyright Act applies to the use of this document. Nanyang Technological University Library

13. S. M. Gates, D. A. Neumayer, M. H. Sherwood, A. Grill, X. Wang and M. “Sankarapandian, Preparation and structure of porous dielectrics by plasma enhanced chemical vapor deposition”, J. Appl. Phys. 101, (2007).
14. J. Ushio, T. Ohno, T. Hamada, S. I. Nakao, K. Yoneda, M. Kato and N. Kobayashi, “Ultraviolet-curing mechanism of porous-SiOC”, Jpn. J. Appl. Phys. Part 2 - Lett. Express Lett. 46, L405 (2007).
15. L. Prager, P. Marsik, L. Wennrich, M. R. Baklanov, S. Naumov, L. Pistol, D. Schneider, J. W. Gerlach, P. Verdonck and M. R. Buchmeiser, “Effect of pressure on efficiency of UV curing of CVD-derived low k dielectric at different wavelengths”, Microelectron. Eng. 85, 2094 (2008).
16. S. Sayan, D. Chandler-Horowitz, N. V. Nguyen and J. R. Ehrstein, “High sensitivity attenuated total reflection Fourier transform infrared spectroscopy study of ultrathin ZrO2 films: A study of phase change”, J. Vac. Sci. Technol. A 26, 270 (2008).

Chapter 5

1. International Technology Roadmap for Semiconductors: 2011 Update.
2. G. S. Haase, E. T. Ogawa, and J. W. McPherson, “Reliability analysis method for low k interconnect dielectrics breakdown in integrated circuits”, J. Appl. Phys. **98**, 034503 (2005).
3. K. Maex, M. R. Baklanov, D. Shamiryan, F. Iacopi, S. H. Brongersma, and Z. S. Yanovitskaya, “Low dielectric constant materials for microelectronics”, J. Appl. Phys. **93**, 8794 (2003).
4. W. Volksen, R. D. Miller, and G. Dubois, “Low Dielectric Constant Materials”,

ATTENTION: The Singapore Copyright Act applies to the use of this document. Nanyang Technological University Library

Chem. Rev. **110**, 56 (2010).

5. M. R Baklanov and K. Maex, “Porous low dielectric constant materials for microelectronics”, Phil. Trans. R. Soc. A **364**, 201 (2006).
6. M. Stucchi, P. J. Roussel, Z. Tokei, S. Demuynck, G. Groeseneken, “A Comprehensive LER-Aware TDDB Lifetime Model for Advanced Cu Interconnects”, IEEE Trans. Device and Materials Reliability **11**, 278 (2011).
7. J. Noguchi, “Dominant factors in TDDB degradation of Cu interconnects”, IEEE Trans. Electron Devices **52**, 1743 (2005).
8. F. Chen, O. Bravo, D. Harmon, M. Shinosky, and J. Aitken, “Cu/low k dielectric TDDB reliability issues for advanced CMOS technologies”, Microelectronics Reliability **48**, 1375 (2008).
9. K. Y. Yiang, W. J. Yoo, Q. Guo, and A. Krishnamoorthy, “Charge trapping at the low k dielectric-silicon interface probed by the conductance and capacitance techniques”, Appl. Phys. Lett. **93**, 122902 (2008).
10. J. M. Atkin, E. Cartier, T. M. Shaw, R. B. Laibowitz, and T. F. Heinz, “Charge trapping at the low k dielectric-silicon interface probed by the conductance and capacitance techniques”, Appl. Phys. Lett. **93**, 122902 (2008).
11. L. S. Chen, W. H. Bang, Y. J. Park, E. T. Ryan, S. King, and C.U. Kim, “Observation of space charge limited current by Cu ion drift in porous low k/Cu interconnects”, Appl. Phys. Lett. **96**, 091903 (2010).
12. C. Cartereta and A. Labrosseb, “Vibrational properties of polysiloxanes: from dimer to oligomers and polymers. 1. Structural and vibrational properties of hexamethyldisiloxane (CH3)3SiOSi(CH3)3”, J. Raman Spectrosc. **41**, 996 (2010).

ATTENTION: The Singapore Copyright Act applies to the use of this document. Nanyang Technological University Library

13. N. J. Trujillo, Q. Wu, and K. K. Gleason, “ltralow Dielectric Constant Tetravinyltetramethylcyclotetrasiloxane Films Deposited by Initiated Chemical Vapor Deposition (iCVD)”, Adv. Funct. Mater. **20**, 607 (2010).
14. A. Grill and D. A. Neumayer, “Structure of low dielectric constant to extreme low dielectric constant SiCOH films: Fourier transform infrared spectroscopy characterization”, J. Appl. Phys. **94**, 6697 (2003).
15. J. Bao, H. Shi, J. Liu, H. Huang, P. S. Ho, M. D. Goodner, M. Moinpour, and G. M. Kloster, “Mechanistic study of plasma damage of low k dielectric surfaces”, J. Vac. Sci. Technol. B, **26**, 219 (2008).
16. H. L. Shi, J. Bao, R. S. Smith, H. Huang, J. Liu, P. S. Ho, M. L. Mcswiney, M. Moinpour, and G. M. Kloster, “Origin of dielectric loss induced by oxygen plasma on organo-silicate glass low k dielectrics” Appl. Phys. Lett. **93**, 192909 (2008).
17. J. C. K. Lam, M. Y. M. Huang H. Tan, Z. Q. Mo, Z. H. Mai, C. P. Wong, H. D. Sun, and Z. X. Shen. “Vibrational spectroscopy of low k/ultra-low k dielectric materials on patterned wafersJ. Vac. Sci. Technol. A, **29**, 051513 (2011).

Chapter 6

1. Teh, Y.W.; Wong, T.K.S.; Sudijono, J.; See, A. High density plasma chemical vapor deposition of fluorinated silicon oxide for low k dielectric applications. In Proceedings of SPIE International Symposium of Microelectronics and Assembly, Singapore, 28–30 November 2000.

ATTENTION: The Singapore Copyright Act applies to the use of this document. Nanyang Technological University Library

2. Ligatchev, V.; Wong, T.K.S.; Liu, B.; Rusli. Atomic structure and defect densities in low dielectric constant SiOCH films deposited by plasma-enhanced chemical vapor deposition. J. Appl. Phys. 2002, 92, 4605–4611.
3. Wong, T.K.S.; Liu, B.; Narayana, B.; Ligatchev, V.; Kumar, R. Investigation of deposition effect on properties of PECVD deposited SiOCH. Thin Solid Films 2004, 462, 156–160.
4. Goh, T.K.; Wong, T.K.S. Investigation of thermal and oxygen plasma stability of mesoporous methylsilsesquioxane low k films by X-ray reflectivity and small angle scattering. Microelectron. Eng. 2004, 75, 330–343.
5. Hacker, N.P. Organic and inorganic spin-on polymers for low-dielectric-constant applications. MRS Bull. 1997, 22, 33–38.
6. Homma, T. Low dielectric constant materials and methods for interlayer dielectric films in ultralarge-cale integrated circuit multilevel interconnections. Mater. Sci. Eng. 1998, R23, 243–285. Morgen, M.; Todd-Ryan, E.; Zhao, J.H.; Hu, C.; Cho, R.; Ho, P.S. Low dielectric constant materials for ULSI Interconnects. Annu. Rev. Mater. Res. 2000, 30, 645–680.
7. Maex, K.; Balkanov, M.R.; Shamiryan, D.; Iacopi, F.; Brongersma, S.H.; Yanovitskaya, S. Low-dielectric constant materials for microelectronics. J. Appl. Phys. 2003, 93, 8793–8841.
8. Beaudoin, S.; Graham, S.; Jaiswai, R.; Kilroy, C.; Kim, B.S.; Smith, S. An update on low k dielectrics. Interface 2005, 14, 35–39.
9. Gill, A. Porous pSiCOH ultra-low k dielectrics for chip interconnects prepared by PECVD. Annu. Rev. Mater. Res. 2009, 39, 49–69.

ATTENTION: The Singapore Copyright Act applies to the use of this document. Nanyang Technological University Library

10. Kohl, P.A. Low-dielectric constant insulators for future integrated circuits and packages. Annu. Rev. Chem. Biomol. Eng. 2011, 2, 379–401.
11. Havemann, R.H.; Hutchby, J.A. High-performance interconnects: An integration overview. Proc.IEEE 2001, 89, 586–601.
12. Fleetwood, D.M.; Pantelides, S.T.; Schrimpf, R.D. Defects in Microelectronic Materials and Devices; CRC Press: Roca Baton, FL, USA, 2011; pp. 123–129.
13. The International Technology Roadmap for Semiconductors 2009. Available online: http://www.itrs.net (accessed on 10 June 2012).
14. Jeffrey C. K. Lam, Maggie Y. M. Huang, Hao Tan, Zhiqiang Mo, and Zhihong Mai, Choun Pei Wong, Handong Sun, and Zexiang Shen. "Vibrational spectroscopy of low k/ultra-low k dielectrics on patterned wafers", J. Vac. Sci. Technol. A 29(5), 051513.
15. Jeffrey C. K. Lam, Maggie Y. M. Huang, Hao Tan, Zhiqiang Mo, Zhihong Mai, Handong Sun, and Zexiang Shen, "FTIR Spectroscopy of Ultra-Low k dielectric on Patterned Wafers", Jpn. J. Appl. Phys. 51 (2012) 111501.
16. International Technology Roadmap for Semiconductors: 2010 Update.
17. Suehle, J. Ultrathin gate oxide reliability: Physical models, statistics, and characterization. IEEE Trans. Electron. Devices 2002, 49, 958–971.Terence K.S. Wong, Time Dependent Dielectric Breakdown in Copper Low k Interconnects: Mechanisms and Reliability Models. ISSN 1996-1944, Published: 12 September 2012.

ATTENTION: The Singapore Copyright Act applies to the use of this document. Nanyang Technological University Library

18. Fen Chen and Mike Shinosky: Addressing Cu/Low k Dielectric TDDB-Reliability Challenges for Advanced CMOS Technologies. IEEE TRANSACTIONS ON ELECTRON DEVICES, VOL. 56, NO. 1, JANUARY 2009
19. Maxime Vilmay, David Roy, Cedric Monget, Fabien Volpi, and Jean-Marc Chaix: Copper-Line Topology Impact on the Reliability of SiOCH Low k for the 45-nm Technology Node and Beyond. IEEE TRANSACTIONS ON DEVICE AND MATERIALS RELIABILITY, VOL. 9, NO. 2, JUNE 2009
20. Jeffrey C. K. Lam, Maggie Y. M. Huang, Tsu Hau Ng, Mohammed Khalid Bin Dawood, Fan Zhang et al: Evidence of ultra-low k dielectric material degradation and nanostructure alteration of the Cu/ultra-low k interconnects in time-dependent dielectric breakdown failure. Appl. Phys. Lett. 102, 022908 (2013); doi: 10.1063/1.4776735
21. T. L. Tan,1,2 C. L. Gan,1,a_ A. Y. Du,2 and C. K. Cheng3: Effect of Ta migration from sidewall barrier on leakage current in Cu/SiOCH low k dielectrics. JOURNAL OF APPLIED PHYSICS 106, 043517 _2009.
22. N. L. Michael, Choong-Un Kim, P. Gillespie, and R. Augur：Mechanism of reliability failure in Cu interconnects with ultralow k materials。Appl. Phys. Lett. 83, 1959 (2003); doi: 10.1063/1.1609242.
23. Yamamoto, Shigehisa Yamamoto, Shigehisa: A NEW TDDB DEGRADATION MODEL ASED ON CU ION DRIFT IN CU INTERCONNECT DIELECTRICS. Reliability Physics Symposium Proceedings, 2006. 44th Annual., IEEE International. Conference Publications Page: 484 – 489.

ATTENTION: The Singapore Copyright Act applies to the use of this document. Nanyang Technological University Library

Publications

1. **Jeffrey C. K. Lam**, Maggie Y. M. Huang, Ng Tsu Hau, M. K. B. Dawood, Fan Zhang, Anyan Du, Handong Sun, Zexiang Shen, Zhihong Mai, Evidence of Ultra-Low k Dielectric Material Degradation and Nanostructure Alteration of the Cu/Ultra-Low k Interconnects in Time-Dependent Dielectric Breakdown Failure, Applied Physics Letter, 102, 022908 (2013).
2. Maggie Y. M. Huang, **Jeffrey C. K. Lam**, Ng Tsu Hau, M. K. B. Dawood, Fan Zhang, Anyan Du, Handong Sun, Zexiang Shen, Zhihong Mai, Current leakage and Electrical Field Dependant Dielectric Degration in Time-Dependent Dielectric Breakdown Failure of a Cu/Ultra-Low k dual Damaseence Process, Applied Physics Letter, Submitted.
3. **Jeffrey C. K. Lam**, Maggie Y. M. Huang, Hao Tan, Zhiqiang Mo, and Zhihong Mai, Choun Pei Wong, Handong Sun, and Zexiang Shen. "Vibrational spectroscopy of low k/ultra-low k dielectrics on patterned wafers", J. Vac. Sci. Technol. A 29(5), 051513.
4. **Jeffrey C. K. Lam**, Maggie Y. M. Huang, Hao Tan, Zhiqiang Mo, Zhihong Mai, Handong Sun, and Zexiang Shen, "FTIR Spectroscopy of Ultra-Low k dielectric on Patterned Wafers", Jpn. J. Appl. Phys. 51 (2012) 111501.
5. **Jeffrey C. K. Lam**, Wei Lin Wang, Maggie Huang, Dandan Wang, Fan Zhang, Wei Shao, Anyan Du, Alan Lek, Handong Sun, Zexiang Shen, and Zhi Hong Mai, A Model Analysis and The Process Improvement on the Cu/Ultra-Low k

ATTENTION: The Singapore Copyright Act applies to the use of this document. Nanyang Technological University Library

Dielectric TDDB Failure Caused by Dielectric Degradation and Barrier Metal Migratation into the degraded dielectrics, Microelectronics Reliability, Submitted.

6. **Lam Jeffrey**, Huang Yamin, Zhang Fan, Sun Handong, Sheng Zhexiang, and Mai Zhihong, To Reveal Failure Mechanism of Low k Dielectric Reliability Fallout with Raman and FTIR Spectroscopy, Submitted to Applied Physics A.
7. **Lam Jeffrey**, Huang Yamin, Zhang Fan, Sun Handong, Sheng Zhexiang, and Mai Zhihong, Experiments and Results of Raman and FTIR Complementary Vibrational Spectroscopy for IC Reliability Failure analysis, Proceedings of 20th Internatinal Symposium on the Physical and Failure Analysis of Integrated Circuits, 15-19 July 2013, Shangri-la Hotel, Suzhou, China.